Università degli Studi di Palermo

AREA QUALITÀ, PROGRAMMAZIONE E SUPPORTO STRATEGICO
SETTORE STRATEGIA PER LA RICERCA
U. O. DOTTORATI

Dipartimento di Scienze della Terra e del Mare (DiSTeM)
Dottorato di ricerca in Scienze della Terra e del Mare
Settore Scientifico Disciplinare GEO/04 Geografia Fisica e Geomorfologia

LANDSLIDES SUSCEPTIBILITY STOCHASTIC MODELLING UNDER EARTHQUAKES AND RAINFALLS TRIGGERING: APPLICATIONS TO 2001 EARTHQUAKES (13TH JANUARY AND 13TH FEBRUARY) AND 2009 TROPICAL STORM (IDA/96E) IN EL SALVADOR

IL DOTTORE
Dr. Claudio Mercurio

IL COORDINATORE
Prof. Alessandro Aiuppa

IL TUTOR
Prof. Edoardo Rotigliano

IL CO-TUTOR
Prof. Christian Conoscenti

CICLO XXXV
ANNO CONSEGUIMENTO TITOLO 2022

LANDSLIDES SUSCEPTIBILITY STOCHASTIC MODELLING UNDER EARTHQUAKES AND RAINFALLS TRIGGERING: APPLICATIONS TO 2001 EARTHQUAKES (13TH JANUARY AND 13TH FEBRUARY) AND 2009 TROPICAL STORM (IDA/96E) IN EL SALVADOR

1. Introduction

In El Salvador (C.A.), landslides are among the most destructive natural phenomena, which can cause mass fatalities and devastation in the built environment. They may occur either due to heavy rains (rainfall-induced landslides) or as a secondary effect of an earthquake (earthquake-induced landslides). Regarding the first trigger, the extreme rainfall events that frequently affect the Central American region are responsible for activating gravitational phenomena consisting of shallow and fast-moving flow landslides that may cause severe economic damage and fatalities. For the second category, large damages are controlled by shaking-related causes (roads and building collapse); however, a seismic event can produce several gravitational phenomena capable of causing more damage and victims than the earthquake itself, a situation that occurs in the country, often affected by high-intensity phenomena.

The intricate geodynamic context in which the small territory of El Salvador is located is characterized by the subduction of the Cocos plate under the Caribbean plate, through the Middle America Trench, with an estimated rate of about 7 cm/year. This active tectonic environment is responsible for the presence of several active volcanoes in the country, aligned in the direction of WNW-ESE, which have frequently erupted and deposited widespread and poorly consolidated tephra in many parts of the country. These lithologies, combined with acid pyroclastites and acid/basic effusive rocks, ensure that volcanic rocks represent 95% of the outcropping lithologies in the country. El Salvador is the smallest country in Central America but has the highest population density (310 inhabitants/km^2). Indeed, the fertility of the soils around the active volcanoes has generated a situation in which much of the population lives in the areas in the proximity of the highest mountains.

The combination of the geodynamic context, capable of generating moderate and strong earthquakes, steep slopes composed of weak volcanic rocks and the presence of the main population centres around them, combined with a warm and humid subtropical climate with heavy rainfalls, all create conditions for recurrent either earthquake- and rainfall-

induced landslides in the country. Because of the destructive nature of these phenomena, in terms of damage to infrastructure and human lives, any hazard and risk assessment must include the hazard associated with earthquake- and rainfall-induced landslides. If a large-scale study is to be carried out, it is necessary to analyze all the possible factors that are supposed to be predisposing factors in causing the gravitational phenomena. In fact, by studying these predictive factors, it is possible to recognize the most susceptible areas to the initiation of future gravitational phenomena following a specific trigger.

The Italian Agency for Development Cooperation (AICS), the University of Palermo and the University of Chieti-Pescara (Italy) has financed the CASTES project, which is dedicated, among the many objectives of this program of international collaboration, to study the unstable seismic effects induced within the El Salvador territory, in order to produce approaches for preventing and reducing these catastrophes and recovering and reconstructing the affected areas, like the landslides susceptibility analysis. In fact, it is essential for land management and civil protection authorities to know the probability of a gravitational event occurring in a specific spatial unit of a definite area. Several methodologies can be used to generate susceptibility maps from landslides; nonetheless, indirect and quantitative are the most effective for the aim.

This doctoral research aims to evaluate the combination of different susceptibility models using various combinations of inventories and variables to predict areas where earthquake-induction phenomena are most likely to occur. In fact, earthquake- and rainfall-induction inventories will be used with different combinations, using variables typically applied for the rainfall-induced landslides susceptibility and dynamic seismic factors.

The case studies of this thesis are related to the sectors affected by two intense earthquakes that occurred on 13th January (M 7.7) and 13th February (M 6.6) and the sectors affected by an extreme rain phenomenon of November 2009 following the combination of the Hurricane Ida and the low-pressure system event 96E.

The thesis work is divided as follows:

- Chapters 2 and 3 are the theoretical section of the projects; Chapters 4, 5, 6 and 7 are the applications section.

- In Chapter 2, the different types of landslides are analyzed. Subsequently, paragraphs related to the susceptibility to landslides to reduce the risk associated with such phenomena will be investigated.

- In Chapter 3, the geodynamic context, the outcropping lithologies and the high susceptibility of the study areas to the manifestation of gravitational phenomena triggered both by extreme rainfall and seismic events are described.

The following chapters correspond to the three main themes that will be analyzed in this thesis:

- In Chapter 4, a methodology for producing a rainfall-induced susceptibility map is developed in an area affected by the combination of Hurricane Ida and the low-pressure system 96E event, which occurred in November 2009. This work was developed using MARS (Multivariate Analysis Regression Splines) statistical technique. The aim is to demonstrate the excellent predictive performance of the MARS stochastic model in predicting rainfall-induced susceptibility phenomena following extreme rainfall phenomena.

- In Chapter 5, earthquake-induced landslide susceptibility output using different inventories and variables (both linked to seismic or extreme rain triggers) are presented and discussed to determine the best combination for assessing earthquake-induced landslide susceptibility maps. Two possible scenarios are analyzed, one in which most gravitational phenomena are known (75%) and another one in which only a reduced number of gravitational phenomena are known (5%), both in order to know the predictive abilities of the models applied for the prediction of the location of the remaining landslides.

- In Chapter 6, earthquake-induced landslide susceptibility output are presented using rainfall-induction inventories for calibration and earthquake-induction inventories for validation by creating two models, one linked to predictive variables common to both types of triggers and one linked by the combination of the variables of the previous model and the

variables used exclusively for seismic triggers. This test was carried out because extreme rainfall events are frequent in Central America; however, the same is not expected for seismic phenomena, with relatively more significant return times. This relatively minor amount of earthquake-induction landslide inventories ensure that the earthquake-induction inventories and the related susceptibility maps are more complex to obtain than rainfall-induction inventories/susceptibility maps. This study aimed to evaluate the possibility of matching the rainfall-induced susceptibility scores obtained from classic and static modelling with the expected seismic parameters to predict earthquake-induced landslides. A positive response could allow this type of map to be generated anywhere, even where no earthquake-induced landslide inventories are available. Due to the active geodynamic context and the passage of hurricanes and low-pressure systems, El Salvador is strongly affected by both trigger categories.

- Finally, in Chapter 7, discussion and conclusions regarding the main objectives of the thesis are given.

Below is a table showing the objective of the application chapters of this thesis, the inventories used for calibration and validation and the predictive variables used for each of the seven models elaborated (Tab. 1.1).

Table 1.1 - Input and output of the seven models produced in this thesis.

Chapter and Title	Inventory for Calibration	Variables	Inventory for Validation	Result
4: Mapping susceptibility to debris flows triggered by tropical storms: a case study of the San Vicente Volcano area	Rainfall-induced landslides (75%)	10 predictive variables	Rainfall-induced landslides (25%)	Rainfall-induced landslides susceptibility map
5: Predicting earthquake-induced landslides by using a stochastic modelling approach which combines preparatory and triggering factors	Rainfall-induced landslides (Scenario 1: 75%; Scenario 2: 5%)	*Model 1*: Probability of occurrences of rainfall-induced landslides by using 11 predictive variables (PSV)	Earthquake-induced landslides (Scenario 1: 25%; Scenario 2: 95%)	Earthquake-induced landslides susceptibility map with features related to rainfall-induction landslides
	Earthquake-induced landslides (Scenario 1: 75%; Scenario 2: 5%)	*Model 2*: PSV; 2 Dynamic predictors (PGA, Epicentral distances)		Earthquake-induced landslides susceptibility map with features related to rainfall-induction landslides
	Earthquake-induced landslides (Scenario 1: 75%; Scenario 2: 5%)	*Model 3*: 11 Static predictors; 2 Dynamic predictors (PGA, Epicentral distances)		Earthquake-induced landslides susceptibility map
	Earthquake-induced landslides (Scenario 1: 75%; Scenario 2: 5%)	*Model 4:* PSV; 11 Static predictors; 2 Dynamic predictors (PGA, Epicentral distances)		Earthquake-induced landslides susceptibility map with features related to rainfall-induction landslides
6: Prediction of the spatial distribution of landslides generated from earthquake by using an approach which combines a rainfall-induced inventory and static with seismic parameters	Rainfall-induced landslides (100%)	*Model Ida2009rain*: 10 Static predictors	Earthquake-induced landslides (100%)	Earthquake-induced landslides susceptibility map
		Model Ida2009rain_pga_dist: 10 Static predictors; 2 Dynamic predictors (PGA, Epicentral distances)		Earthquake-induced landslides susceptibility map

THEORETICAL SECTION

2. Methodology

This chapter discusses the theoretical aspect of landslides, the danger and risk associated with these phenomena and the possible risk mitigation.

2.1. Landslides

Landslides are among the most destructive natural processes, capable of causing death and destruction following their activation.

Depending on the type and intensity of the trigger and the geo-environmental characteristics of the involved areas, gravitational phenomena can be produced with different distribution areas, densities and dimensions. Gravitational phenomena can be triggered by heavy rainfalls or as a secondary response to an earthquake. As for the first category, the rains increase the weight of involved lithologies and, concomitantly, a reduction in effective stresses, consequently reducing shear resistance. These factors increase the active forces compared to those resistant, resulting in the trigger of gravitational phenomena. As for the latter category, fatalities are controlled by shaking-related causes; however, seismic events can produce several gravitational phenomena capable of causing more damage and victims than earthquakes.

Knowing the areas where gravitational phenomena can be triggered (or reactivated) is of fundamental importance to prevent infrastructure, housing and, consequently, human lives from being involved in its destructive action. After careful studies by geologists, it may be possible to prevent the construction of new buildings in some regions of the earth's surface that may be located along the transport and/or accumulation area of landslides. In addition, where the site is inhabited, it is necessary that regular studies and monitoring are carried out to check its activation status. In fact, a landslide can be quiescent, and it should be possible to know its reactivation by studying precursor phenomena and indicators.

Therefore, the study of landslides is an indispensable instrument by which it is possible to safeguard the territory and, consequently, the artefacts and human lives.

Identifying the characteristics of all types of landslides, and then the shape of the relief, the volumes involved, the speeds, the kinds of movement and the triggering causes is fundamental, and, given the specific type of gravitational phenomenon analyzed, it is necessary to carry out adequate monitoring and any appropriate work of intervention.

It is essential to be aware of the direction in which the gravitational process will evolve to predict the possible occurrence of risk situations for people or infrastructure. For this reason, the concept of "activity" is introduced, whose conditions are defined in terms of state (temporal evolution), distribution (spatial evolution) and style (kinematic relations between different portions of the landslide area). The state of activity refers to the temporal evolution of the phenomenon, differing in the following levels: *active* and *inactive*. Landslides in inactivity are diversified as *quiescent* and *stabilized* (Tab. 2.1).

Tab 2.1 – Activity state of landslides.

Activity state		**Description**
Activated or reactivated		if it is currently in motion.
Inactivated	*quiescent*	if it moved the last time before the last season cycle but can be reactivated by its original causes.
	artificially or naturally stabilized	if it moved the last time before the last season cycle but whether it has been protected from its original causes by resettlement or whether the gravitational phenomenon has run out naturally, that is, whether it is no longer affected by its original causes.

The *activity distribution* describes in which direction the gravitational phenomenon is moving and allows to predict the type of instability evolution (Tab. 2.2).

Tab 2.2 – Activity distributions of landslides.

Activity distribution	**Description**
Advancing	the rupture surface extends in the direction of movement.
Retrogressive	the rupture surface extends in the direction opposite to the movement of the displaced material.
Enlarging	the rupture surface of the landslide extends in two or more directions.
Diminishing	the volume of displaced material is decreasing.
Confined	there is a scarp but no rupture surface visible at the foot of the displaced mass.
Moving	the displaced material continues to move without any visible change in the rupture surface and the volume of the ejected material.
Widening	the rupture surface extends into one or both flanks of the landslide.

The *activity style* indicates how the different movement mechanisms contribute to the landslide. Depending on the activity style, a landslide is defined (Tab. 2.3):

Tab 2.3 – Activity style of landslides.

Activity style	**Description**
Complex	exhibits at least two types of movement in sequence.
Composite	exhibits at least two types of movement simultaneously in different parts of the displacing mass.
Successive	phenomenon characterized by a movement of the same type of a previous and adjacent phenomenon.
Single	a single movement of displaced material.
Multiple	shows repeated development of the same type of movement.

2.2. Landslides classification

During the last decades, many definitions of *landslide* have been enunciated. However, most of these presented imperfections and ambiguities, seeing the quantity and the heterogeneity of the possible gravitational phenomena in nature. Brunsden defined them as mass movements (Brunsden, 1984), distinguishing them from mass transport, as he felt that the gravitational process did not require a means of transportation different than gravity. However, this definition conflicts with the debris flow landslides and lateral spreads, because they depend, respectively, on the fluid conveying and the tangential forces, orthogonal to the acceleration gravity vector. Varnes (1978) defines landslides as a *gravity-controlled, shallow or deep, fast or slow movement of material that can affect part or an entire mountainous relief*. At last, Varnes, together with Cruden, define the word landslide as a *movement of masses of rock, earth and debris along a slope* (Cruden & Varnes, 1996). As for the classification of gravitational phenomena, many debates have been opened among the experts and different classifications have been presented. Among these, the classification of Desio (1973) proposes a classification based on the typology of movement, creating a classification of six types of gravitational phenomena. Hutchinson's (1988) classification distinguishes gravitational phenomena into eight classes based on morphological differences, mechanisms, typology, and velocity of the material involved. In 1996, Cruden and Varnes created a classification based on the distinction of six types of landslide phenomena according to their type of movement; they also differentiated them according to the nature of the material involved, distinguishing them into three further classes. The latter classification is the most widely used in the field of geomorphology.

2.2.1. Nature of material involved in landslides

As for the nature of the material involved, Cruden and Varnes distinguish three types of materials, distinguishing between them according to their mechanical characteristics:

- *consistent materials*: solid stone or metamorphic rocks, rigid materials with a stone behaviour, massive or stratified, which have high cohesion (between 5 and 10 MPa) and therefore have a significant mechanical strength;
- *inconsistent materials*: clastic deposits free of natural constraints, such as blocks, pebbles, gravel and sand; therefore equipped with low cohesion and low mechanical strength;
- *pseudo-consistent materials*: clayey rocks that behave like consistent materials under anhydrous conditions, while when they are saturated, they exhibit a behaviour similar to that of inconsistent materials.

The material involved in the landslide movement is divided into *rock*, *debris* and *earth* (defined in the EPOCH project 1991-1993), which correspond, respectively, to *consistent*, *inconsistent* and *pseudo-consistent materials*; it was decided that soil and debris categories should be distinguished according to the particle size of the material involved in the movement (respectively < 2 mm and > 2 mm).

2.2.2. Type of material involved in landslides

There are five types of movement provided by the classification of landslides of Cruden and Varnes: falls, topples, slides (rotational and translational), lateral spreading and flows. To these types is added that of complex landslides, the combination of two or more types of landslides just mentioned. By crossing the two classification criteria described above, it is possible to arrive at an overall table of the different types of landslides provided by the classification of Cruden and Varnes (Tab. 2.4).

Tab 2.4 – The classification of landslides of Cruden and Varnes with the respective classes, generated by the type of movement and type of material involved.

Type of movement		**Type of material involved**		
		Hard rock	*Dissolved rock*	
		Rock	*Debris*	*Earth*
Falls		Rock fall	Debris fall	Earth fall
Topples		Rock topple	Debris topple	Earth topple
Slides	*Rotational*	Rock slide	Debris slide	Earth slide
	Translational			
Lateral spreading		Rock spread	Debris spread	Earth spread
Flows		Earth flow	Debris flow	Earth flow
Complex		Phenomenon presenting two or more main types of movement in sequence		

The following paragraphs describe the five types of landslides according to the classification of Cruden and Varnes, as included within the study areas of this thesis, with particular attention to flows and slides, the most prevalent types in the study areas.

2.2.3. Falls

Falls are a type of landslide in which masses of rock, debris and/or earth detach from a topographic surface with a high slope, after a movement in the air, impact the foot of the slope, generating a propagation phenomenon dependent on different factors than those that generated the same detachment. When the hazard linked to collapse phenomena is analyzed, it will be necessary to study both the possibility that blocks will fall off and how the phenomenon will evolve. The first depends on the presence/absence of secondary fractures, the discontinuities' spacing and the lithological bodies' mass and volume. The latter depends on the morphology (concavity, convexity), the slope, the presence/absence of vegetation and the coefficient of mechanical absorption of lithologies located on the slope's foot.

The presence of secondary fractures in the blocks is a significant factor, as, at the time of impact, they can shatter into several parts of a smaller size. Among the predisposing factors of these phenomena, there are the height of the escarpment (the higher it is, the greater the kinetic energy at the moment of impact) and the mass (the block size dependent on the

gap spacing of discontinuities). Thanks to these two parameters, it would be possible to know how much kinetic energy corresponds to the moment of impact.

2.2.4. Topples

A topple is a type of landslide in which there is a rotation of rock prisms towards the outside of the slope, with a centre of rotation located at a point on foot or outside the prism itself. The kinematic evolutions can present both rapid evolutions in the case of homogeneous rigid rocks in the slope and controlled and slow (diachronic) evolutions in structures that contain rigid rocks above ductile rocks. In the latter case, there may also be a retro-rotation of the basal part and a forward rotation of the block's upper part involved, in which collapse phenomena may occur.

2.2.5. Slides

Slides are movements of a mass of rock, debris or earth that occur along a breaking surface or within a shear deformation band. These can be *translational* or *rotational*, depending on the shape of the breaking surface, and can be differentiated between rock/debris/earth slides, depending on the type of material involved.

Rotational slides have a semicircular breaking surface with the concavity facing upwards and a rotation centre of a portion of the slope located outside its slope. This landslide occurs when the slope has a geometry to allow the development of a breaking surface capable of overcoming the resistance forces of the material that constitutes the slope.

The radius of curvature depends on the mechanical characteristics of the material; the shape of the surface indicates the type of shear strength the material possesses. Indeed, that is a diagnostic indicator: a rotational slide affecting a side characterized by rigid material will have a wide slope area and a minimal accumulation area. In fact, the rupture surface must be deep to obtain a shear force that can overcome the shear strength and rise steeply towards the topographical plane. If a ductile lithology characterizes a landslide, it needs less lithostatic load for its trigger, presenting a relatively less steep breaking plane.

Translational slides mainly manifest along structural discontinuities such as stratification and fracture surfaces with a *dip slope* structure. Many phenomena of this type exploit mechanical discontinuity as sliding surfaces. The most widespread of these surfaces is the horizon separating the bedrock from the regolith, as the latter has higher permeability and infiltration than the first one.

2.2.6. Lateral spreads

Lateral spreads differ from previous gravitational phenomena since the breaking plane is horizontal and tangential forces are orthogonal to the acceleration gravity vector. They can occur either in contexts involving the entire relief with homogeneous lithology with the formation of double ridges and consequent graben, or in contexts with heterogeneous lithologies, where rigid rocks are superimposed on masses with ductile behaviour.

2.2.7. Flows

Flows are gravitational movements that occur mainly in loose soils and are evidenced by deformations of a plastic type of material. These movements present variable speeds in the landslide area. The rupture is manifested by loss of resistance due to a decrease in cohesion and/or an increase in neutral pressures. From a kinematic point of view, each lithological element before the landslide is connected to the others, presenting a cohesive force. At the moment of the trigger, the individual elements are divided, presenting an independent behaviour.

Depending on the particle size of the dissolved rocks, the eventual channelling, the cohesion value and the water content in the landslide, there should be different types of flows (*debris/mud/earth flows/avalanche*).

Debris flows are rapid mass movements characterized by a mixture of non-cohesive material, air and water that rapidly move downstream along impluvium lines (Brabb, 1984), usually gullies and first- or second-order channels. From a physical-mechanical point of view, debris flows are viscous fluids that are in an intermediate position between solid

transport and sediment-laden water floods. Debris flows can be initiated by debris slides or avalanches or rock falls occurring on open and steep slopes. Once the moving material reaches steep impluvium lines, these phenomena turn into debris flows.

The definitions of landslides as phenomena in which only the force of gravity acts, contrast with this type of gravitational phenomenon. For this reason, Brunsden (1984) classifies them as intermediate phenomena between landslides and concentrated outflow processes.

Debris flow can occur due to both cohesion losses and increased neutral pressures. In the first case, the water infiltrates and saturates the volume of lithology and the failure point of the slope occurs where the rupture of cohesion compromises the stability of the slope. As for the second case, a significant rise in groundwater level/infiltration occurs, leading to a consequent increase in neutral pressures with a resulting reduction in shear strength. Their activation depends on the inflow of water on the topographic surface, the infiltration capacity and the lithologies' permeabilities.

Rupture fringes occur because the breaking surface does not correspond to a flat line, since the lithologies in the regolith are not homogeneous; therefore, there is a portion of lithology in which the state of cohesion loss or increase of neutral pressures that trigger the gravitational phenomena.

In the initiating phase, the speed of such gravitational phenomena is remarkable (up to 20 m/s), and adjacent debris flows can also flow into the same channel, thus increasing their speed and thus their erosive and destructive power. The deposition area is often located at the base of the slope, but it can also reach several kilometres from it, depending on the amount of water included in the phenomenon.

The difference between this type of flow and the *debris avalanche* is that, for the first, the transport phase takes place in a channel, while the debris avalanche is manifested uniformly in the slope. Sometimes, slide debris can form instead of debris flow when the material does not disarticulate as for debris flow but tends to maintain its cohesion, therefore not generating a flow. However, if the soil's disformity tends to lose cohesion due to the

various impacts with the morphology, it tends to become a debris flow. Another difference is their depth; slides involve relatively greater depths than a slope, while flows are more superficial phenomena involving the regolith.

The *earth flows* have a characteristic shape in which there is a *source of detachment* upstream with a circular shape, a *propagation zone*, more reduced and narrower, with fractures of rupture and an *accumulation zone*, with a circular shape. The viscosity of the material is shown by the possible presence of radial fractures, which form only in the presence of even a minimum cohesion, while, in the absence of it, a deposition cone is formed in which the material is deposited uniformly. Earth flows, unlike debris flows, can also involve the clay substrate and not just the regolith.

The *mud flows* have a longer shape, the cohesion of the material is lower than that of the earth flow, showing more similar kinematics to that of debris flow.

In the category of *rock flow*s, there is also *sackung*, located in an intermediate zone between the flow type and that of lateral expansion. *Rock avalanches* are rapid flows of coarse-grained rocks that develop on slopes with a high slope. Often, a rock avalanche can be generated as a secondary collapse event when the impacted blocks disintegrate during their descent downstream; in this case, it is called *rock fall avalanche*.

2.3. Predisposing and triggering factors

Landslides typically occur under a combination of complex geological conditions.

All those actions that disturb the natural stability of a slope, modifying its stress regime, are the causes of gravitational phenomena. Such actions can be distinguished into *predisposing* and *triggering causes*.

The *predisposing factors* create the conditions for the generation of gravitational phenomena. Finding the combination of predisposing factors is significant in studying and, therefore, reducing the associated risk. In fact, their predisposition depends on the lithology and permeability of the material involved, the geometry of the slope, the possible presence of vegetation, their mechanical strength characteristics, and their grain size. A gravitational

phenomenon is manifested thanks to several slope factors; in fact, the variation of the value of at least one of the elements described in Tab. 2.5 can trigger a landslide.

Tab 2.5 – Parameters whose modification can determine the trigger of the landslide.

Element	**Description**
Slope	the gravity acting on the slope.
Cohesion	the intensity of the force that tends to keep the elements of the rock connected. Cohesion becomes null if the slope consists of inconsistent rocks, such as loose sand. In light of this, it can be stated that the slope is stable only if the inclination is equal to or less than the material's resting angle (Earle, 2015).
Friction	the value of resistance offered by lithologies.

The *triggering factors* are those that cause the alteration of natural balances, as, for example, extreme meteoric events, rapid melting of snow, accelerated erosion, erosion on the foot of the slopes by the action of water currents, earthquakes and rapid rise of the aquifer.

The succession of extended dry periods with intense and concentrated rainy events is a triggering factor of landslides. This situation is manifested, with short return times, in El Salvador, as well as in other states of Central America that are in a tropical context, characterized by the alternation of the dry season with the wet one. High values of cumulative precipitation can determine the soil saturation and the aquifer's high stationing, representing a factor both predisposing and triggering the landslide movements that may involve the substrate. However, rains should not be considered an immediate trigger of a landslide; it is necessary to consider the water content that a slope can contain. In fact, as the water content increases, cohesion decreases progressively, which leads to exceeding a threshold in which there is the trigger of a gravitational phenomenon. For the same reason, the rains can trigger landslides even without an intense rainy phenomenon; the possible trigger depends on the state of saturation of the lithologies involved.

The anthropic activities, concerning the characteristics of the context in which they are carried out, can act both as triggers and as predisposing causes (e.g., improper agricultural use and management of the woods, pastoralism and extractive activity).

The recurrent and intense seismic activity that affects the country of El Salvador can trigger, in conjunction with the most relevant events, the gravitational phenomena that present spatial distributions (both as regards the density of gravitational phenomena and the maximum distance at which they can be activated) which depends on the Magnitude. The topic will be dealt with in Chapter 3.2.

2.4. The Landslide Risk

The *Risk* is defined as the combination of three factors, corresponding to *hazard*, *vulnerability* and *exposed value*. Risk is the probability of damage, so the *landslide risk* is the probability of damage caused by a landslide. That is one of the main existing natural risks, capable of causing many fatalities and damage to artefacts yearly. Considering its definition, if at least one of these three factors has a zero value, it will equal the risk to null. Thus, for example, despite a large number of landslide phenomena, the risk in an area without artefacts and human lives, such as a desert area, is null. The risk is the result of the effects of a trigger on the territory and depends on the characteristics of the natural phenomenon, the strength of anthropic structures and the presence of people and activities.

A fundamental component of the Risk formula is the *hazard*, which represents the probability that a specific event occurs in a given area. This component is one of the fundamental objects of applied geomorphology studies, in which geomorphologists try to estimate the future morphodynamic responses of the slope, classifying them in terms of energy and return time. "*Any process or potential event that threatens a community's health, safety and well-being or any population's economy is considered a geological hazard*" (USGS, 1977). According to this definition, an earthquake or landslide occurring in an uninhabited area does not constitute a geological hazard. In the UNESCO report of Varnes

(Varnes & IAEG, 1984), this concept is modified, and geomorphological hazard is defined as the "*probability that a potentially destructive phenomenon occurs in a specific time and area*". It was therefore decided to separate the landslide hazard into two factors: *probability* and *intensity*. Probability represents the possibility of the manifestation of an event; it varies from 0 to 1, where 0 indicates the impossibility of the event and 1 indicates the certainty of the event. The intensity is the magnitude, the energy, which is mechanical in gravitational phenomena. Thanks to these statements, it is possible to indicate that the landslide hazard is entirely independent of the presence of inhabited areas and infrastructure.

V*ulnerability* is the attitude of a structure to suffer damage of a certain intensity following a landslide occurrence. Its value depends on the *rate of the resource* (a structure or an artefact that if damaged can cause economic and human loss, e.g., the value is very high in the case of a hospital or a school) and on the intrinsic resistance that presents the structure compared to the landslide phenomenon (e.g., characteristics of foundations).

The work of the geologist, in this case, must be finalized on the knowledge of the possible reactivation of the phenomena that are currently quiescent and also be able to recognize a scenario of new activation. He must suggest all those works that can consolidate the structure or slope in such a way as to reduce the value of the vulnerability and, consequently, the value of risk.

The *exposed value* represents the population and economic activities exposed to natural risk in a given area. The rate of the exposed value is expressed in monetary or numerical terms or in terms of the amount of units exposed to the risk.

2.5. Methods to mitigate the Landslide Risk

Recognizing the predisposing and triggering factors of landslides and the parameters for which an area is subject to high-risk values, it is essential to carry out interventions in order to mitigate the risk and monitor the slopes, in order to have information about possible

scenarios of new activation or reactivation of gravitational phenomena. For this purpose, the concept of *Factor of Security* (FoS) has been created to evaluate quantitatively the resistance of the slope against the action of natural or artificial forces that lead to its instability.

The forces to be considered in the study of the equilibrium of a slope can be summarized in two components: breaking forces, responsible for the tangential stresses (or shear forces) and those opposite, which contribute to the shear resistance (or internal resistance) of the slope. The Factor of Safety can be defined through these two elements, expressed by the relationship between *yield stress* and *working stress*. When the acting forces are more significant than the resistant forces, the landslide is triggered; in these conditions, the value of the Factor of Safety is below the unit. On the contrary, positive values will indicate stability conditions.

By referring to the numerator and denominator of the Factor of Safety, the following mechanisms of triggering a landslide can be identified:

- An *increase in cutting force*, which can be caused by several factors such as seismic stress, increase in the load on the slope, increase in the specific gravity of the soil (as a result of the growth in the water content), increase in the slope acclivity (e.g., due to human interventions such as excavations at the base of the slope).

- A *decrease in the shear strength*, that may depend on: a decrease in cohesion (due to physical, chemical or biological phenomena), an increase in neutral pressures (for meteoric events or for particular conditions in the area which determine a decrease of shear strenght) and the generation of seismic stresses. Shear strength is related to the friction force and is equal to the product of the *tangent of the internal friction angle of a material* for the *normal load* acting on it, where the latter factor is given by the difference between the *lithostatic load* and the *neutral pressure*. From this, it can be shown that the increase in neutral pressure leads to a decrease in the resistance factor.

To stabilize a landslide or to increase the Factor of Safety of a slope and, therefore, to mitigate the risk, interventions are needed to reduce the denominator and/or increase the numerator, so that this value would be as high as possible. These are basically distinguished in interventions that reduce the shear forces (e.g., re-profiling of the slope, poles and anchorages) and interventions that increase the material's shear strength characteristics (e.g., retaining structures and improvements in soil geotechnical characteristics and drainage). Knowing the type of landslide in the area under consideration is fundamental, as the interventions that tend to increase the Factor of Safety must be chosen according to the type of gravitational phenomenon. For example, a fall-type landslide will require the use of tools capable of constraining the block under consideration and rockfall nets, while a rotational sliding landslide will require interventions that tend to affect the saturation state and the stabilization of the landslide even below the breaking surface.

In addition to carrying out fundamental interventions to increase the Factor of Security, it is necessary to evaluate the area's movements and know their spatial and temporal evolution. It is, therefore, necessary to control the kinematic trend of the slope through its monitoring; this is fundamental to proposing a forecast model of the phenomenon. In fact, careful and continuous monitoring can be valuable from the point of view of risk management in the field of civil protection. Monitoring means observing the variation of some signals that generate phenomena that are believed to be connected to the process being studied (such as a rainfall meter, which measures the amount of rain falling in a given unit of time), so study their *precursors*.

The monitoring can be assumed as a work of mitigating the risk from landslides, since it works to identify the valuable precursors. Of course, to affirm the usefulness of a precursor, it must estimate the percentage of error with which it is giving a specific alarm. In fact, there is also necessary to consider the hazard associated with a false alarm, especially in economic terms. In this case, a *type 1 error* is generated, that is an alarm is given for a possible landslide when, in reality, it does not manifest itself, this is a *false positive*. That is a less severe error

than that of *false negatives*, the *type 2 error*, in which no alarm is given as a gravitational phenome is not expected when, in reality, this is manifested.

Damage to landslides due to rainfalls and earthquakes are closely related to economic development and the ability to prevent and reduce disasters. Developed countries, indeed, have the economic and scientific resources to project and manage structures designed to contain blocks of rock and stop or divert both slow and rapid flows (Chen, 2006; Matthew Larsen and Wieczorek, 2006). They may also activate direct or indirect protection and alarm systems to favor a prompt and rapid general evacuation.

Projecting effective defensive engineering structures and alarm systems requires knowing where landslides are more likely to occur. This information, which is also fundamental for land use planning aimed at mitigating landslide risk, is provided by landslide susceptibility maps.

2.6. Landslide susceptibility

Landslide risk can be mitigated by predicting where slope failures are most likely to occur. In fact, a landslide susceptibility map represents the relative probability of landslide occurrence for each spatial unit of a given area (Brabb, 1984; Conoscenti et al., 2016). Developing this output provides a practical and valuable tool to the authorities dealing with territory management and civil protection, as they indicate where new slope failures are more likely to occur in the future, thus showing areas where risk mitigation is a high priority.

Landslides susceptibility differs from the hazard analysis as it does not provide the magnitude and return times, but generates a spatial assessment of the conditions of greater or lesser probability of occurrence of a landslide phenomenon.

Several methodologies could be used to generate landslide susceptibility maps, however, the most effective for the purpose are the stochastic ones (Reichenbach et al., 2018; Carrara et al., 1986; Agnesi et al., 1983; Chung and Fabbri, 2003; 2008; Guzzetti et al., 1999; 2005; 2006; Clerici et al., 2006; Conoscenti et al., 2008). These are characterized by high objectivity since they use statistical tools to determine the influence of the factors of

instability and, consequently, the link between the latter and the distribution of gravitational phenomena in a given area. The stochastic approach is based on the principle that “the past is the key to the future”; thus, triggering future landslides is more probable under the same environmental conditions that produced slope failures in the past. The statistical approach relies upon inventories of landslides and maps revealing the spatial variability of a set of environmental attributes. If predisposing causes are considered immutable in time, the only factors that change are the triggers. Only a study of the previous triggers can allow knowing what can occur in a slope following a comparable trigger.

The first step for generating a landslide susceptibility map is to produce an inventory, which must refer to a specific trigger. For this purpose, analyzing aerial/satellite photos after a specific trigger is necessary to map the phenomena. To avoid including the gravitational phenomena that occurred with a previous trigger in the inventory, comparing the aerial/satellite photos with those previous trigger events is required. In fact, including antecedent phenomena, which occur with different triggers, involves an error that can compromise the final result.

A valid inventory must represent every landslide through an identifying point or a polygon that encloses the whole phenomenon. Although no agreement exists on the best location of a point to identify a landslide, numerous recent studies have successfully adopted LIPs for landslide susceptibility zoning (Rotigliano et al., 2011; Lombardo et al., 2014; Cama et al., 2015). In case of debris flows, which are usually shallow, LIPs are expected to be even more suitable for identifying pre-failure conditions (Rotigliano et al., 2011, 2018).

Subsequently, the landslides susceptibility study involves dividing the area into specific mapping units, distinguished from adjacent units according to defined characteristics and boundaries (Hansen, 1984; Carrara et al., 1995; Guzzetti et al., 1999). There are several mapping units; the selection depends on the available data, the research objective, the prediction images and the geomorphological proprieties. In this thesis, the mapping unit was realized using pixel-partition, then with cells with a size equivalent to those adjacent ones. Research (Rotigliano et al., 2012; Cama et al., 2017; Martinello et al.,

2020) has shown that the pixel-partition gives excellent model performance when landslide initiation points need to be detected, as in the case of flow landslides, present in a high number in the analyzed territory following triggers of earthquakes or extreme rainfall events.

The dependent variable reflects the presence or absence of landslide polygons or LIPs in a given location or mapping unit.

In the study of landslide susceptibility, geo-environmental attributes should be chosen as independent variables (predictive variables) based on their supposed influence on the triggering mechanisms of the phenomenon. In fact, these act as proxies for the factors mainly controlling landslide occurrence in the study area and are expected to be predictors of the spatial distribution of the landslides included in the inventories (Costanzo et al., 2012).

Understanding the connections between landslides and influencing factors is critical for susceptibility mapping studies; research about susceptibility mapping shows no systematic procedure or general agreement about influencing factors (Shao and Xu, 2022). Because these depend on the predisposing factors, it is more probable that the landslide manifests where the factors are more determinant for the production of gravitational phenomena (e.g., a fall landslide would occurs where the slope is higher).

Since a landslide susceptibility map should be generated for all types of gravitational phenomena, it is necessary to select the common predisposing factors, those with the same relations of manifestation/absence of the gravitational phenomenon.

Once a set of predictors is defined, a value for dependent (presence/absence of LIPs or polygon) and independent variables (continuous or categorical) is assigned to each of the mapping units (Rotigliano et al., 2012).

Unlike geomorphological or heuristic methods, which strongly depend on the skill and experience of the operator, the stochastic approach is characterized by high objectivity, since it uses statistical tools to determine the influence of the instability factors and, consequently, the functional relationship between the latter and the distribution of gravitational phenomena in a given area (Verstappen, 1983). The statistical approach aims to achieve the best possible compromise between costs (money and time) and the reliability of the landslide

susceptibility models. The input data quality controls the landslide predictive models' accuracy and relative susceptibility maps.

This thesis calculated the likelihood of landslide occurrences at each grid cell in the study areas using the Multivariate Adaptive Regression Splines (MARS; Friedman, 1991) statistical modelling technique. The statistical analyses were realized using R Studio software with the "earth" package (Milborrow, 2020).

MARS is a non-parametric regression method that allows to model non-linear relationships between dependent and independent variables. This technique splits the range of the covariates into intervals, whose extreme values are called “knots”, and finds an optimal linear function between two consecutive knots, which is known as “basis function” (Gómez-Gutiérrez et al., 2015; Conoscenti et al., 2018; Garosi et al., 2018; Vargas-Cuervo et al., 2019).

The MARS method has been successfully applied recently in some geomorphological studies (Gutiérrez et al., 2009, 2015; Conoscenti et al., 2018, 2020), but there are relatively few tests in the literature in the field of landslide susceptibility zoning (Gutiérrez et al., 2009, 2015; Conoscenti et al., 2014, 2015, 2016, 2018; Garosi et al., 2018; Rotigliano et al., 2018; Rotigliano et al., 2019; Vargas-Cuervo et al., 2019). In fact, the statistical techniques most frequently used to map landslide susceptibility in the recent past have been: conditional analysis, discriminant analysis, logistic regression, artificial neural networks and classification and regression trees (Costanzo et al., 2012; Rotigliano et al., 2012; Clerici et al., 2006; Carrara et al., 2008; Van Den Eeckhaut et al., 2009; Costanzo et al., 2014; Lombardo et al., 2014; Cama et al., 2016).

The MARS model is the result of the weighted sum of terms that include a basis function or a product of two or more basis functions. Mathematically, a MARS model is expressed as:

$$y = f(x) = \alpha + \sum_{i=1}^{N} \beta_i h_i(x)$$

where y is the dependent variable predicted by the function $f(x)$, α is the constant, h_i is the basis functions and β_i its coefficients, N is the number of basis functions.

Modelling landslide susceptibility by using a statistical approach requires a validation procedure to measure the model's predictive skill. Without validation, the model is unusable and deprived of any scientific significance (Chung and Fabbri, 2003).

The calibration subset of landslides (training subset) is exploited to produce a prediction model, while the validation subset (test subset) simulates future landslides which are exploited to measure the predictive skill of the model (Conoscenti et al., 2008). In this work, calibrations are made both within the same dataset (using a certain percentage for calibration and the remaining for validation) and an entire inventory as calibration and another different inventory for validation. This method verifies whether the training subset can predict test landslides.

A susceptibility map is obtained with values from 0 to 1, indicating the probability of manifestation of gravitational phenomena. A summary of the procedure is shown in Fig. 2.1.

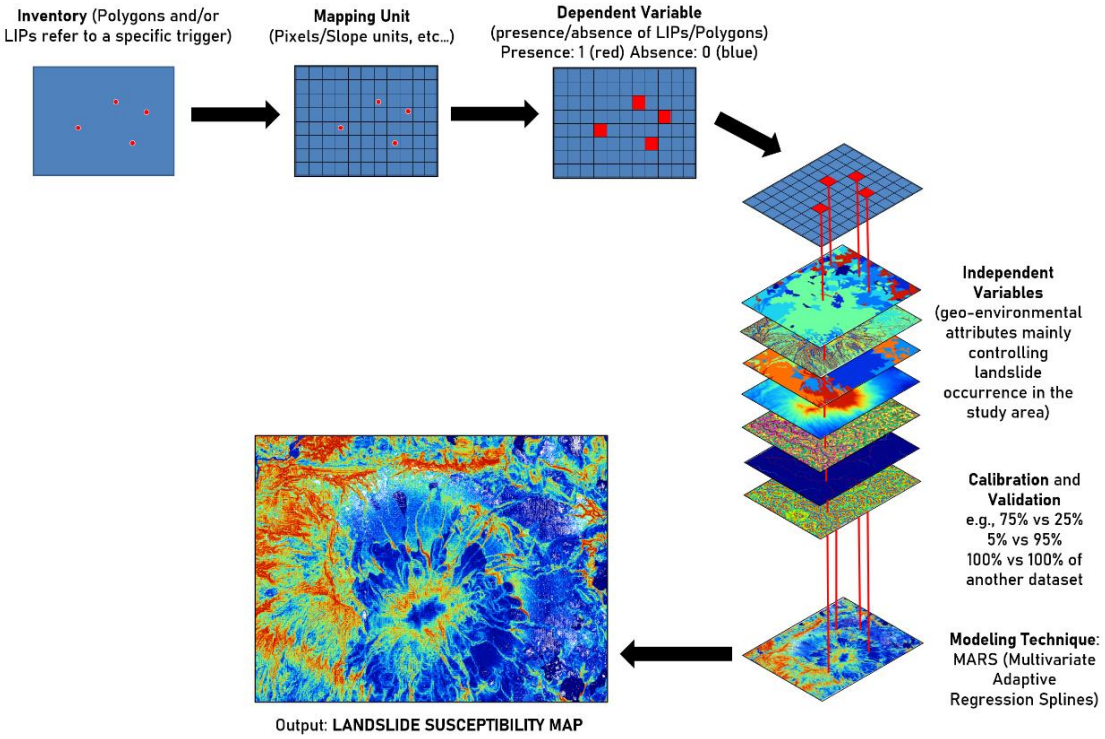

Figure 2.1 – Procedure for obtaining a landslide susceptibility map.

The models' performances are evaluated by preparing Receiver Operating Characteristic (ROC) curves and analyzing the Area Under the ROC Curve (AUC) values. ROC curves plot, across all possible cut-off values, *sensitivity* (or True Positive Ratio, TPR) against 1 - *specificity* (or False Positive Ratio, FPR). TPR is the ratio between the number of true positives (TP) (i.e. positives that were correctly classified) and the total number of positive cells. In contrast, FPR corresponds to the ratio between the number of false positives (FP) (i.e. negatives that were incorrectly classified as positive) and the total number of negative cells. AUC values close to 1 indicate the perfect discrimination ability of the model, whereas values close to 0.5 indicate no discrimination ability; values equal to or higher than 0.7, 0.8 and 0.9 can be interpreted as acceptable, excellent or outstanding, respectively (Hosmer and Lemeshow, 2000). In order to evaluate the model's performance by also using cut-off dependent metrics, an optimal cut-off value for the ROC curves should be calculated by using Youden's index (*J*) (Youden, 1950; Cama et al., 2017; Rotigliano et al., 2019; Conoscenti et al., 2020). This method allows finding the threshold that maximizes the sum of sensitivity and specificity. The value of *J* was used as a threshold to separate cells predicted as negatives and positives.

The optimized cut-off allows binarization of the landslide susceptibility map; values below the cut-off value are predicted as negative (absence of landslide), while those above are predicted as positive (presence of landslide). By comparing the validation dataset with the binarized map, it is possible to evaluate the model's performance with a confusion matrix by calculating the amount of true positive (TP), true negative (TN), false positive (FP) and false negatives (FN).

TP and TN represent correct predictions, in fact a pixel in a landslide is correctly predicted in the first case and a stable pixel is predicted as stable in the second case. In contrast, FP and FN represent *type 1* and *type 2 errors* (Chapter 2.5). Indeed, TN represents an error in the production of maps of susceptibility from landslides, as predicted a specific pixels unstable while the analyzed pixel has not presented triggers of gravitational phenomena in the validation check. However, this is a less severe error than type 2 (FN),

which means that a pixel is predicted to be stable when, in reality, a landslide is triggered by comparison with the validation data. That is a serious problem as an alarm or evacuation signal may not be given incorrectly in an area rated stable.

Each row of the matrix represents the instances in an actual class, while each column represents the instances in a predicted class, or vice-versa (both versions can be found in the literature). Thanks to this table is effortless to know if the system foresees if each landslide/non-landslide event is assessed as a gravitational phenomenon or not. Thanks to the obtained values it is possible to evaluate the *sensitivity* and the *specificity*. The first one is the true positive rate, defined as TP/(TP+FN) and refers to the probability of a positive test, conditioned on truly being positive. The latter is the true negative rate, defined as TN/(TN+FP) and refers to the probability of a negative test, conditioned on truly being negative. A summary of the procedure after the optimized cut-off generation is shown in Fig. 2.2.

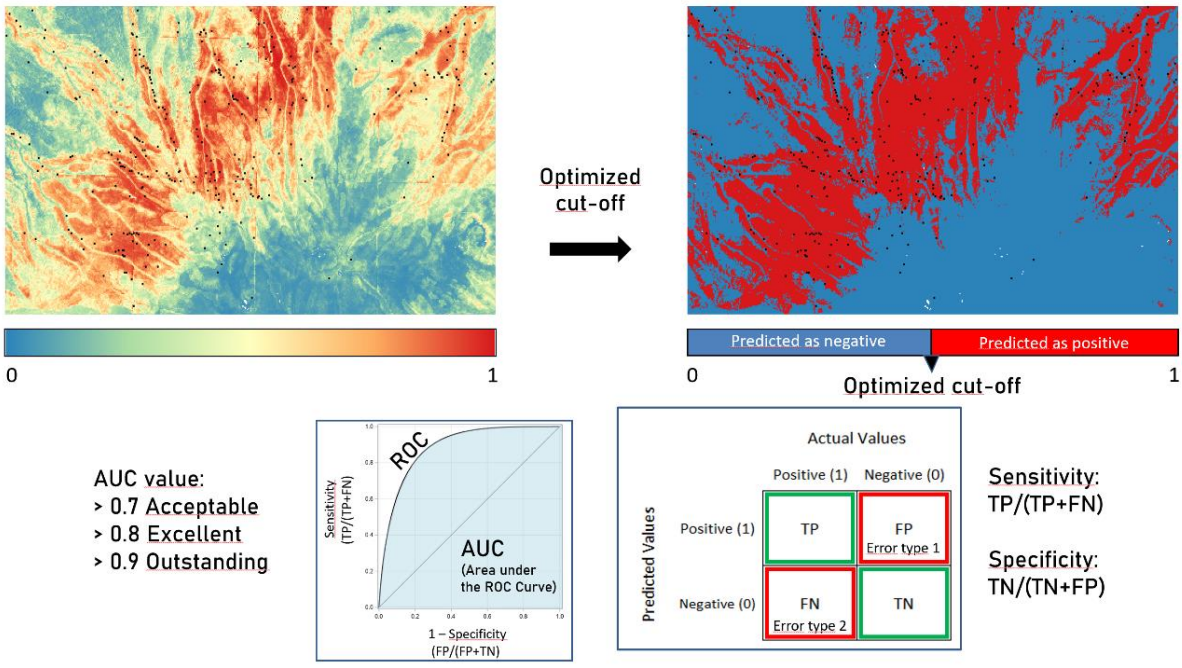

Figure 2.2 – The production of an optimized cut-off allows binarising the landslide susceptibility map to generate a confusion matrix that evaluates the susceptibility model's predictive ability generated.

APPLICATIVE SECTION

3. Geomorphological hazards in El Salvador

With an area of just over 21,000 km^2, El Salvador is the smallest country in Central America. It is situated on the Pacific coast and is bordered by Guatemala (East) and Honduras (North and West). The intricate geodynamic context in which El Salvador is located is characterized by the convergence of the Cocos plate with the Caribbean plate, through the Middle America Trench, with a rate of about 7 cm/year (Dewey and Suárez, 1991). This active tectonic environment is responsible for several active volcanoes in the country, aligned in the direction of WNW-ESE, which have frequently erupted and deposited widespread and poorly consolidated tephra in many parts of the country (Jibson et al., 2004). These lithologies, combined with acid pyroclastites, volcanic ashes and acid and basic effusive rocks, ensure that volcanic rocks represent 95% of the outcropping lithologies in the country (Fig. 3.1).

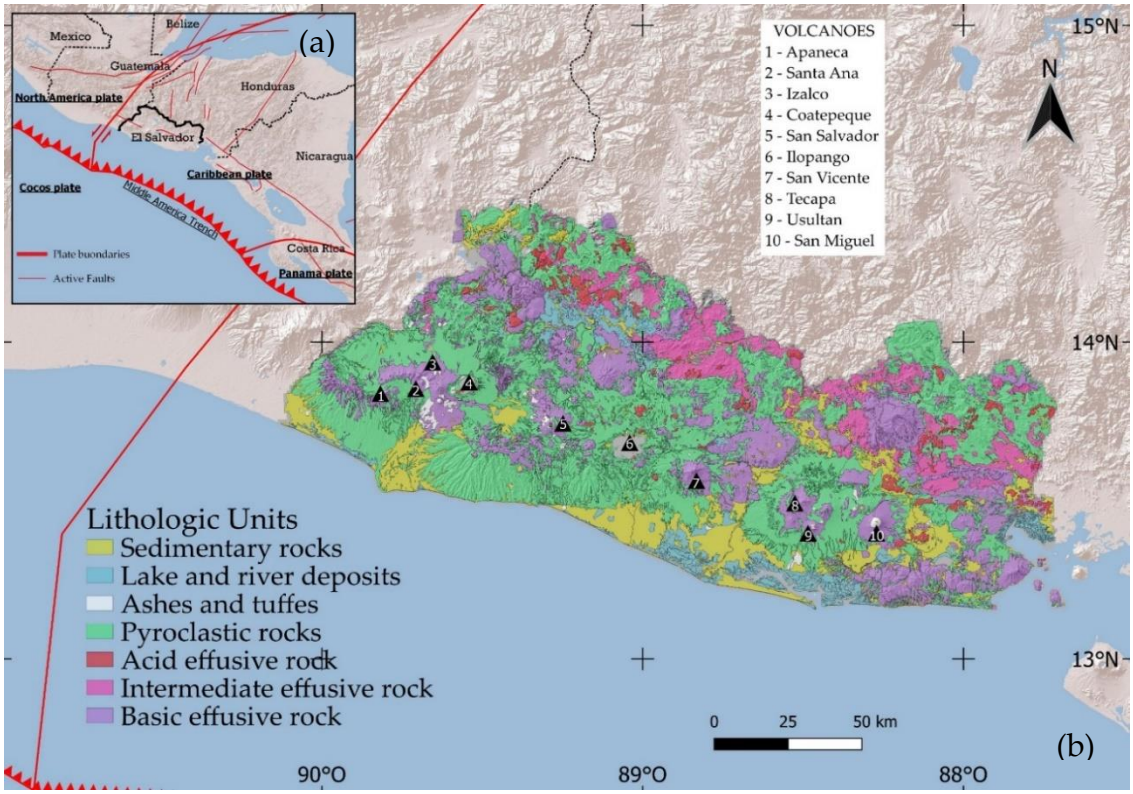

Figure 3.1 - Location and geological setting of the study area. El Salvador is located in Central America, where the Cocos Plate is subducted beneath the Caribbean Plate into the Middle American Trench (**a**); the geological setting of El Salvador, mainly characterized by volcanic outcropping rocks formed by the volcanoes chains (**b**).

The combination of the geodynamic context, responsible for medium and high earthquakes, steep slopes due to rugged volcanic ranges, incoherent rocks and a subtropical climate characterized by heavy storms, cause a high probability of earthquake- and rainfall-induced landslides occurrence in most of the country. The consequences of these gravitational phenomena are devastating for the country, which is the smallest country in Central America but the one with the highest population density (310 inhabitants/km^2). Indeed, the fertility of the soils around the volcanoes, oriented WNW-ESE due to the tectonic assessment (Bommer et al., 2002) and, most recently, to the production of geothermal energy, has generated a situation in which a large part of the population lives in the areas of the country most susceptible to the gravitational phenomena. This situation has meant that almost half of the Salvadoran population lives a few kilometres from the volcanic buildings of Santa Ana and Izalco, San Salvador, San Vicente and San Miguel (Major et al., 2004), thus increasing the elements at risk and, consequently, the consequences of the damage caused by landslides that are triggered by volcanic reliefs. As a confirmation, El Salvador has the highest ratio between the destroyed houses and the affected risks of Central America (Quesada-Román and Campos-Durán, 2022).

3.1. Extreme rainfall events

The extreme rainfall events that frequently affect the country are responsible for activating gravitational phenomena consisting in shallow and fast-moving flow landslides that may cause severe economic damage and even victims. These landslides are related to the outcropping of unconsolidated material on steep slopes, which can be rapidly moved by gravity and travel hundreds of meters to several kilometres from its origin (Crone et al., 2001).

Dramatic examples of their destructive potential in America are given by the disasters that occurred in Vargas (Venezuela), which caused about 15,000 victims in December 1999 (Larsen and Wieczorek, 2006; Larsen 2008), or in the mountainous regions of Rio de Janeiro (Brazil), in January 2001, where numerous debris avalanches and debris flows triggered by

an extreme rain event lasting two days caused around 1,500 victims (Avelar et al., 2013; Hungr et al., 2014).

Regarding El Salvador, since most population centres are located close to volcanoes, mainly consisting of inconsistent rocks, the risk is very high and civil protection institutions cannot give adequate notice to the population during extreme rainfall events. The short time between the extreme rainfall events, indeed, creates a situation in which the time for the alarm is reduced. In this case, a fundamental step is to provide sufficient advance to restrict the displacement of civilians and stop commercial activities, as well preventing future construction in the most susceptible areas. In fact, the country, as well as much of Central America, is often affected by the action of the passage of tropical storms and hurricanes that have caused several damages down the ages. Among them, *Hurricane Mitch*, which occurred on November 1998, caused devastation in Honduras, Nicaragua and El Salvador. During the event, 61 h of continuous rain generated 787 mm of rainfalls that caused the death of 374 Salvadorans (Hellin et al., 1999). *Hurricane Stan*, occurred on October 2005, caused 69 fatalities in El Salvador, rapid debris flows and floods that involved 300 communities, with 54,000 people forced to leave their homes after 500 mm of rainfalls (USAID, 2005). This event has joined to the destruction that occurred following the eruption of the volcano of Santa Ana, manifested a few days earlier, which also caused debris flows and lahars (USGS, 2005).

During the 7th and 8th of November 2009, most of El Salvador was struck by the simultaneous action of *Hurricane Ida and the low-pressure system 96E*. Hurricane Ida has been evolving since 4th November 2009 as a tropical depression in the southern-western sector of the Caribbean Sea and increased its strength until it evolved to tropical storm grade on 7th November while crossing Nicaragua's coast. It arrived at the stage of a second-level hurricane on the 8th, then shifted northward to the Gulf of Mexico and the Caribbean Sea, returning to the tropical storm grade and then depression on the 9th, until its total disappearance on the 12th of November. At the same time, the low-pressure system 96E from the eastern Pacific Ocean arrived in El Salvador territory (Avila and Cangialosi, 2009).

This event caused heavy rainfall between the 7th and 8th. The combined action of these two events resulted in about 350 mm in 24 h in an area of about 400 km^2 located between Ilopango Lake and San Vicente Volcano.

As a consequence, floods and thousands of landslides occurred in this area, causing about 200 victims, huge damage to infrastructures and buildings, with an economic loss estimated to be approximately a quarter of a billion dollars (Avila, 2009b.). These landslides, mostly debris flows, seriously affected the villages of Verapaz and Guadalupe, located in the north-western sector of the study area (Figures 3.2 and 3.3).

Figure 3.2 - An area hit by a debris flow in Verapaz after the simultaneous action of Hurricane Ida and the low-pressure system 96E. Photo by Yuri Cortez, 9th November 2009.
AFP/Getty Images, *https://volcano.si.edu/volcano.cfm?vn=343070*.

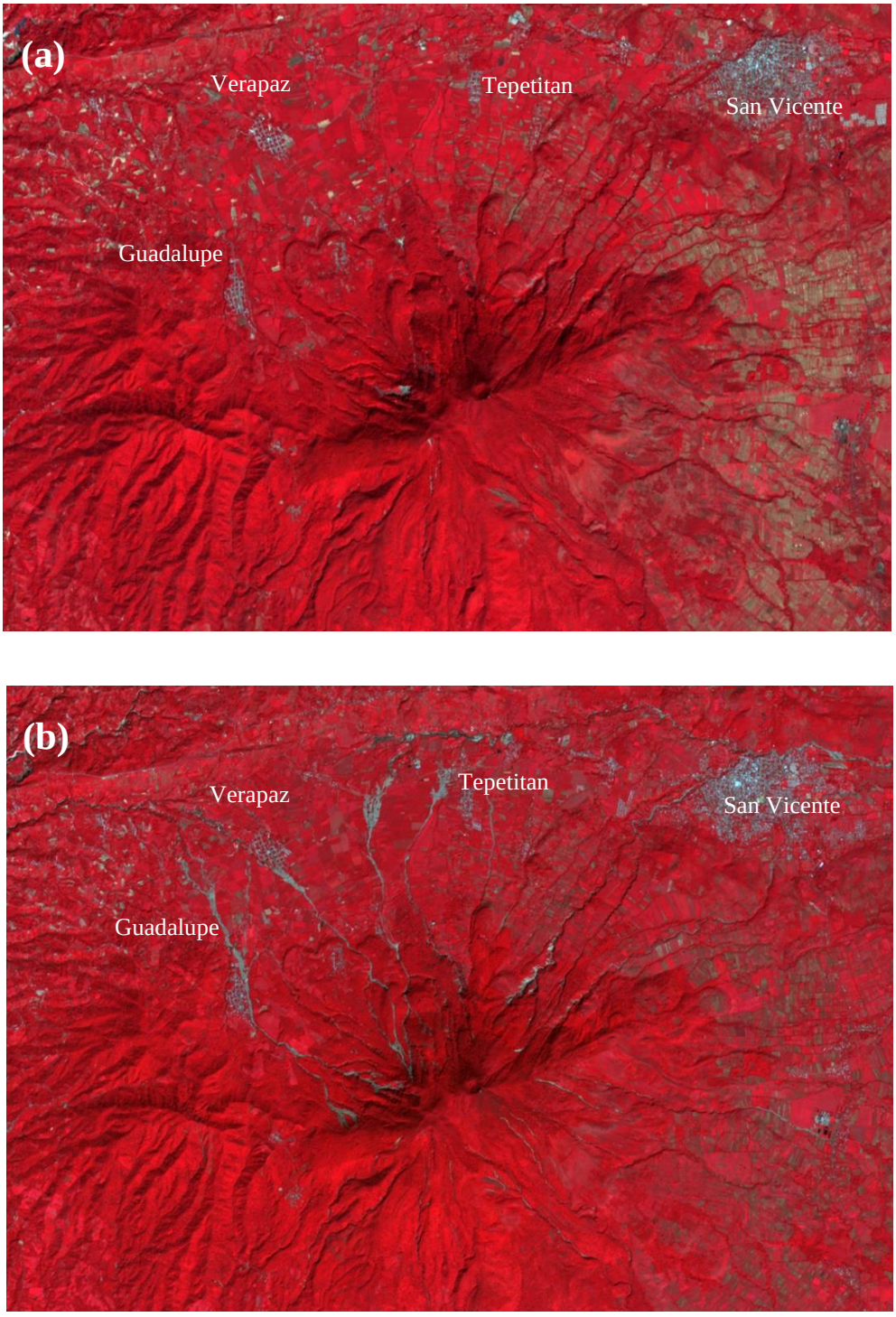

Figure 3.3 - These two false color images generated by the ASTER on NASA's TERRA show the area under examination before (**a**) and after (**b**) the event of 7th and 8th November 2009. The images were prepared with artificial colors to distinguish the vegetation (in red) from the bare ground (in grey). Based on data from the NASA/GSFC/METI/ERSDAC/JAROS, and U.S./Japan ASTER Science Team, NASA Earth Observatory image by Robert Simmon *https://earthobservatory.nasa.gov/images/41365/landslides-on-volcan-de-san-vicente*.

The government is increasingly accepting the importance of preventing these phenomena, which will continue to manifest due to the geographical context. In fact, between the 10th and 11th of October 2022, El Salvador, Guatemala and Nicaragua were affected by *Hurricane Julia*, which started as a *category one hurricane* with winds higher than 140 km/h. The event gradually decreased its speed to 65 km/h near Nicaragua, when it was downgraded to a *tropical storm event*. This event was able to cause numerous fatalities in the affected countries and numerous debris flows. The civil protection authorities of Guatemala have reported the loss of at least thirteen people, four missing and eleven injured due to the gravitational and flooding phenomena that occurred following the rains. The government of El Salvador, now habituated to events of this intensity that manifest with short return times, has trained 19,000 people (including soldiers, police, firefighters, tactical operative teams, rescue teams and employees of the MOP (Ministry Public Work of El Salvador) and the DOM (National Directorate of Public Works)) to: build barricades and temporary tents to accommodate refugees and evacuated people in areas less susceptible to landslides and floods, save people at risk, avoid displacement of people and raise awareness of the inhabitants. Ambulances were also set up to bring up to 1,000 people to the nearest hospital at the same time. The government also provided early warning to limit the damage as much as possible. Unfortunately, despite this operational framework, El Salvador has reported the deaths of ten people, including five soldiers who expired after a wall collapsed where the refugees were, while they did their defence work. However, without these proceedings, the victims and the damage would certainly have been more significant, consistent with those following the previous extreme events.

Due to the continuous occurrence of these hazardous events, the country must continue to increase the efficiency of the production of susceptibility maps from landslides, monitoring systems and development of emergency plans. All these tools must be used for risk mitigation.

3.2. Earthquakes

An earthquake is a natural process with a high destructive potential, which frequently causes considerable economic damage due to damage to buildings and infrastructure but, above all, loss of life. However, some processes resulting from the earthquake, such as landslides (earthquake-induction landslides), can be even more destructive than the seismic phenomenon. That is due to the passage of the mechanical waves through the lithologies, which takes place through a transfer of forces. As a result, the waves passing through lithologies close to the collapse conditions, increase the value of tangential forces and/or increase neutral pressures, resulting in a decrease in effective stresses and shear strength of the material, thus triggering the landslide phenomena.

Landslides usually occur during or shortly after a seismic event and have different spatial distributions according to slope gradient, lithology, earthquake magnitude and hypocentral and epicentral distances (Agnesi et al., 1982, 1983; Carrara, 1986).

Research shows a correlation between earthquake intensity and landslide occurrence; Keefer (1984) identified a critical Richter Magnitude of 4.0 and observed that the area affected by gravitational phenomena grows progressively up to 500,000 km^2 for an earthquake having a magnitude of 9.2.

In fact, Keefer, in 1984, considered 40 historical earthquakes chosen to sample many climatic, geologic, and seismic settings in Earth's major seismic regions. These earthquakes, which have magnitudes from 5.2 to 9.5, occurred between 1811 and 1980 that triggered thousands of landslides grouped by kinematics: falls, slides and lateral spreading. Keefer did not take into account the lithology involved in landslides. Thirty years later, Martino et al. (2014) used the Italian Database of co-seismic instability phenomena to compare Keefer's study worldwide with the recent one. They considered 166 earthquakes over the 1908-2012 period to reduce the scatter in data. They did not group the landslides by kinematics but considered the lithologies involved. They examined a minimal number of volcanic rocks. They all traced curves in a graph (Fig. 3.4) where on the abscissa there is the Magnitude of the considered earthquakes and on the ordinates the maximum distance of the landslides

from the source (that is, the maximum epicentral distance). From these graphs, it can be pointed out that Keefer's curves are all higher than Martino's one.

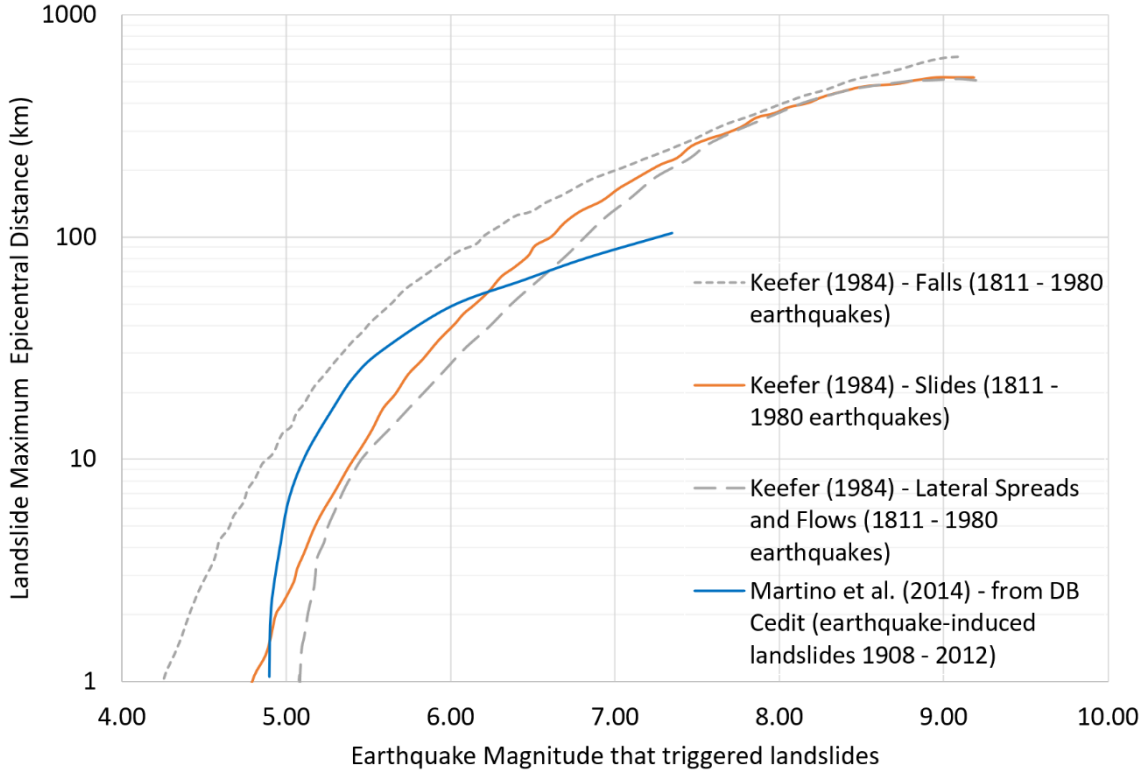

Figure 3.4 – The curves produced by Keefer (1984) and Martino et al. (2014) show the relationship between the maximum distance for the manifestation of gravitational phenomena and the Magnitude.

However, these correlations may present exceptions. A landslide indeed could be initiated even by a weak shaking if the failure of a slope is imminent before the seismic event or if the involved material includes weakly cemented and/or incoherent rocks. Volcanic rocks, widely distributed across the country, are among these lithologies, as they are usually characterized by higher mobility than non-volcanic rocks due to differences in material properties such as granularity, collapsibility and water content (Legros, 2002; Hayashi and Self, 1992). These geological conditions can significantly increase the frequency of gravitational phenomena triggered and the areas affected by landslides compared to areas that experienced comparable magnitudes (Bommer et al., 2002; Jibson et al., 2004).

The complex geodynamic context in which El Salvador is located (convergent structure characterized by the interaction between the Cocos Plate and the Caribbean Plate), added to the lithological characteristics of the outcropping rocks (e.g., ignimbrites, acid and basic effusive rocks, acid pyroclastites and volcanic ash) create a situation in which high-magnitude seismic phenomena occur, causing thousands of gravitational phenomena and resulting in many fatalities and enormous economic damage.

During the last century, many seismic phenomena have been manifested (Table 3.1), and the number of victims has been different in relation to the Magnitude, the hypocentral depth and the distance of the epicenter from the main inhabited centres.

Table 3.1 – Major seismic phenomena (M > 5.7) that have occurred in El Salvador since 1917.

Data (Y/M/D)	**M_w**	**Fatalities**
2001-02-13	6.6	315
2001-01-13	7.7	944
1986-10-10	5.7	3,000
1982-06-19	7.2	43
1965-05-03	6.5	125
1951-05-06	6.2	400
1936-12-19	6.1	200
1919-04-28	5.9	100
1917-06-07	6.5	1,050

The continuous uncontrolled increase of the suburbs of the cities, with structures often inadequate to withstand seismic shocks, has raised the number of casualties. This data can be seen from the correlation between increased mortality trends in seismic events and the growth in the size of population centres by comparing several aerial and satellite photos of the last forty years.

Bommer et al. (2002) report that the country is experiencing earthquakes from two major seismic sources. The first source of seismicity originates deep earthquakes in the Benioff-Wadati zones of the subducted Cocos plate beneath the Caribbean plate, characterized by relatively high magnitude values (surface wave magnitude Ms and moment magnitude Mw often with values > 6.0), capable of involving large areas of El Salvador. The territory is also geologically influenced by the interaction of the tectonic plates of the

Pacific and North America; however, the main seismic activity has been interpreted as the result of activity driven by the convergence between the Cocos and Caribbean plates (White, 1993).

Numerous seismic phenomena with this genesis were witnessed in the last century; many were particularly destructive and dramatically impacted the country. Among them, the September 1915 event, Ms 7.8, caused destruction in the country's western area, while the earthquake of Ms 7.3 occurred in June 1982 caused 49 victims and hundreds of earthquake-induced landslides. The last seismic event belonging to this seismic source was the event that took place on 13th January 2001, in which the country was hit by a violent earthquake, belonging to the first source of seismicity, at a depth of 60 km with 7.7 Mw. This event caused thousands of gravitational phenomena, causing 844 fatalities and 5,565 injured, with the destruction of over 100,000 buildings. Besides the difference in magnitude values, the discrepancies in damage and fatalities between this event and the one of 1982 are only in the increase of the elements at risk, which has led to an expansion of the neighbourhoods, which continued to increase more towards the flanks of volcanoes, as witnessed by the difference between the urban areas in the topographical maps of the country dating back to the year 1981 and aerial photos of 2010.

The second source of seismicity is a zone of upper-crustal earthquakes that coincides with the volcanoes array, orientated WNW-ESE (Bommer et al., 2002); these intraplaque earthquakes occur at relatively lower hypocentral depths. Since the main Salvadoran cities are located just along the volcanoes' alignment, it is not hard to figure out the catastrophic consequences of the seismic events that can occur, often with more significant damage than seismic phenomena with genesis in Benioff-Wadati zones. Among the most significant events in the last century with this genesis, there are the earthquake of 8th June 1917 (Ms 6.7), which caused 101 victims, the 20th December 1936 (Ms 6.1) event that resulted in more than 200 victims and the 10th October 1986 event (Ms 7.5), which caused more than 1,500 fatalities. On 13th February 2001, El Salvador experienced a further intense earthquake,

which more destroyed the country. This event, belonging to the second source of seismicity, was of 6.6 Mw, with a hypocentre placed at 10 km depth, resulting in 315 fatalities and 3,399 injured caused by ground-shaking and landslides (Fig. 3.5). Nearly 45,000 homes were destroyed and 16,000 seriously damaged. This earthquake affected areas comparable to those affected by the 1936 event, with the same genesis. Once again, the increased risk factors have led to more damage and victims.

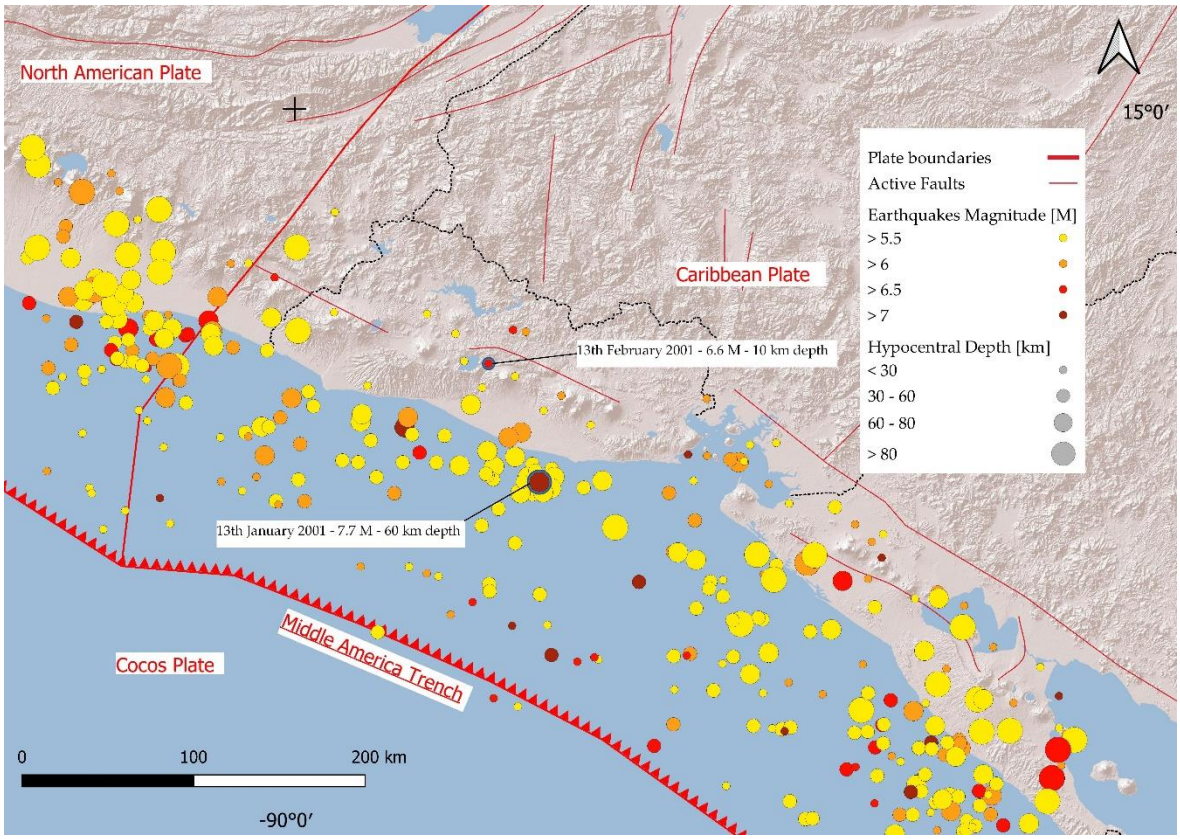

Figure 3.5 – Major seismic phenomena of the last century including January and February 2001 events.

There are several doubts about whether these two seismic sources are related. However, Lomnitz et al. (2001) and Bommer et al. (2002) reported that normal faulting subduction earthquakes in Central America tend to be followed by either large thrust events or shallow intraplate events within four years. This trend can also be observed in El Salvador, where earthquakes belonging to the second type of seismic genesis have occurred even after a month, as in the case of the earthquakes of 2001.

To mention additional examples of this trend, Bommer et al. (2002) cite 1915 subduction earthquakes, 1932 and 1982, followed by 1917, 1936 and 1986 intra-crustal earthquakes, respectively.

Because of the destructive power of these phenomena, in order to mitigate the risk, it is necessary, also for this type of phenomenon, to foresee the regions where landslides are most likely to take place, concerning what has happened in the past. This information is given from the landslide susceptibility analysis.

3.3. Susceptibility studies in El Salvador

In El Salvador, studies on landslide risks and susceptibility analysis are relatively recent. Indeed, the National Government and the local authorities did not investigate this issue during the whole period of the civil war, which took place between 1980 and 1992. With the end of this event, the continuous occurrence, with short return times, of extreme events of rainfalls, together with the continuous scientific progress of the 90s, led to the foundation by the Government of the SNET (Servicio Nacional de Estudios Terriroriales), an institution dedicated to the analysis of the country's natural risks. After an initial phase, in which only possible scenarios of future eruptions by the many active volcanoes were analyzed, the events of extreme rainfall that occurred in the late 1990s and the destructive seismic phenomena of 13th January and 13th February of 2001 have shifted the focus to the scenarios of susceptibility, danger and risk associated with seismic shocks and correlated earthquake-induced landslides. As a result of these destructive earthquakes, scientific studies were carried out (Bommer et al., 2002, Jibson et al., 2004, Evans et al., 2004; Bent et al., 2004; Rolo et al. 2004) that perfectly reported the damage associated with the seismic events and the earthquake-induction landslides triggered as a consequence. These works have been constructive from the perspective of post-event reports, also showing the lithologies more affected by gravitational phenomena. However, they do not present the inventory of all the manifested gravitational phenomena, showing only a limited number of the present ones by

analyzing only the most affected areas and the more significant gravity phenomena within them.

The first approach to the risk associated with these phenomena was carried out by Major et al. (2004), in which the debris flows hazard near the volcanoes of San Salvador, San Vicente and San Miguel were investigated due to their high probability of triggering landslides that could reach the inhabited centres. This study was carried out through conoid analysis to estimate the average volume of debris flows that could trigger in the future, thus generating a susceptibility map.

In 2004, some Central American civil protection authorities, including MARN (Ministerio de Medio Ambiente y Recursos Naturales), located in El Salvador, used the Mora-Vahrson heuristic method (1994). That classifies the risks of landslides in seismically active tropical areas. The model receives five input factors divided into two groups: susceptibility by passive elements (slope, lithology, soil moisture) and susceptibility by active elements (seismic intensity and rainfall intensity). For each factor, an inflation index is defined for a given site and, when combined with a specific weight, a relative threat level is obtained through multiplication and summation of the indices. The efficiency of the methodology is confirmed by some studies (Castillo et al., 2011; Quesada and Feoli-Boraschi, 2018); however, the authors recommend that this methodology be applied on a scale not larger than 1:50,000 due to the difficulty of obtaining detailed information from lithology, altitude and meteorology. This method does not use inventories.

Further studies on the susceptibility and hazard of landslides in El Salvador include Garcia Rodriguez et al. (2008, 2010) evaluated the probability of occurrence of earthquake-induced landslides at the regional scale, using Multivariate Logistic Regression (MLR) and Artificial Neural Network (ANN) technique using the retro-propagation learning algorithm. These studies were carried out by grouping the seismic phenomena of January and February 2001 in a single landslides inventory, mapping phenomena through polygons and using a spatial resolution of 100-m pixels for both dependent and independent variables, conditioned by the resolution of the input data. The results obtained in the Receiver Operating

Characteristics (ROC) curves show a high concordance, with values close to 1, testifying to near perfection of the model's performance, showing a high concordance between the inventory of landslides and the area estimated high susceptibility. However, the lack of validation on a dataset of earthquake-induced events provides issues, making the work impossible to confirm. In fact, in prediction modelling, the essential component is to validate the prediction results (Chung and Fabbri, 2003); without this, the prediction model and image have hardly any scientific significance.

A study by Kopačková and Šebesta (2007) was also conducted to generate a susceptibility map from landslides. In this case, a rainfall-induced susceptibility map was produced following the generation of an inventory of 363 landslides in an area affected by Hurricane Mitch in 1998. That was obtained by multivariate analysis using rasters extrapolated from a DEM, a geological map of the study area, and a land use map. Also in this specific case, a percentage of the dataset was not used for validation, making the work of low validity.

Recently, thanks to international cooperation projects that have led to a collaboration with the MARN by the University of Palermo (RIESCA and CASTES project), studies have been carried out on the susceptibility of landslides induced as a result of both extreme and not extreme phenomena but still destructive. Among these, the work of Rotigliano et al. (2018), in which maps of landslide susceptibility are made with both BLR and MARS in the Ilopango Caldera area, showed a better predictive ability for debris flow phenomena for the latter technique, although the first was the one most used for the purposes until then. In addition, Rotigliano et al. (2019) also studied two different rainfall-induced landslides events, both on Ilopango, studying predictive performances using a dataset of landslides generated by a non-extreme rainfall event of 2003 and validating it with an inventory of landslides generated by the extreme event generated by the combination of the Hurricane Ida and the low-pressure system event 96E of 2009 and vice versa (thus using forward and backward chrono-validations, in addition to self-validation models), showing that all of the

tested models produced broadly acceptable AUC values, even as a loss in the predictive performance from self-validation to chrono-validation was observed.

The work presented in Chapter 4, extracted and re-elaborated from an article by Mercurio et al. (2021) published in the Earth journal (MDPI) (https://doi.org/10.3390/earth2010005), produced a susceptibility map from rainfall-induced landslides in the San Vicente volcano area following the 2009 Ida/96E event.

In work presented in Chapter 5, the susceptibility from earthquake-induced landslide is carried out using earthquake- and rainfall-induction inventories with different types of predictive variables, both static (categorical and continuous), which can be used both for the analysis of the susceptibility of the landslide-induced and earthquake-induced, if the predisposing factors are considered as the same for both types of triggers, together with the use of variables that can only be used for this type of triggers, such as Peak Ground Accelerations and epicentral distances.

Chapter 6 presents an analysis of earthquake-induced landslide susceptibility using an inventory generated by rainfall-induction events and static and dynamic predictive variables.

4. Mapping susceptibility to debris flows triggered by tropical storms: a case study of the San Vicente Volcano area

Chapter constructed from: Mapping Susceptibility to Debris Flows Triggered by Tropical Storms: A Case Study of the San Vicente Volcano Area (El Salvador, CA) - Mercurio, C.; Martinello, C.; Rotigliano, E.; Argueta-Platero, A.A.; Reyes-Martínez, M.E.; Rivera-Ayala, J.Y.; Conoscenti, C. [https://doi.org/10.3390/earth2010005] – published on "Earth" MDPI journal.

4.1. Introduction

In El Salvador, landslides are among the most destructive natural processes, capable of causing fatalities and destruction. Among the possible triggers, these can manifest as a response to extreme rainfall events. In this study, an inventory of landslides that occurred in San Vicente (central sector of El Salvador) were prepared, following a combination of events that hit El Salvador in November 2009, when most of the country was hit by the passage of Hurricane Ida and low-pressure system 96E event. Most of the landslides that occurred in this sector can be classified as debris flows (Chapter 2.2.7). Following heavy rains, these phenomena can reach high velocities that may further increase if different debris flows can flow into the same channel. The deposition fan is often located at the base of the slope but can also reach several kilometres from it. For this reason, this type of landslide is extremely hazardous in the San Vicente area, where the base of the volcano slopes is densely populated and crossed by major transportation routes.

This work aims to predict the spatial distribution of the landslides that occurred in the San Vicente area by using the MARS statistical modelling technique (Friedman, 1991) to generate a landslide susceptibility map. The model's performance will be evaluated by using confusion matrices and also preparing ROC curves and analyzing the values of the resulting AUC.

4.2. Materials and Methods

4.2.1. Study Area

The study area, which extends for 287 km^2, is located along the slopes of the San Vicente Volcano, El Salvador (Figure 4.1).

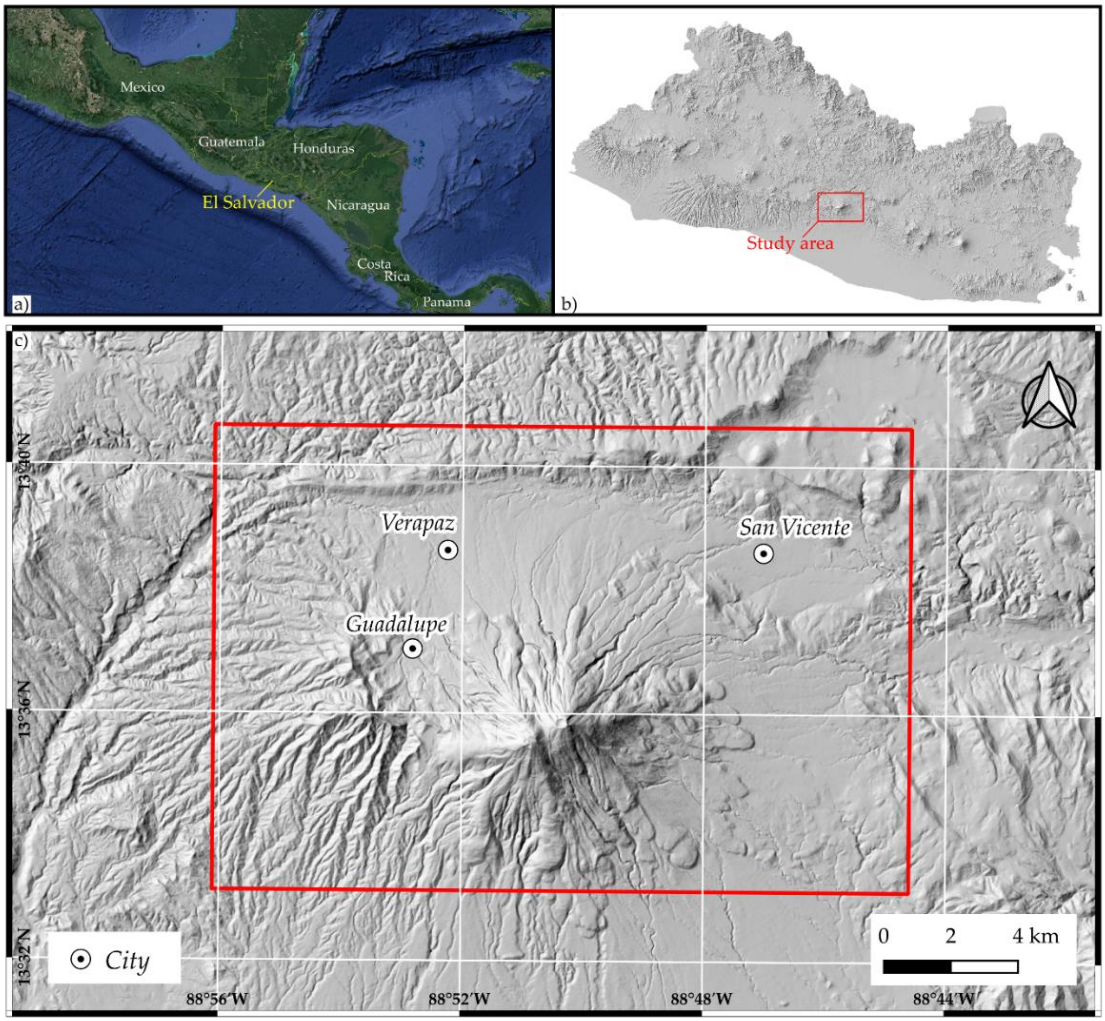

Figure 4.1. Location of the study area. This is located in the central sector of El Salvador, Central America (**a**); within the area under study (**b**) there are three towns: Guadalupe, Verapaz and San Vicente (**c**).

The San Vicente volcano, also known as *Chichontepec* (in the indigenous language *nahuat* it means "the mountain of the two breasts" for its double summit), is one of the twenty-two volcanoes of the volcanic arc of El Salvador and is situated next to the town of San Vicente (hence the name), located about 50 km east of the capital city San Salvador. This composite stratovolcano is the second-highest volcano (2,182 m) and one of the most

significant volcanos in the country (also with San Salvador, San Miguel, Ilopango, Santa Ana, Izalco and Conchaguita).

Although San Vicente has not erupted in the past 1,700 years, powerful hot springs and geothermal developments located on the volcano's north side suggest that past eruptions are youthful enough and that the volcanic system maintains residual heat from magmatic sources. Thus, the volcano should be considered active and likely to erupt again (Major, 2001).

Predicting the style of future eruptions is difficult due to poorly known eruptive history; however, based on past eruptive activity, future eruptions might involve the emplacement of lava flows and the growth and collapse of small-volume lava domes. In addition, the collapse of lava domes might generate pyroclastic flows and surges that might travel several kilometres over the volcano’s base.

However, possible future eruptions do not represent the main problem of the volcano, as the main current risk in the area is given by the manifestation of massive debris flows.

Due to a tropical-humid climate regime, with an average annual rainfall of about 1,500 mm and average annual temperatures between 21°C and 32°C, the slopes of San Vicente volcano experience intense physical-chemical degradation with consequent lowering of the level of cohesion of the rocks, also favoured by the pyroclastic and ashy nature of the outcropping materials. This climatic and geological setting favours the occurrence of numerous gravitational phenomena, such as debris flows, involving weathered pyroclastic materials which cover steep slopes. This type of landslides, which can destroy or damage everything in their paths through burial or impact, occurred many times in Central America, causing enormous economic damages and, above all, death. An example is that of 1934, in which an impressive debris flow on the north side of San Vicente destroyed the village of Tepetitan (Major, 2001).

4.2.2. Mapping strategy

Mapping the landslides triggered by heavy rainfalls in a tropical area, where vegetation recovers rapidly, such as that of San Vicente, requires aerial/satellite images taken not long after the event. The landslides archive used in this study was prepared by analyzing high-resolution remote sensing imagery dated 11/21/2009 (mm/dd/yyyy), thus only two weeks after the combined action of Hurricane Ida and 96E low-pressure system, and freely available in Google Earth. Each slope failure was identified through a Landslide Identification Point (LIP; (Costanzo et al., 2014)), located at the highest point of the landslide crown line.

4.2.3. Environmental variables

As seen in Chapter 2.6, landslide susceptibility zoning requires adopting a mapping unit technique, which allows dividing the study area into portions with specific properties and distinguishing each unit from adjacent ones according to clear and definable boundaries (Guzzetti et al., 1999). In this study, grid cells were used as mapping units. These divide the territory into regular squares of predefined size and are usually preferred when working with raster data. The size of the cells was set to 10 m, based on the horizontal resolution of the available Digital Elevation Model (DEM), which was employed to derive most of the predictor variables. This resolution of the input data has been demonstrated to produce landslide susceptibility models with good predictive performance (Cama et al., 2016). For all the selected independent variables, a value or a category was assigned to each cell. As regards the dependent variable, which reflects the presence or absence of a LIP within a mapping unit, a binary value was given to each cell (0: absence; 1: presence).

In this study, ten environmental attributes were selected as predictive variables of the mapped landslides, based on their presumed influence on the triggering mechanism and on the availability of data: GEO (lithology), USE (land use), LCL (landform classification), SLO (slope), ELE (elevation), PRC (profile curvature), PLC (plan curvature), TWI (topographic wetness index), NORTH (Northness), EAST (Eastness). All the variables, with

the exception of GEO and USE, were derived from the 10-m resolution raster DEM available for the area by using QGIS and SAGA GIS (Conrad et al., 2015) software. GEO, USE and LCL are categorical variables whereas all the others are continuous.

Geology (GEO) = The lithology layer was prepared on the basis a regional geological map at a scale of 1: 100,000 (Weber et al., 1975), which was modified and improved using field checks. The study area is characterized by seven lithological units that can be distinguished based on their different physic-chemical characteristics (Figure 4.2).

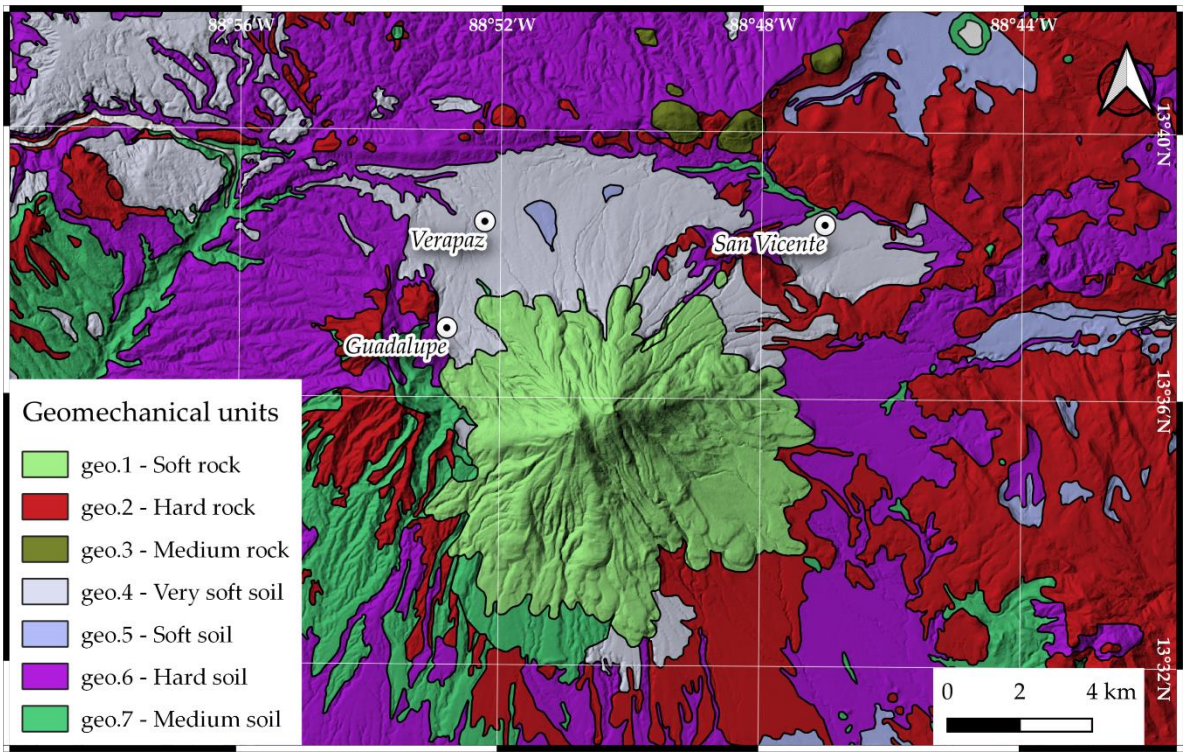

Figure 1.2 - Geological map of the study area.

In the area of the San Vicente volcano, the outcropping rocks are intermediate and basic effusive rocks with alternations of pyroclastites (geo.1). Moving eastward from the crater, large outcroppings of intermediate basic effusive rocks and subordinate pyroclastites (geo.3) can be observed, alternating with acid pyroclastic rocks, volcanic epiclastites and volcanic epiclastites and pyroclastites with locally effusive basic-intermediate rocks (geo.6 and geo.7) in the western sector of the area. In the northern sector, where the localities of San Vicente (north-eastern sector of the area), Guadalupe and Verapaz (north and north-

western sector) are located, there is a strong presence of acidic pyroclastites and subordinate volcanic epiclastites and effusive acid rocks, or lithologies belonging to the Tierra Blanca, a member of the San Salvador formation (geo.4). All these deposits are highly weathered and may favour the triggering of debris flows following extreme rainfall events.

As shown in Table 4.1, the lithology class with the most significant extent is that of hard soil, i.e. acid pyroclastic rocks and volcanic epiclastites; this class contains almost half of the identified landslides.

Table 4.1 - The seven lithological classes are shown with their corresponding descriptions and the percentage value of the presence of each class compared to the total area.

COD	TYPE	DESCRIPTION	% presence of the factor in the area
geo.1	Soft rocks	intermediate basic effusive rocks and subordinate pyroclastites	23.00%
geo.2	Hard rocks	intermediate basic effusive rocks and subordinate pyroclastites	20.84%
geo.3	Medium rocks	acid effusive and acid intermediate rocks	0.80%
geo.4	Very soft soil	Tierra Blanca: acidic pyroclastites and subordinate volcanic epiclastites and acid effusive rocks	17.25%
geo.5	Soft soil	Quaternary sedimentary deposits	0.91%
geo.6	Hard soil	acid pyroclastic rocks, volcanic epiclastites	29.77%
geo.7	Medium soil	volcanic epiclastites and pyroclastites, locally effusive basic-intermediate rocks	7.42%

Land use (USE) = The land use raster map includes eleven classes and was created by rasterizing the CORINE Land Cover shapefile, which was prepared by using satellite images dated 2002. Most of the investigated territory is characterized by crops of different natures, whereas only about 3% of the area is characterized by anthropogenic structures (Table 4.2).

Landform classification (LCL) = This variable was extracted by using an automated procedure that recognizes landforms on a gridded elevation distribution. Table 2 reveals that open slopes (lcl.5) are the most frequent class.

Table 4.2 - Percentage frequency distribution of land use (left) and landform classifications (right).

COD	TYPE	% presence of the factor	COD	TYPE	% presence of the factor
use.1	Urban areas	3.13%	lcl.0	Streams	4.86%
use.2	Woods	5.05%	lcl.1	Midslope drainages	7.88%
use.3	Annual crops	17.61%	lcl.2	Upland drainages	0.59%
use.4	Mixed crops	20.11%	lcl.3	Valleys	5.39%
use.5	Permanent crops	45.96%	lcl.4	Plains	18.21%
use.6	Wetlands	0.00%	lcl.5	Open slopes	42.47%
use.7	Mangroves	0.00%	lcl.6	Upper slopes	7.12%
use.8	Minings	0.00%	lcl.7	Local ridges	0.41%
use.9	Pastures	1.73%	lcl.8	Midslope ridges	8.98%
use.10	Rivers	0.24%	lcl.9	High ridges	4.08%
use.11	Shrub vegetations	6.18%			

Slope (SLO) = This variable represents the steepness of the ground measured as a percentage.

Elevation (ELE) = The altitude above sea level of each cell corresponds to the value of the DEM.

Profile curvature (PRC) = This variable reflects the geometry of the surface in the direction of the maximum incline of the slope. Positive cell values indicate an upward convexity of the surface, while negative values indicate a downward concavity; a value of 0 indicates the absence of concavity/convexity and, therefore, a constant slope steepness.

Plan curvature (PLC) = This variable reflects the curvature measured perpendicular to the direction of the maximum slope, thus reflecting the curvature along the contour lines. Positive and negative values indicate a convex and a concave surface, respectively, while a value of 0 indicates the absence of concavity/convexity at the cell along contour lines. Profile and plan curvature, which reflect flow acceleration/deceleration and flow convergence/divergence across the land surface, respectively, can also be used to identify areas of activation and propagation of landslides (Ohlmacher, 2007).

Topographic wetness index (TWI) = This variable is calculated as $\ln(A_s/\tan\beta)$, where A_s is the specific contributing area and β is the local slope angle. TWI should reflect soil saturation and, thus, is expected to control the spatial distribution of debris flows.

Northness (NORTH) and *Eastness (EAST)* = These two variables were computed by applying cosine and sine transformations of slope aspect expressed in radians. The slope aspect may influence the spatial distribution of landslides, as it can reflect the difference in exposure to solar radiation temperature, humidity and type and density of vegetation cover. Northness ranges between 1, if the aspect is north, and -1, if the aspect is south, with 0 associated to slopes facing east or west. Accordingly, eastness is in the range 1 (east) – -1 (west), with 0 indicating either north or south slope aspect.

Since the employed modelling technique requires excluding multicollinearity among covariates, the Variance Inflation Factor (VIF) was calculated for the selected continuous predictors. This metric allows measuring the degree of correlation between predictors. Predictors with VIF values equal to or higher than 10 indicate multicollinearity (Allison, 1999; Hair et al., 2010; Keith, 2014). VIF values were calculated by using the R package "usdm" (Naimi, 2015).

4.2.4. Modelling technique

Multivariate Adaptive Regression Splines (MARS; (Friedman, 1991)) was used as modelling technique of landslide susceptibility.

In this paper, MARS models were prepared by using the “earth” package (Milborrow, 2020) of the R software. The “evimp” function of the “earth” package was used to estimate the importance of each of the selected predictors (Rotigliano et al., 2019). This was evaluated according to the number of model subsets that include the variable or a category, in the case of categorical variables (i.e., GEO, USE, LCL). The higher the number is, the more significant the contribution of the variable/category is.

4.2.5. Calibration and validation of the models

In this work, MARS models were calibrated and validated by using different random samples extracted from the landslide archive (Chung and Fabbri, 2003). This approach requires that the random selection of learning and test samples is repeated many times, in order to assure that the validation results, and related conclusions, are not produced by chance. Estimating the variability of the model's performance allows for evaluating the robustness of the modelling approach, whereas the average values of the performance metrics can be employed to reveal the overall predictive ability. To this aim, 100 datasets were created by randomly selecting the 25% of positive cells (cells intersecting LIPs) and the same number of negative cells (cells not intersecting LIPs). Then, each of the 100 datasets was randomly divided into a training and a test group, both with the same number of positive and negative cells, containing 75 and 25% of the LIPs, respectively. Finally, a MARS model was calibrated and validated on each of the datasets, thus obtaining 100 measures of the model's performance.

The predictive skill of the models was evaluated by preparing, for each of the 100 models' run, a ROC curve and by calculating the AUC curve. In order to evaluate the model's performance by using also cut-off dependent metrics, an optimal cut-off value for the 100 ROC curves was calculated by using Youden's index (J) (Youden, 1950; Cama et al., 2017; Rotigliano et al., 2019; Conoscenti et al., 2020).

4.2.6. Landslide susceptibility map

The 100 MARS replicates allowed to calculate for each of the cells of the study area an average value of probability of debris flow occurrence. These values, which vary in the range between 0 and 1, were classified into four levels (low, moderate, high and very high) and employed to produce a final debris-flow landslide susceptibility map. The optimal cut-off value J was used as a limit between moderate and high susceptibility levels. Two other Youden's indexes, J_{low} and J_{high}, calculated for the cells with probability lower and higher

than *J*, respectively, were employed to separate low/moderate and high/very high susceptibility levels.

4.3. Results

4.3.1. Landslide inventory

The visual analysis of the Google Earth images dated 11/21/2009 and available for the study area allowed to identify of 5,609 LIPs relative to the debris flows triggered by the paroxysmal event that happened on 7th and 8th November 2009 (Figure 4.3).

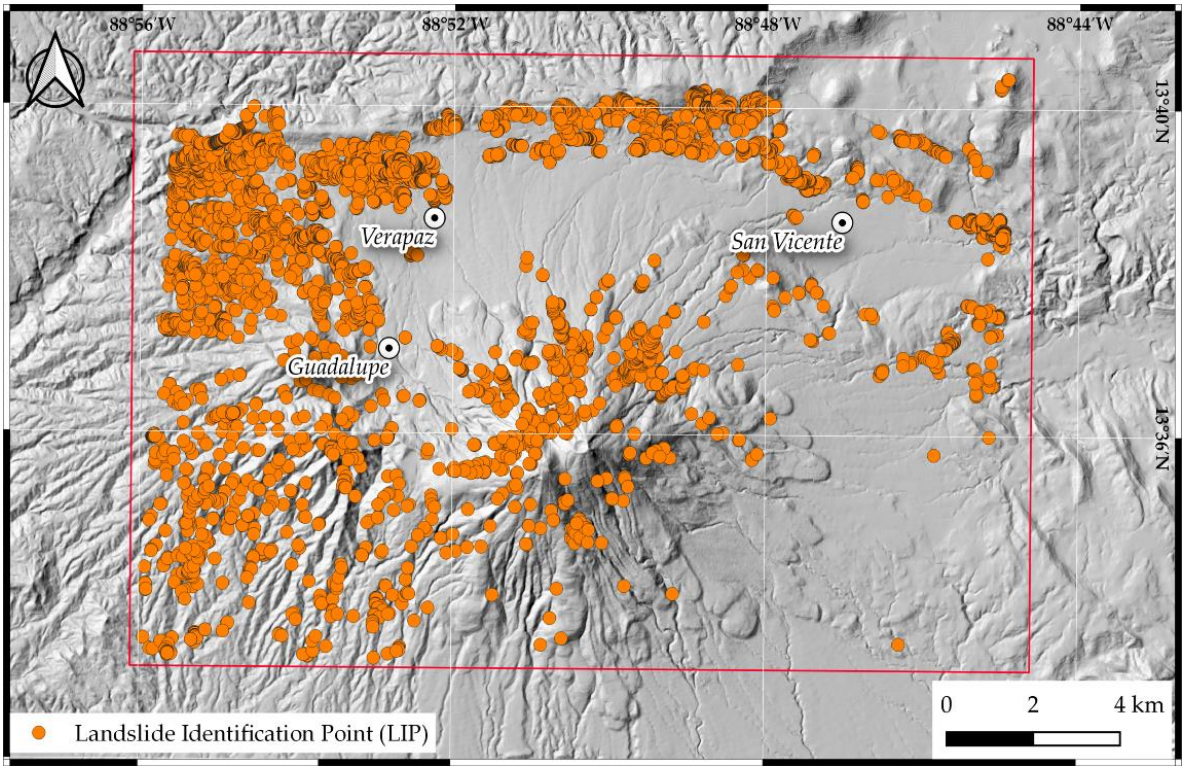

Figure 4.3 - Map of the 5,609 LIPs identified in the study area.

LIPs are mainly located in the study area's northern, western, and north-western sectors, as well as in the slopes of the San Vicente volcano. Almost half (i.e., 2,753) of the LIPs are located over the hard soil unit (Figure 4.4), which includes acid pyroclastic rocks and volcanic epiclastites, is the class with the greatest areal extension (Table 4.1). The second highest frequency of LIPs (i.e., 979) is observed for the Tierra Blanca unit, which includes acidic pyroclastites and subordinate volcanic epiclastites and acid effusive rocks.

The class geo.1 (intermediate basic effusive rocks and subordinate pyroclastites), which is the second largest lithological unit, hosts 612 LIPs, representing around 11% of the LIPs' inventory.

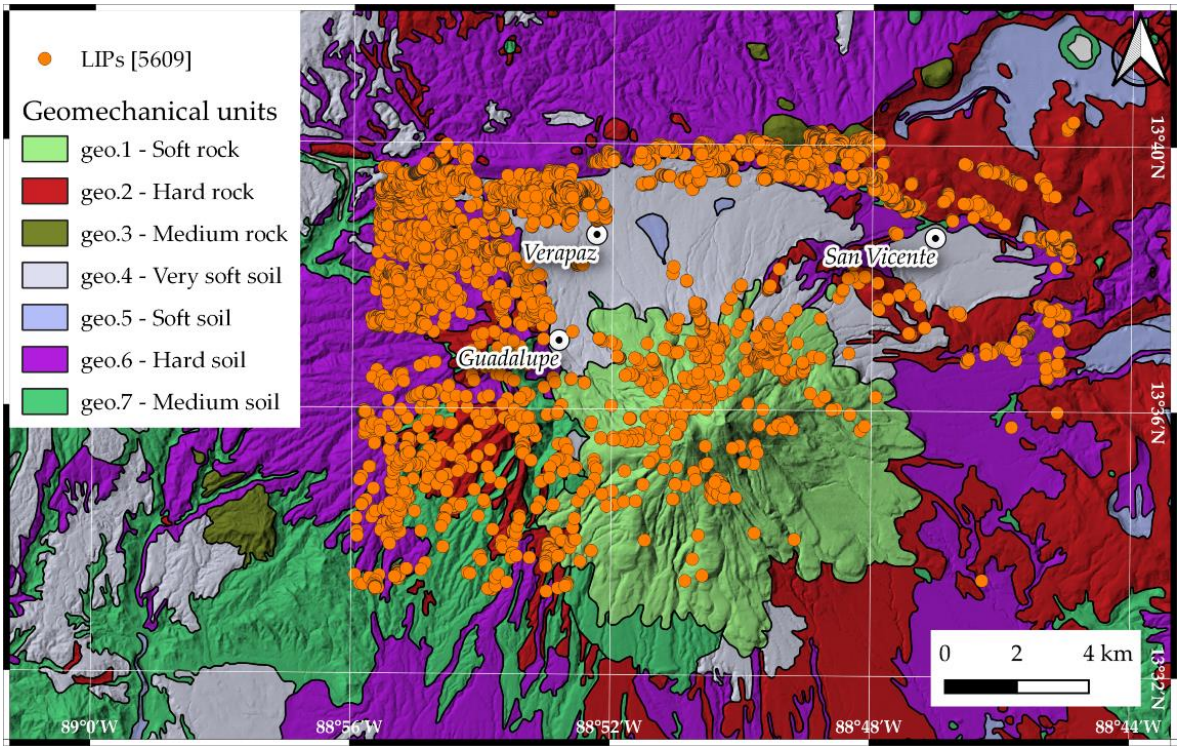

Figure 4.4 - Spatial distribution of the 5,609 LIPs over the lithological map.

Figure 4.5 shows the relative frequency distributions [%] of the selected predictors calculated over the entire study area and only on the pixels intersecting one or more LIPs (i.e. positive pixels). Different distributions of a predictor observed in the entire area and where LIPs occur are expected to indicate a relationship between the spatial variability of that predictor and the LIPs' positions. On the other hand, similar distributions should suggest no correlation between predictor and target variable. The distributions of elevation share the same centre but that observed on positive pixels is clearly less dispersed, indicating that pixels in the range 500–600 m asl are more likely to host a LIP. The slope frequency distribution observed on positive pixels is centred at a higher steepness than that observed on the entire area, reflecting that debris flows are more likely to start on pixels with slope angle between 10° and 30°. Frequency distributions of northness and eastness reflect the

distribution of the LIPs over the study area (Figure 4.5), which occur more frequently on slopes facing east and north. Frequency distributions of plan and profile curvature calculated on the entire dataset and on positive pixels appear very similar, whereas those of TWI are differently skewed revealing that LIPs occur more frequently at low to moderate values and thus on the middle and upper portions of the slopes. Frequency distributions of USE and LCL show small to moderate differences, whereas those of GEO indicate that hard soil (geo.6) is the lithology class most prone to debris flows and soft (geo.1) and hard (geo.2) rocks are the most stable.

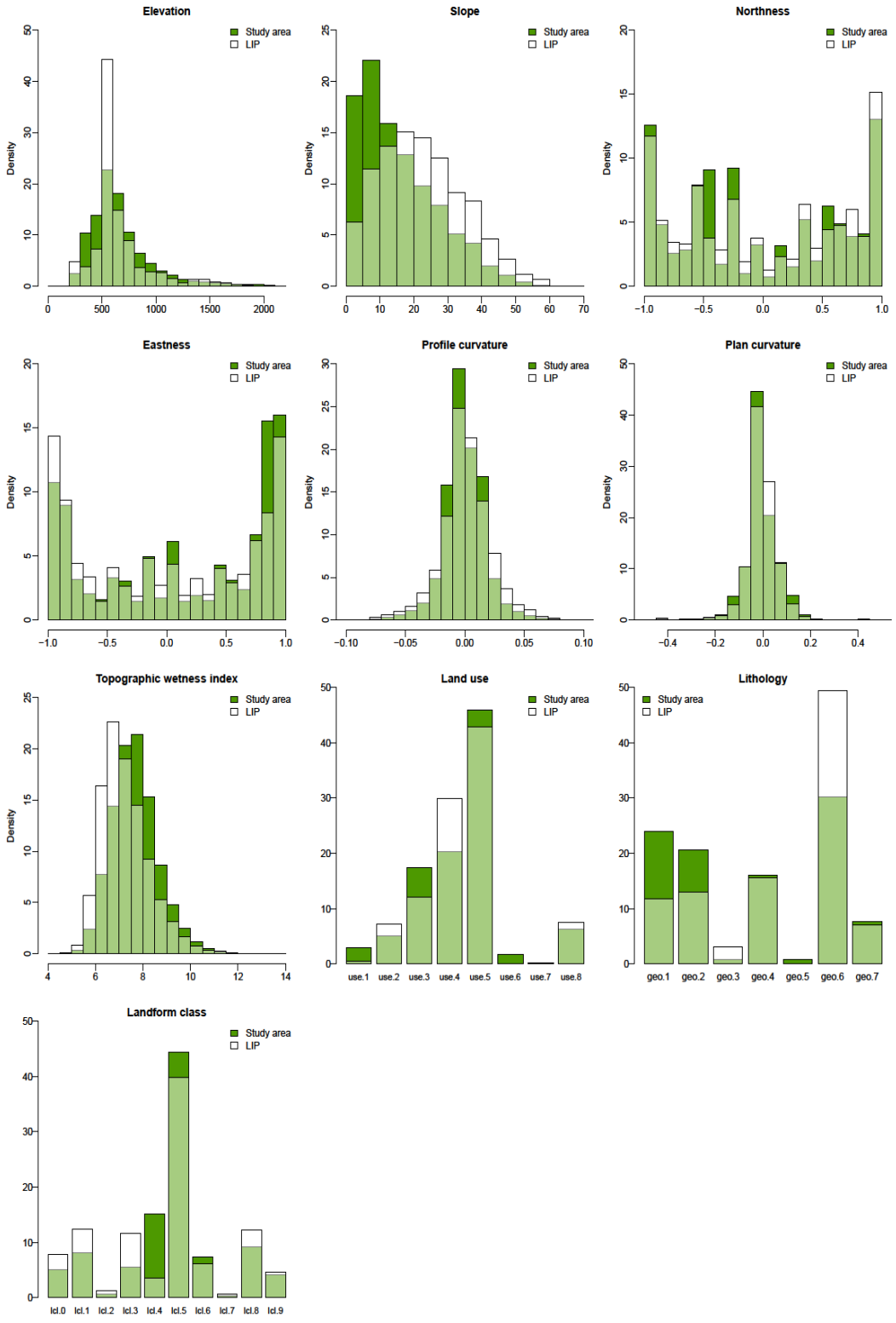

Figure 4.5 - Relative frequency distributions [%] of the selected predictors calculated over the entire study area and only on the pixels intersecting one or more LIPs.

4.3.2. Calibration and validation of the models

Calibration and validation of MARS models were performed by using all the selected environmental variables as predictors. The Variance Inflation Factor (VIF), indeed, which is below the threshold of ten for all the independent continuous variables, revealed no strong correlations among them (Table 4.3).

Table 4.3 - Variance Inflation Factor values calculated for the seven continuous variables.

VARIABLES	VIF
ELE	1.308
PLC	1.491
PRC	1.276
SLO	2.013
TWI	2.205
NORTH	1.003
EAST	1.035

The dataset employed to calibrate and validate the debris flows predictive models includes 2,794,399 pixels of 10 m, which cover the entire study area. 4,975 of these pixels host one or more LIPs and are classified as “positive cells”. The remaining 2,789,424 pixels are classified as “negative cells”. The first step of the validation procedure consisted in preparing 100 random samples, including 1,244 pixels (25% of the total positive cases) and the same number of negative cases. Then, each of the 100 samples was split into a training and a test subset, both balanced in terms of positive and negative cases and including 75% and 25% of the 1,244 pixels, respectively.

Figure 4.6 shows 100 ROC curves, each revealing the fit of a MARS model to a test subset, as well as the average ROC curve. The latter achieves an AUC value of 0.80, which reflects excellent predictive performance of the MARS models. Moreover, the standard deviation of the 100 AUC values, which is equal to 0.01, demonstrates the robustness of the procedure to changes of the learning and validation samples.

The average ROC curve was employed to calculate Youden’s index *J*, which is equal to 0.46 and represents the optimal cut-off value allowing to maximize of the sum of

sensitivity and specificity. This value was employed to calculate an average confusion matrix for all the 100 random samples of 2,488 pixels, with a 1:1 ratio of positive-to-negative instances, as well as for the entire dataset, which has a high prevalence of negative pixels (Table 4.4).

Table 4.4 - Validation results for the balanced and all-area MARS models.

MODELS	N° PIXELS	CUT-OFF	POSITIVE CASES	NEGATIVE CASES	TP	FP	TN	FN
Balanced	2,488	0.46	1,244	1,244	985	417	827	259
All-area	2,794,399	0.46	4,975	2,789,424	3,992	933,454	1,855,970	983
MODELS	**ACCURACY**	**SENSITIVITY**	**SPECIFICITY**	**PPV**	**NPV**	**AUC**		
Balanced	0.73	0.79	0.66	0.70	0.76	0.80		
All-area	0.67	0.80	0.67	0.00	0.99	0.81		

Sensitivity of the 100 model runs (balanced models) and that calculated for the average probability values computed for all the pixels of the area (all-area model) is 0.79 and 0.80, respectively, demonstrating a good predictive skill of event pixels; on the other hand, specificity values are 0.66 and 0.67, respectively, thus reflecting a lower ability of the MARS models to detect true negatives. The accuracy of the balanced models (0.73) is substantially higher than that achieved by the all-area model (0.67), due to the very high number of false positives (FP) predicted over the entire dataset. Positive predictive value (PPV) and negative predictive value (NPV), which are calculated as TP / (TP + FP) and TN / (TN + FN), are 0.70 and 0.76 for the balanced models, whereas they are 0.00 and 0.99 when computed on the entire study area. The values of PPV and NPV calculated for all-area model reflect the high number of FP and the high ratio of TN to FN, respectively.

The AUC value (0.80) achieved by the all-area model, also reported in Table 4.4, indicates, in accordance with the classification proposed by Hosmer and Lemeshow (Hosmer and Lemeshow, 2000), the excellent ability of the predictive model to discriminate between observed presences and absences.

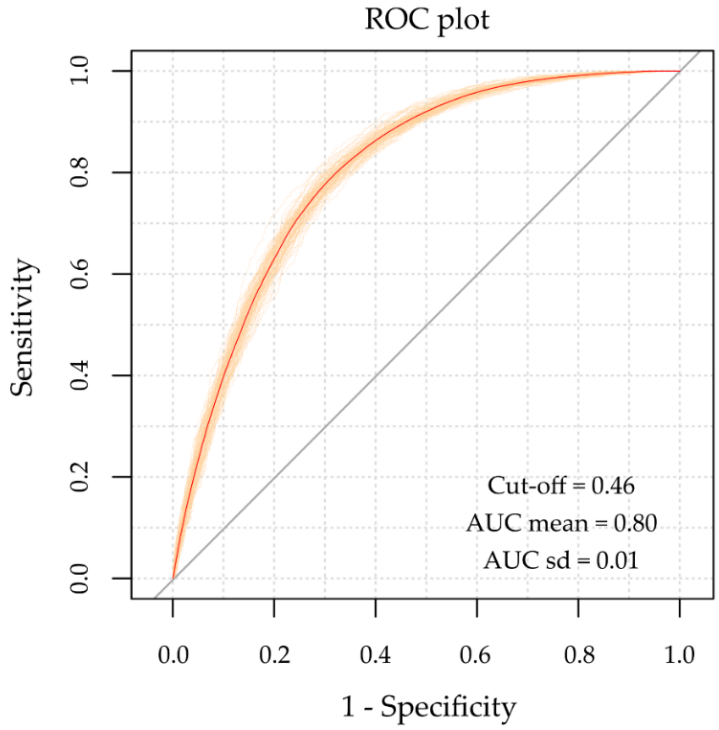

Figure 4.6 - ROC curves processed using the MARS method in the study area.

Figure 4.7 displays the relative importance of the predictor variables assessed by using the nsubsets criterion (Conoscenti et al., 2016; Rotigliano et al., 2019; Martinello et al., 2020). Slope is the most important independent variable, followed by three classes of GEO (i.e. geo.1, geo.2 and geo.7) and LCL (i.e. lcl.3, lcl.4 and lcl.5), and by ELE, which achieve a relative importance higher than 30%.

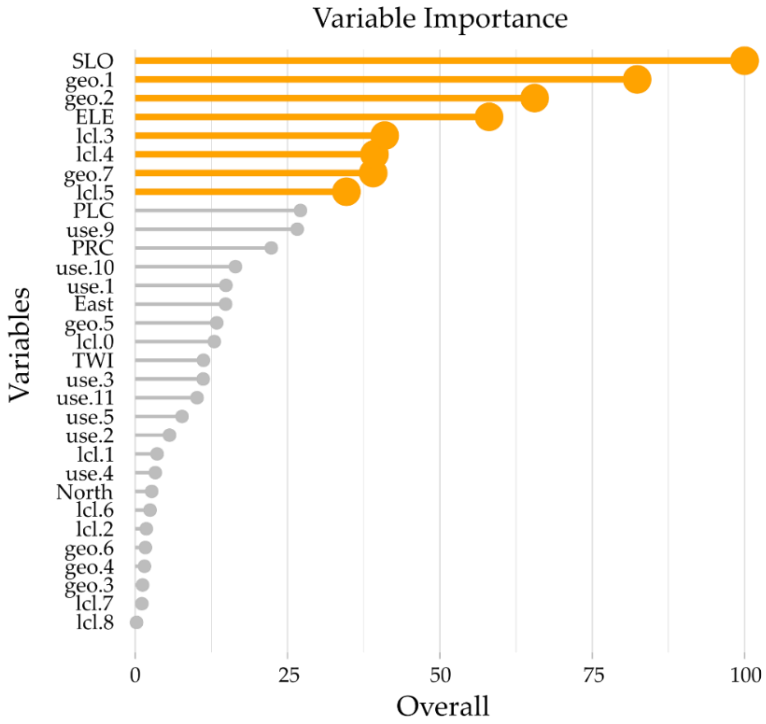

Figure 4.7 - Relative importance of the predictor variables. Thicker lines and bigger circles indicate importance higher than 30%.

4.3.3. Landslide susceptibility map

This results in the final debris flow susceptibility map, obtained by averaging the probability values calculated by the 100 MARS model runs for each of the 2,794,399 pixels of the study area. MARN and municipalities have provided this map, which now uses as cartography for susceptibility to rainfall-induced landslides for the municipalities of San Vicente, Verapaz and Guadalupe (Mendez Alfaro, 2022) (Fig. 4.8).

The map was created by classifying the probability values into four levels, according to the optimal cut-off value *J* (0.46) and the subsequent two different Youden's indexes (equal to 0.25 and 0.7, respectively) calculated to discriminate very low/low and high/very high susceptibility levels. The “degree of fit” between the susceptibility map and the spatial distribution of the LIPs is shown in Figure 4.9. The latter reveals that the frequency of the probability classes decreases from the lowest to the highest levels, whereas the frequency of LIPs shows an inverse trend achieving the highest value in the highest susceptibility class.

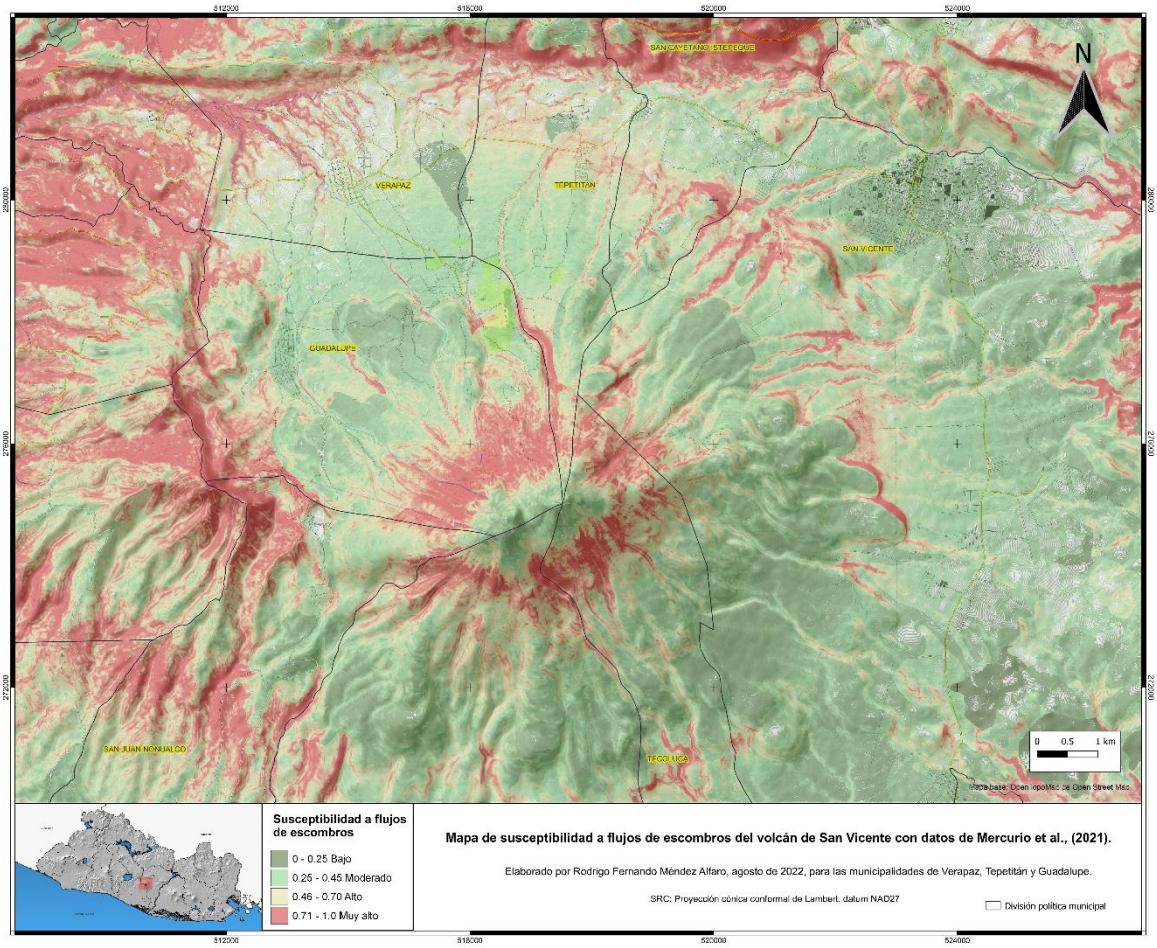

Figure 4.8 - Debris flows susceptibility map of the study area. Created by Mercurio et al. (2021) and modified from Mendez Alfaro (2022) and now used for the municipalities of Guadalupe, Verapaz and Tepetitan.

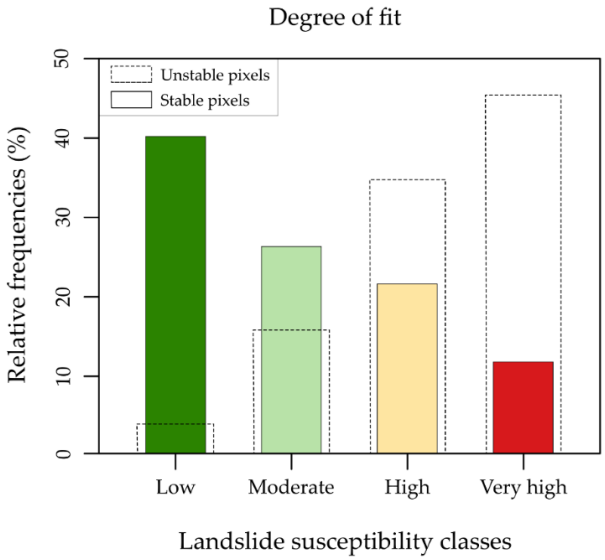

Figure 4.9 - Relative frequency distributions of the debris flow susceptibility levels (solid outline) and of the LIPs (dotted outlines) calculated for the four levels.

4.4. Discussion and Conclusions

In this experiment, susceptibility to debris flow initiation in the area of the San Vicente volcano was evaluated by preparing an inventory including thousands of landslides triggered by heavy rainfalls due to Hurricane Ida and the 96E low-pressure system (November 2009) and by modelling the relationship between the location of these landslides and the spatial variability of a set of environmental variables by using MARS as modelling technique.

The validation of the MARS models, which was performed on 100 random samples of pixels, revealed an overall excellent ability to predict the debris flows that occurred in the San Vicente area, as attested by an average AUC value equal to 0.80. Moreover, the very low standard deviation of AUC values (0.01) demonstrated the robustness of the modelling procedure, which achieved very similar performance when changing the learning and validation samples. The cut-off dependent metrics, which were calculated by applying Youden's index as a threshold to discriminate between pixels predicted as positives and negatives, revealed a different ability of the models to identify the event (sensitivity = 0.79) and stable (specificity = 0.66) cells. This difference in performance reflects a relatively low number of false negatives, on the one hand, and a high number of false positives on the other. The number of false positives increases proportionally when the model is applied to the entire study area (i.e. all-area model). This data indicates that the model tends to overestimate the susceptibility to debris flows in the area of San Vicente. However, it is worth noting that an excess of false positives constitutes a less serious prediction error than that due to a large number of false negatives. In fact, while landslides could occur in the future in pixels erroneously predicted as unstable, those pixels that have been considered stable and where landslides have occurred, constitute an irreversible error. Besides, in light of the geomorphological setting of the area and its high exposure to severe rainfall-triggering events, false positive cases are to be considered as potential future initiation points.

The ability of MARS to predict debris flow source sites in the San Vicente area is very similar to that measured in the Ilopango Caldera, El Salvador (Rotigliano et al., 2018, 2019), by using an inventory of landslides also triggered by Hurricane Ida and the 96E low-pressure

system (AUC = 0.81-0.82; Std. dev. = 0.006). The performance of MARS observed in this study is even slightly better than that evaluated by Vargas et al. (2019) in Mocoa (Colombia) with debris flows triggered by a heavy rainfall event, where the average AUC was 0.78, but with a very low standard deviation (0.007). As regards the threshold-dependent metrics, similar values of sensitivity (0.84) and specificity (0.66) were found in the area of the Ilopango Caldera by Rotigliano et al. (2018, 2019). The specificity values also found in these previous studies indicate that future research should address the issue of the high number of false positives generated by the MARS model.

The evaluation of the importance of the predictor variables revealed that slope angle (SLO) and elevation (ELE) are the most important continuous predictors, whereas, among the categorical variables, three classes of lithology (GEO) and landform classification (LCL) achieved a high relative importance (> 30%). The analysis of the importance of the variables, which was based on the nsubsets criterion, partially confirms what can be inferred from the comparison of the variables' relative frequency distributions observed on the entire area and on the positive pixels (Fig. 4.7). These distributions are, indeed, somewhat different for SLO and ELE, but also for TWI, EAST and NORTH, which instead exhibited low importance (< 20%). Based on the high density of LIPs, we would have expected high importance of the lithology category geo.6 (hard soil), whose relative contribution to the MARS models is, however, very low.

A strong relationship between landslide locations and slope angle variability and elevation was also found in other landslide susceptibility studies that employed MARS as modelling techniques (Rotigliano et al., 2018; Vargas-Cuervo et al., 2019). As regards the Ilopango Caldera area, Rotigliano et al. (2019) calculated high importance of elevation and terrain ruggedness index. The latter variable is usually strongly correlated with slope steepness; thus, it is possible to infer that the importance of the continuous predictors of debris flows is somewhat similar in the two areas of El Salvador. On the other hand, the analysis of the importance of the categorical variables revealed different results, as GEO and

LCL exhibited low importance in the Ilopango Caldera area, whereas a relatively strong relationship was found between some of the USE classes and the location of debris flows.

Based on the results obtained in this experiment, the following conclusions can be drawn for the area of San Vicente volcano:

- MARS is able to predict the locations of debris flows with excellent accuracy (AUC = 0.80) by using as predictors a set of environmental variables that can be extracted from available thematic maps and a DEM with 10-m horizontal resolution;
- The ability of MARS to predict the spatial distribution of debris flows is stable when changes of the learning and validation samples are performed (AUC Std. dev. = 0.01);
- The cut-off dependent metrics revealed that MARS models produce a large number of false positives and thus their ability to identify stable cells is moderate (specificity = 0.66);
- MARS exhibits in the San Vicente area the same predictive skill as that achieved in other study areas located in El Salvador and Colombia;
- MARS modelling revealed that slope angle, elevation, lithology and landform classification are the most important predictors of the debris flows that occurred in the study area.

The modelling procedure described in this paper allows for preparing debris flow susceptibility maps using data typically available on a large scale. These maps may help land planners and environmental agencies to adopt actions to mitigate landslide risk and avoid severe damages or even casualties caused by their occurrence in urbanized areas. At the same time, the obtained susceptibility model and map optimized for detecting the initiation points for future debris flow phenomena are the basis for the now-running step of this research aimed at implementing a propagation routing algorithm to produce a full predictive scenario.

5. Predicting earthquake-induced landslides by using a stochastic modelling approach which combines preparatory and triggering factors

Chapter constructed from: Predicting earthquake-induced landslides by using a stochastic modelling approach which combines preparatory and triggering factors: a case study of the coseismic landslides occurred on January and February 2001 in El Salvador – Mercurio, C., Martinello, C., Argueta-Platero, A. A., Azzara, G., Rotigliano, E., and Conoscenti, C (presented at 10th IAG International Conference on Geomorphology (ICG) https://doi.org/10.5194/icg2022-543, 2022a).

5.1. Introduction

On 13th January 2001, El Salvador was hit by an intense earthquake (M 7.7) which, both the soil shaking and the thousands of coseismic landslides generated, caused 844 fatalities, 5,565 injured and the destruction of over 100,000 buildings. The areas most affected by this seismic phenomenon correspond to the south-western and south-eastern sectors of the country (e.g., San Salvador, Santa Tecla, Comasagua, La Libertad and Usultan). The country, still injured by the seismic event, precisely a month later, on 13th February 2001, was affected by a further intense earthquake of M 6.6 which added fatalities and destruction in the country. This event caused 315 victims and thousands of gravitational phenomena in the central sector of El Salvador (Fig. 3.5, Chapter 3.2). Since the main population centres are located just along the volcanoes' alignment, the phenomenon has caused catastrophic consequences.

There are types of landslides that have a greater predisposition to earthquake-induction than others (Keefer; 1984); the minimum magnitude of activation depends, in addition to the lithological characteristics, also from the initial conditions of the involved slopes. In fact, if a specific area is in conditions close to instability, even a slight seismic event would be sufficient to generate a landslide. The gravitational phenomena triggered by the two earthquakes of 2001 caused devastating effects on the country, often affecting very intense seismic phenomena (twelve earthquakes above M 6.0 in the last century). Indeed, along the

Cordillera del Bálsamo, In Las Colinas and Las Barrioleas, two massive gravitational phenomena caused almost 1,000 deaths (Abate et al., 2014).

The main aim of this chapter is to evaluate the ability of rainfall- and earthquake-induced landslide susceptibility models to predict the geographical distribution of the coseismic slope failures that occurred in 2001 events. The experiment was performed in fourteen sectors of El Salvador, accounting for a total extent of 396.97 km^2. Eight of these sectors (91.85 km^2) were strongly hit by the January earthquake, whereas most of the landslides triggered by the February earthquake occurred in the other six sectors (305.72 km^2). The modelling strategy was based on both rainfall- and earthquake-triggered landslide susceptibility models. The first model was calibrated by using the inventory of 5,609 (Chapter 4.3) landslides triggered on November 2009, by the combined action of Hurricane Ida and the low-pressure system 96E, in a sector extending 287 km^2 along the slopes of the San Vicente Volcano, El Salvador (Mercurio et al., 2021). The rainfall-triggered model, which was trained by using only static independent variables, was applied to all fourteen study areas to verify its ability to predict the position of the coseismic landslides that occurred on January and February 2001. On the other hand, the earthquake-induced landslide predictive models were calibrated by using both static and dynamic variables, the latter reflecting the intensity of ground shaking. In order to estimate the predictive skill of the models and the goodness of fit of the susceptibility models, the results will be evaluated thanks to the AUC value.

5.2. Materials and Methods

5.2.1. Study areas

This work was performed in 14 areas along the volcanic chain (Fig. 5.1), which were among the areas most affected by the two intense earthquakes occurred in the first two months of 2001.

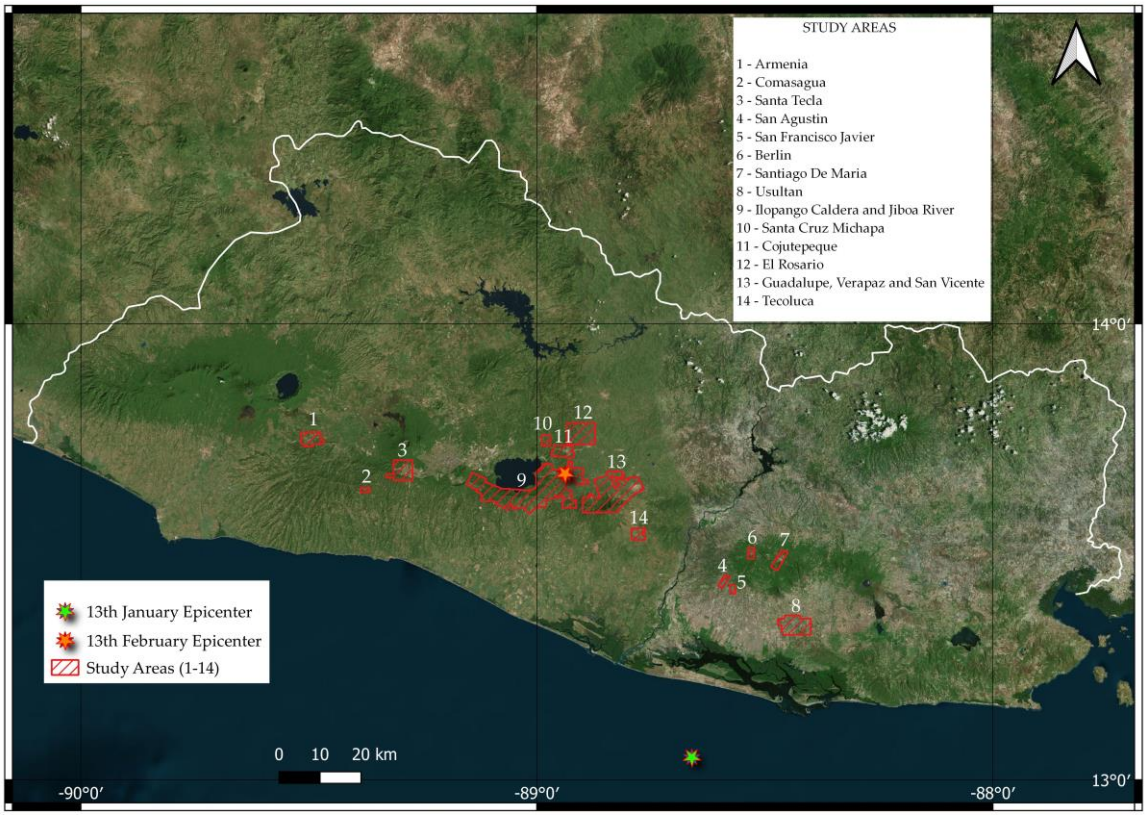

Figure 5.1 - Location of the fourteen study areas: sectors 1-3 and 4-8 are located in the south-eastern and south-western areas of El Salvador and were affected by the earthquake of 13th January 2001, sectors 9-14 are located in the central area of the country and were affected by the earthquake of 13th February 2001.

The first eight study areas, numbered from 1 to 8, were selected because of the high number of landslides triggered by the January 2001 earthquake. Sectors 1 to 3 are in the south-western part of the country, close to the San Salvador volcano, whereas sectors 4 to 8 are located in the southern-eastern portion of El Salvador. Sectors from 9 to 14 are placed in the south-central part of the country and were selected because they were close to the February 2001 earthquake epicenter and strongly affected by coseismic landslides. Table 5.1

reports the extent, average and standard deviation of altitude and slope angle, and the main outcropping lithology of the 14 study areas.

Table 5.1. This table reports for each area, the extent, average and standard deviation of altitude and slope angle, and the main outcropping lithology. Lithology classes: GEO1 soft rocks (intermediate basic effusive rocks and subordinate pyroclastites) GEO2 hard rocks (intermediate basic effusive rocks) GEO3 medium rocks (acid effusive and acid intermediate rocks) GEO4 very soft soils (Tierra Blanca: acidic pyroclastites, subordinate volcanic epiclastites and acid effusive rocks) GEO5 soft soils (Quaternary sedimentary deposits) GEO6 hard soils (acid pyroclastic rocks, volcanic epiclastites) GEO7 medium soils (volcanic epiclastites and pyroclastites, locally effusive basic-intermediate rocks).

Sector	**Area [km^2]**	**Altitude [m a.s.l.]**		**Slope angle [°]**		**Two main lithology classes**	
		Mean	Std.dev.	Mean	Std.dev.		
1	15.41	577.73	64.19	15.10	11.22	GEO7 (83.92%)	GEO2 (15.39%)
2	2.31	1039.00	50.69	25.17	10.02	GEO2 (84.42%)	GEO7 (15.58%)
3	23.89	975.86	70.16	14.71	12.96	GEO7 (42.38%)	GEO4 (26.70%)
4	3.98	286.16	41.14	20.51	10.71	GEO7 (100.00%)	-
5	2.66	287.80	31.01	16.38	9.41	GEO7 (98.44%)	GEO1 (1.56%)
6	3.89	1008.35	85.91	12.11	9.23	GEO1 (72.80%)	GEO7 (27.20%)
7	8.29	862.50	70.54	11.05	8.79	GEO1 (50.97%)	GEO7 (49.03%)
8	31.42	78.34	22.40	3.29	4.28	GEO7 (95.32%)	GEO5 (1.81%)
9	155.32	618.41	122.58	24.23	12.43	GEO7 (30.17%)	GEO6 (27.98%)
10	5.32	685.48	28.97	16.46	12.00	GEO6 (56.19%)	GEO4 (41.14%)
11	13.79	781.87	74.31	16.09	10.14	GEO2 (51.69%)	GEO6 (31.39%)
12	34.80	699.61	51.11	16.30	10.01	GEO2 (10.39%)	GEO6 (73.24%)
13	87.65	833.88	365.10	17.93	13.55	GEO4 (36.26%)	GEO1 (31.78%)
14	8.84	266.62	39.17	5.12	5.55	GEO6 (90.25%)	GEO2 (8.57%)

The sectors under consideration contain different: areal extensions (in a range from about 2.6 to 155 km^2), average elevation (from about 78 to 1.039 m), average slopes (from about 3 to 25°) and different types of lithological classes present, thus showing a wide heterogeneity.

Most of the landslides' activation of both the 2001 earthquakes corresponds to thousands of shallow debris flows/avalanches and rotational slides (Chapters 2.2.7 and 2.2.5, respectively), but there are also numerous falls in rock and debris (Chapter 2.2.3), according

to Cruden & Varnes's classification of landslides (1996). Moreover, both earthquakes triggered a few large and deep landslides that were highly damaging.

El Salvador is in a tropical-humid climate system, characterized by a dry season from November to April and a wet season from May to October, where about 75% of annual precipitation falls. The earthquakes of 2001 occurred in the first two months of the year, thus during the dry season, confirmed by the study of precipitation data recorded close to the study areas. Furthermore, gauge stations showed cumulative precipitation in the 12 months preceding the earthquakes of 2001 lower than the annual average of the same gauge stations in the 29 years before the earthquakes (Tab. 5.2).

Table 5.2 - Precipitation in the 12 months preceding the seismic events of 2001 and the average annual precipitation in the period 1971-1999 in the 14 areas under consideration.

Sector	1	2	3	4	5	6	7	8	9	10	11	12	13	14
Rainfall [mm] Mar 2000-Feb 2001	1166	1614	1614	1571	1571	1571	1571	1571	1632	1632	1632	1632	1632	1632
Average rainfall [mm] 1971-1999	1657	1847	1847	1650	1650	1650	1650	1650	1836	1836	1836	1836	1836	1836

In addition, also by studying the monthly data in detail, it was also observed that November 2000 was the last month that experienced rainfall, which was lower than the average, and the following months until the earthquakes of 2001, unlike the averages of previous years, were without rains. These data suggest that the water's content has not been decisive in the genesis of gravitational phenomena, a situation that could have increased the extension, the amount and the damage of landslides due to a possible increase in volume weight and decrease in the cohesion of soils and outcropping rocks.

5.2.2. Mapping strategy

Landslide inventories are valuable tools for investigating slopes' morphological evolution and analyzing the dynamics following determinant triggers that caused gravitational phenomena. These have to be referred to a specific event to know the phenomena following a specific trigger, so excluding the gravitational phenomena that occurred before or after. The presence or absence of a gravitational phenomenon within a selected mapping unit performs the function of a dependent variable in landslide susceptibility analysis carried out by stochastic and empirical models. It turns out that their completeness is decisive in the accuracy of a model's results (Galli et al., 2008; Steger et al., 2016, 2017; Rotigliano et al., 2018; Martinello et al., 2022). In fact, for the lack of several landslides, an error is made that compromises the performance of the statistical model. Since the 2001 landslide inventories available to date are incomplete, as they present only the main gravitational phenomena, it has been found suitable to create a complete inventory, attempting to include their entirety.

To prepare the earthquake-induced landslide inventory after the two main shocks occurred on 13th January and 13th February 2001, aerial photos were obtained by the CNR (*Centro Nacional de Registros de El Salvador - Instituto Geográfico y del Catastro Nacional*). Regarding the January earthquake, 136 aerial photos were taken, covering 91.85 km^2, while 313 aerial photos covering 305.72 km^2 were taken during the February earthquake (Fig. 5.2). Recognizing and mapping landslides in tropical areas, where vegetation recovers rapidly, requires aerial/satellite images taken not long after the event (Mercurio et al., 2021).

These aerial photos were obtained the following days of both earthquakes, when displaced materials had not yet been removed (Fig. 5.3). In fact, the photos related to the first event were obtained on 17th January, those related to the second event on 19th February.

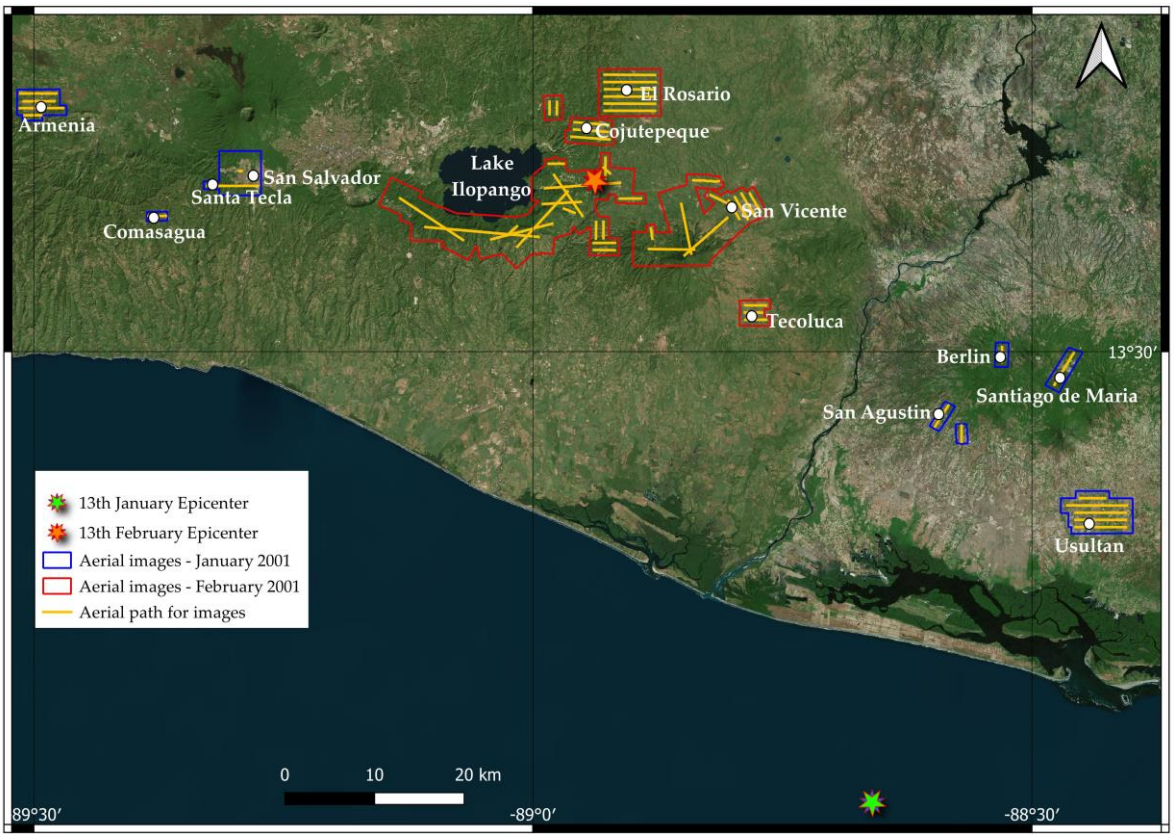

Figure 5.2 - The eight and six sets of aerial photos were used for the study areas of January and February 2001 seismic events.

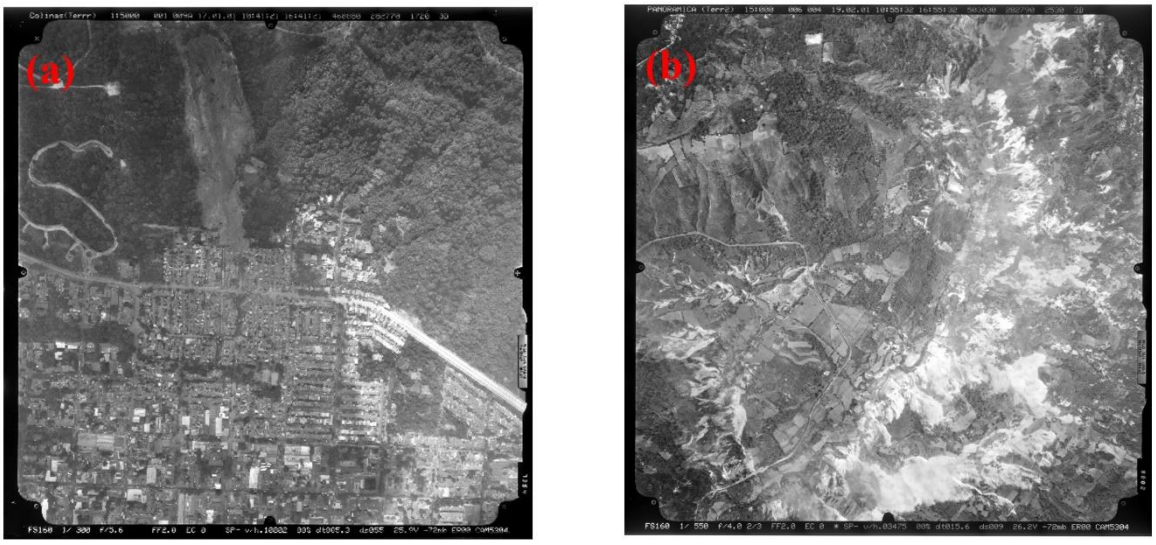

Figure 5.3 – Two examples of aerial photos obtained by CNR. A sector related to the photos of the CNR associated with the event of January 2001 (**a**), it is possible to observe a complex phenomenon (rotational sliding + flow) that will be argued in Chapter 5.2. (**b**) A sector related to the CNR photos associated with the February 2001 event. There are numerous rotational sliding phenomena and debris flow/avalanche.

The aerial photos, taken at different heights on each aerial path, so with varying lengths and widths for each path, were carried out in the most seismically affected areas, corresponding to sectors in the eastern and western parts of the country in the case of the January earthquake and to the central sector in the case of the February earthquake, thus not presenting areas of study intersection between the two events.

First, the manual georeferencing of all the 449 aerial photos was realized, then the polygons were manually mapped, taking care to map all the gravitational phenomena contained, as the eventual lack of phenomena can compromise the final result. Then, the LIPs were extrapolated with an automatic process carried out on QGIS software; in fact, they were automatically placed at the highest points of the landslide polygons. A valid inventory must represent every landslide through an identifying point or a polygon that encloses the whole phenomenon. In this study, since we wanted to analyze the susceptibility of the landslide linked to its positions of initiation, we decided to use an inventory characterized by points. Although there is no agreement on the best position of a point allowing to identify of a given landslide and the conditions which triggered its specific slope failure, several recent studies have successfully adopted LIPs to identify pre-failure conditions, positioning it in the crown of the landslide (Rotigliano et al., 2011; Lombardo et al., 2014; Cama et al., 2015; Rotigliano et al., 2018, 2019).

In order to avoid errors in the mapping and including gravitational phenomena in the inventory that have been triggered in a previous seismic or rainy event, satellite images from ESA (European Space Agency) 10-m satellite resolution SPOT-4 prior to the 2001 events were analyzed and the landslides that were not generated by that specific trigger were removed. In addition, in the areas where the aerial photos were taken in February, SPOT-4 satellite images of 21st January were also analyzed in order to assess if, among the landslides mapped in February, there are phenomena belonging to the trigger of the previous month and then to know if the mapped phenomena are of new initiation or reactivation of the previously seismic event. Previous events that have not been reactivated must be removed from the inventory as they are unrelated to that trigger.

5.2.3. Dependent and independent variables

Indirect and quantitative methods are the most effective among the several methodologies used to generate a susceptibility map from landslides. These are characterized by high objectivity since they use statistical tools to determine the influence of the factors of instability and, consequently, the connections between the latter and the distribution of gravitational phenomena in a given area. In the field of geomorphology, the primary hypothesis of quantitative statistical methods is that landslides that have occurred in the past can reactivate in the future under the same conditions that generated them in the past, both in the same area and in zones with similar geological characteristics. Due to this statement, it would be possible to assign a predictive character to gravitational phenomena through the regression functions that connect the past and present landslide conditions (dependent variable) to a series of predictors or instability factors (independent variables). The techniques used to assess landslide susceptibility must find the best possible compromise between the accuracy and reliability of the forecast models. The quality of the input data is necessary to obtain an output equivalent as possible to reality.

As for the binary dependent variable, which involves the presence or not of the LIP within the selected mapping unit, a binary value has been assigned to each cell (0 = negative, absence; 1 = positive, presence).

As for the independent variables, in this work, eleven predictive variables have been selected that are supposed to affect the rainfall and earthquake-induction trigger phenomena: Aspect (*ASP*), Catchment Area (*C_AR*), Convergence Index (*C_IND*), Downslope Curvature (*D_CUR*), Elevation (*ELE*), Geology (*GEO*), Normalized Difference Vegetation Index (*NDVI*), Slope (*SLO*), Topographic Positioning Index (*TPI*), Topographic Wetness Index (*TWI*) and Upslope Curvature (*U_CUR*). Two additional dynamic predictive variables have been added to the subsequent earthquake-induction susceptibility analysis, the Peak Ground Accelerations (*PGA*) values, obtained from the rasterization of a shapefile obtained from the USGS Shakemap and the distances from the epicenter (*DIST*) related to their specific seismic trigger, obtained from the elaboration of a raster of distances from the coordinates of the

seismic triggers. These variables are considered predisposing factors for initiating gravitational phenomena after an earthquake. All variables are continuous except for GEO, which is a categorical variable. The variables used are shown in Table 5.3.

Table 5.3 - Independent variables used in rainfall- and earthquake-induction landslide susceptibility applications.

Independent variable	Application for rainfall-/eartquake-induction landslide susceptibility (Y: yes, N: no)	Type	References
ASP Aspect	Y/Y	Static	Geospatial Data Abstraction Library QGIS
C_AR Catchment Area	Y/Y	Static	SAGA GIS
C_IND Convergence Index	Y/Y	Static	SAGA GIS
D_CUR Downslope Curvature	Y/Y	Static	SAGA GIS
ELE Elevation	Y/Y	Static	10-m DEM resampled from a 5-m DEM from ESA
DIST Epicentral Distance	N/Y	Dynamic	USGS website
GEO Geology	Y/Y	Static	Geological map from Weber et al. 1975 (modified)
NDVI Normalized Difference Vegetation Index	Y/Y	Dynamic	Terra/MODIS Satellite NASA
PGA Peak Ground Acceleration	N/Y	Dynamic	USGS Shakemap
SLO Slope	Y/Y	Static	Geospatial Data Abstraction Library QGIS
TPI Topographic Positioning Index	Y/Y	Static	Geospatial Data Abstraction Library QGIS
TWI Topographic Wetness Index	Y/Y	Static	SAGA GIS
U_CUR Upslope Curvature	Y/Y	Static	SAGA GIS

5.2.4. Modelling technique

In order to assess predictive model accuracy, landslide susceptibility processing requires initial model calibration and subsequent validation (Chung and Fabbri, 2003). As pixel-cell partition is largely and effectively employed in landslide susceptibility mapping, this strategy was employed in our experiment. That is made with regular squares of predefined size, thanks to a DEM with a resolution that must be suitable for the investigation.

For this work, a 10-m cell DEM was employed, resulting from the resampling of a 5-m cell DEM of the European Space Agency (ESA). This cell size was selected aiming to find a compromise between spatial resolution and computation time needed to train and test the models (Cama et al. 2016). In fact, works (Conoscenti et al. 2015; Garosi et al. 2018) have demonstrated the effectiveness of pixel-based models resulting from 10-m cell DEM.

To this aim, the study areas were divided into 7,096,231 10-m grid cells, corresponding to the pixels of the employed DEM. This dataset includes 6,464 positive and 7,089,890 negative cells. The likelihood of landslide occurrences at each 10-m grid cell of the study area was calculated using Multivariate Adaptive Regression Splines (MARS; (Friedman, 1991)) as modelling technique. The statistical analyses were realized using R Studio software with the "earth" package (Milborrow, 2020).

5.2.5. Calibration and validation strategy

In this study, landslide predictive models were calibrated and validated using five datasets, which correspond to the LIPs contained in the fourteen study sectors (JAN, FEB and JF), in the area of the San Vicente (SV) volcano and in the intersection between the latter and sectors 9 and 13 (FSE), the sectors are shown and described in Figure 5.4 and Table 5.4.

Table 5.4 - Datasets used to calibrate and validate the landslide predictive models.

Dataset code	Area	Trigger	Landslides date
SV	San Vicente (Mercurio et al., 2021)	Rainfall	Nov 2009
JAN	Sectors 1 to 8	Earthquake	Jan 2001
FEB	Sectors 9 to 14	Earthquake	Feb 2001
JF	Sectors 9 to 14	Earthquake	Jan 2001
FSE	Intersections between FEB and SV areas	Earthquake	Feb 2001

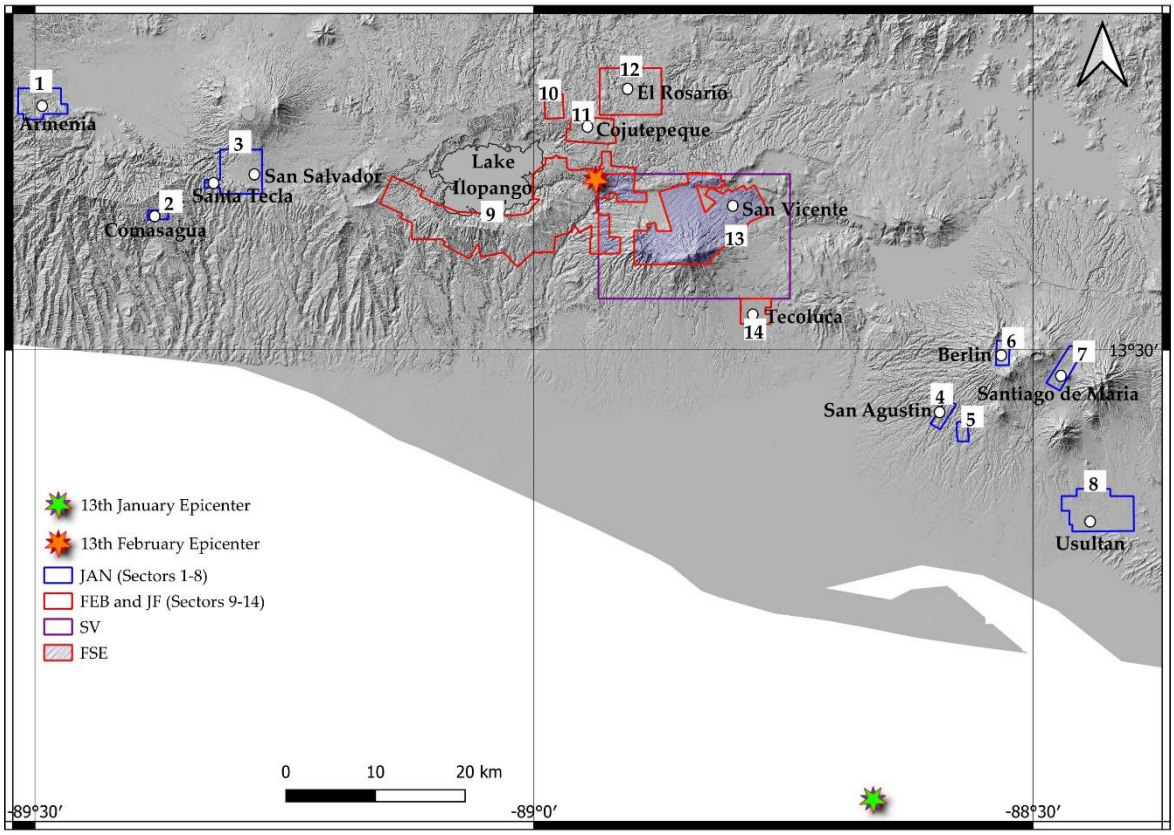

Figure 5.4 - Locations of the datasets used for the landslide susceptibility applications.

These datasets are matrices where rows correspond to the pixels of a specific area, while columns report the values of the dependent and independent variables calculated for each pixel. The dataset of rainfall-triggered landslides (i.e., SV) includes only static predictors, whereas those of the coseismic landslides (i.e., JAN, FEB, JF and FSE) can report the values of both static and dynamic independent variables, depending on the model used. Indeed, the MARS predictive models were prepared using different calibration datasets or sets of predictors (Table 5.5).

The models named M1 were trained with the dataset SV, which includes rainfall-induced landslides and static independent variables. The M1 model, calibrated with the SV dataset, was then transferred to all fourteen study sectors of El Salvador, calculating a probability (PSV) of landslide occurrence for each pixel of these areas. The values of PSV were then employed as a new predictor when training the models M2 and M4. The M2, M3 and M4 models were calibrated with the earthquake-induced landslides of January and February

2001. The predictor variables PSV, PGA and DIST were used in the M2 models, whereas the M3 and the M4 models include all the selected predictors, with the latter also using PSV as an independent variable.

Table 5.5 – Inventories for calibrations, variables and inventories for validations used in M1, M2, M3, M4 models.

	Model			
Area/Inventory for Calibration	**M1**	**M2**	**M3**	**M4**
SV (rainfall-induction)	X			
JAN, JF, FEB (earthquake-induction)		X	X	X
Variables				
PSV	X	X		X
Static Predictors			X	X
PGA, DIST		X	X	X
Area/Inventory for Validation				
JAN, JF, FEB, FSE (earthquake-induction)	X	X	X	X

The predictive ability of the M1 models was evaluated by comparing the PSV values and the presence or absence of coseismic landslides in the datasets JAN, FEB, JF and FSE.

Calibration and validation of the MARS models consisted of the following steps. First, ten subsets from each dataset were randomly selected, including all the event cells and the same number of non-event cells. The subsets of cells extracted from the SV dataset were used to train ten M1 models. Second, two calibration samples from the ten subsets of all the datasets were extracted excluding SV, by randomly selecting the 75% and the 5% of the event cells, respectively. The remaining event cells (25% and 95%, respectively) were included in the validation samples. Both calibration and validation samples were completed by randomly picking the same number of non-event cells. This second step thus produced twenty calibration and twenty validation samples extracted from the datasets JAN, FEB, JF and FSE. The two ratios of event/non-event cells were chosen in order to evaluate the predictive performance of the MARS models under two different scenarios: the first one, in which the positions of a large part (i.e. 75%) of the earthquake-induced landslides are

known; the second scenario that simulates the situation just after the earthquake occurrence when only a very small part (i.e. 5%) of the landslides had been identified.

The probability of landslide occurrence was calculated for each cell of the validation samples by averaging the score obtained from the ten MARS model runs (one for every calibration sample). This strategy was applied to increase the stability of the landslide predictions and mitigate the rare-events issue (Heckmann et al., 2014; Van Den Eeckhaut et al., 2012; Vargas-Cuervo et al., 2019). For all the validation samples, the ROC curve was prepared by comparing the average MARS score and the value (0:absence; 1:presence) of the dependent variable of each pixel. Then, the AUC curves were calculated, thus obtaining ten values for the prediction of the datasets JAN, FEB, JF and FSE obtained from the models M1 to M4. The Wilcoxon signed-rank test was employed to identify significant differences between the models' predictive skill performance, by setting the significance level at 0.01.

5.3. Results

5.3.1. The 2001 earthquake-induced landslide inventories

The JAN inventory was obtained following eight sets of aerial photos taken a few days after the earthquake of 13th January 2001, which correspond to inhabited areas that have experienced the most significant damage due to the seismic shaking and the consequent triggered earthquake-induction landslides, mainly corresponding to debris flows, rotational slides and earth and rock falls. These correspond to sectors with higher PGA values than adjacent zones (blue polygons in Fig.5.5).

The resulting study area (sectors 1 to 8, counted from West to East, are respectively: Armenia, Comasagua, Santa Tecla, S.Agustin, S.Francisco Javier, Berlin, Santiago De Maria and Usultan) is 91.85 km^2, corresponding to 1,260,811 10-m pixels.

The inventory consists of 997 LIPs, placed in 997 10-m pixels. The percentage of positive cells, compared to the total of the pixel of the study area, is equal to 0.079%, while the cells containing the landslides are 9,556, for a total pixel amount of 0.76%.

As mentioned, inventories must be related to a specific trigger. Landslides in the 9-14 sectors (counted from West to East, are respectively: Ilopango south and Rio Jiboa, S. Cruz Michapa, Cojutepeque, El Rosario, San Vicente and Tecoluca; red polygons in Fig. 5.5) could have been triggered already after the 13th January event, despite relatively lower PGA values than in the January areas. Since there were no aerial photos available, it was decided to analyze the area using satellite photos. An essential step to the aim was to find a satellite photo taken after the January and before the February events and compare it with a previous satellite photo to verify that these were exclusive phenomena of January 2001. Satellite photos were found for this purpose from ESA 10-m satellite resolution SPOT-4 of 21st January that allowed to map the phenomena of January (Fig. 5.6).

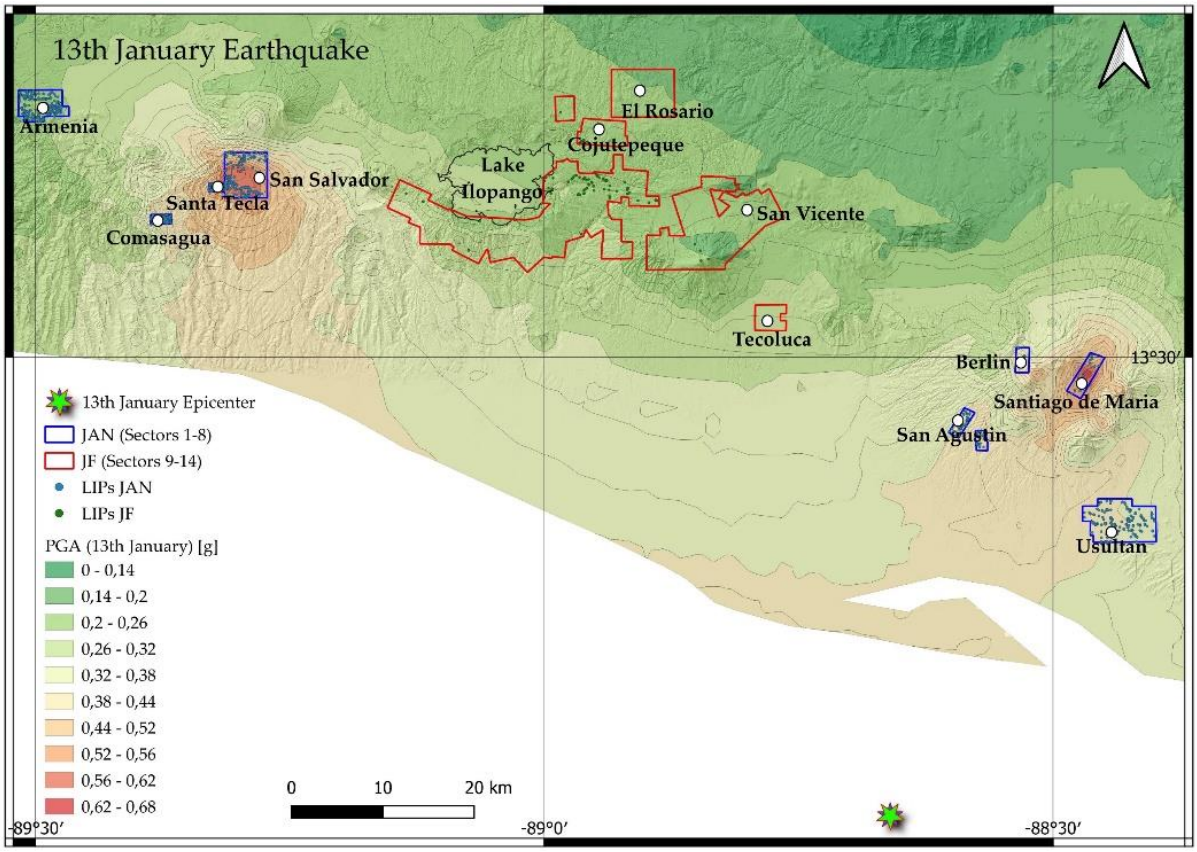

Figure 5.5 - PGA values and LIPs related to the seismic event of M 7.7 of 13th January 2001 in the 14 study areas.

These landslides also needed to analyse the subsequent landslides mapped in February in sectors 9-14 to verify if the landslides of the following month are reactivations or if there

are phenomena of the previous month that have not reactivated in February, to the aim to remove them from the subsequent February inventory.

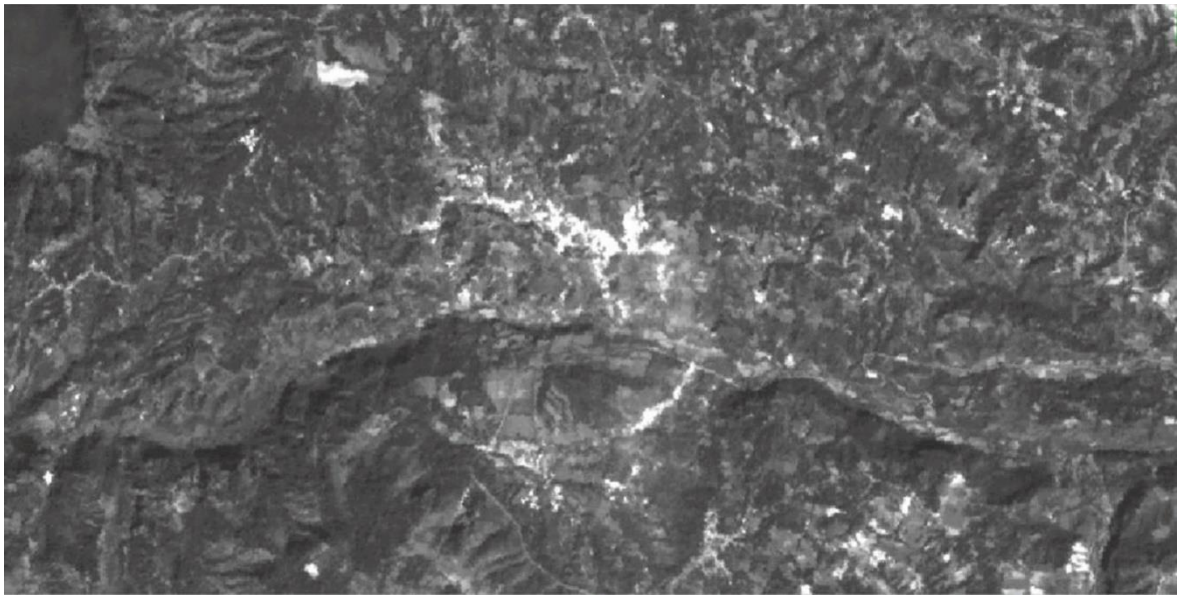

Figure 5.6 – Landslides triggered by 13th January event and mapped in sectors 9-14.

These landslides were added to an inventory called JF, consisting of 123 LIPs between sectors 9 and 14. These are placed in 123 10-m cells, for a total of 0.002% of the LIPs compared to the area under examination. When landslide pixels are analyzed, it turns out that the pixels in which the landslides are located are 11,42, corresponding to 0.2% of the area.

If JAN and JF inventories are merged, the percentage of the LIPs and landslide pixels in relation to the total area (sectors 1 to 14) are significantly reduced (0.017 and 0.30, respectively) due to the low PGA values within sectors 9 to 14. However, the landslides triggered in these sectors, despite being about 1/10 compared to those of the inventory JAN, are in a more significant number of pixels occupied by landslides (Tab. 5.6). The reason is the high slopes characterized by thick deposits of poorly consolidated, late Pleistocene and Holocene Tierra Blanca rhyolitic tephras erupted from Ilopango caldera, an area particularly susceptible to the initiation of gravitational phenomena (Rotigliano et al., 2018, 2019). Indeed, in that region, the January earthquake resulted in a reduced number of debris flows and rotational slides, which, however, have massive surface extensions, also demonstrated

by the number of gravitational phenomena that have an area > 10,000 m^2, which are respectively two and twenty-two in the JAN and the JF inventory sectors. Despite the modest number, the two gravitational phenomena generated the most fatalities and damage, both located in sector 3 (Las Colinas neighbourhood of Santa Tecla, just west of the capital San Salvador). One of these is a complex landslide (rotational slide + earth flows) of about 200,000 m^3, where about 585 people lost their life. This landslide (Fig. 5.7), sadly became famous all over the world for the devastation it has generated, is a phenomenon about 800 m long, 150 m wide with a 50 m high escarpment activated on the north side of El Balsamo Ridge, composed by the andesitic cinders and some interbedded tephra of the El Balsamo Formation (Bommer et al., 2002). The second event, located at a distance of approximately 2,5 km from the first landslide, is a debris flow about 1,500 m long that also started from the north side of El Balsamo Ridge and has reached and destroyed a sector of the Carrera Panamericana, the most crucial road in the country, which connects the capital with the western part of El Salvador. The highway interruption has hindered the arrival of aid, creating enormous damage to the population.

The absence of small landslides in sectors 9 to 14 compared to that of sectors 1 to 8 (41.42%) is related to the different resolution sizes of the tools used for mapping, as phenomena with an extension less than 100 m^2 can be undetectable in a satellite analysis with a 10-m resolution (Tab. 5.6).

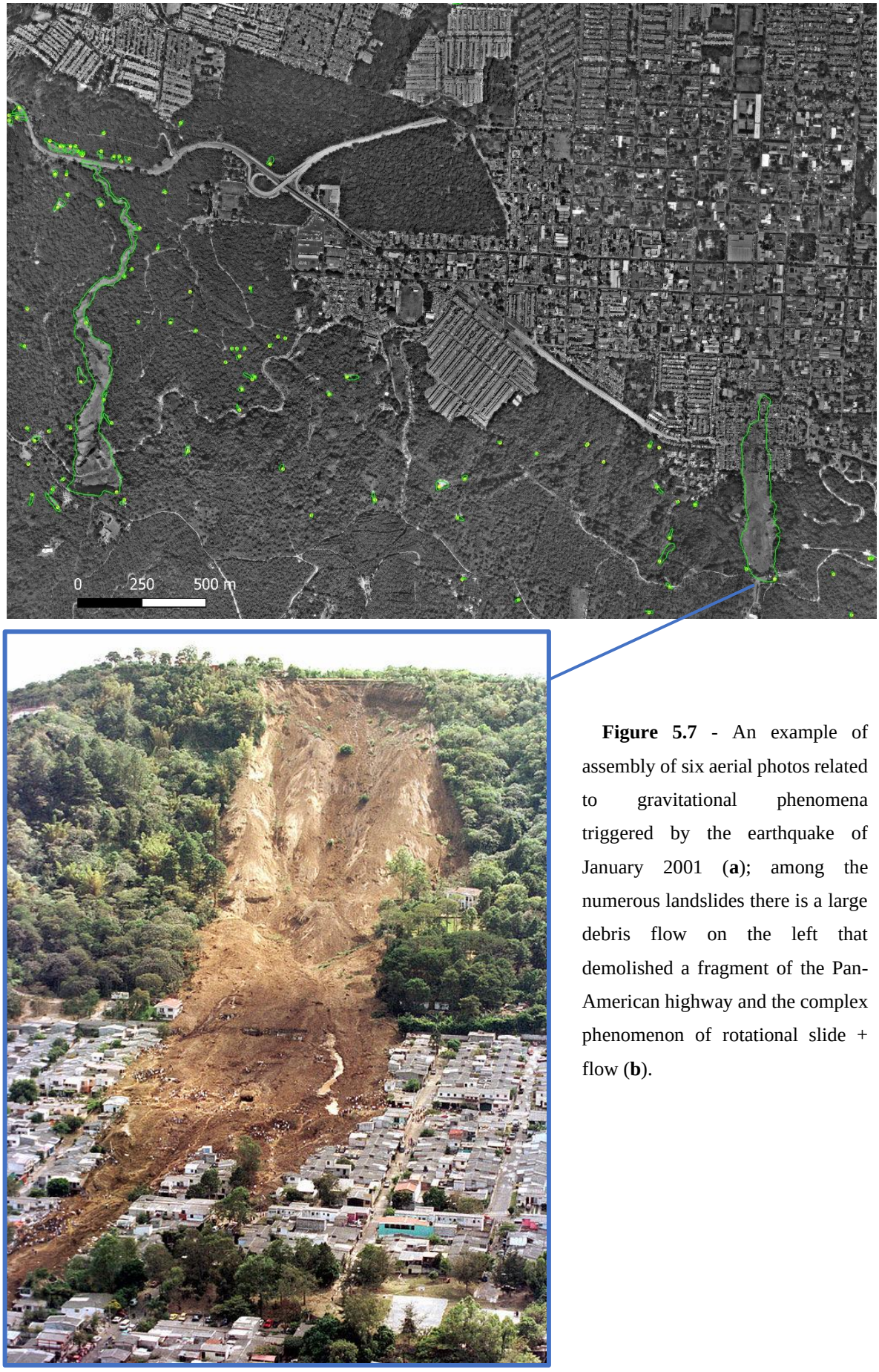

Figure 5.7 - An example of assembly of six aerial photos related to gravitational phenomena triggered by the earthquake of January 2001 (**a**); among the numerous landslides there is a large debris flow on the left that demolished a fragment of the Pan-American highway and the complex phenomenon of rotational slide + flow (**b**).

Table 5.6 - Amounts and characteristics of the gravitational phenomena of landslides belonging to sectors 1 to 14 related to the January earthquake (LIP = Landslide Identification Point, LAND = landslide).

Sector	Area (km$^{2)}$	N° LIPs	% LIPs	N° LAND areas < 100 m^2 ; (%)	N° LANDs areas 100-1,000 m^2 ; (%)	N° LANDs areas 1,000-1,0000 m^2 ; (%)	N° LANDs areas > 10,000 m^2 ; (%)	LANDs areas average m^2	% LANDs
1	15.41	245	0.10	84 (34.29)	143 (58.37)	18 (7.35)	0 (0)	297.69	1.24
2	2.31	128	0.52	67 (52.34)	57 (44.53)	4 (3.13)	0 (0)	190.91	3.16
3	23.89	296	0.10	107 (36.15)	159 (53.72)	28 (9.46)	2 (0.68)	870.79	1.45
4	3.98	67	0.07	38 (56.72)	29 (43.28)	0 (0)	0 (0)	145.82	0.39
5	2.66	43	0.15	27 (62.79)	14 (32.56)	2 (4.65)	0 (0)	151.94	0.74
6	3.89	8	0.02	1 (12.50)	6 (75.00)	1 (12.50)	0 (0)	328.59	0.19
7	8.29	17	0.01	1 (5.88)	16 (94.12)	0 (0)	0 (0)	267.09	0.06
8	31.42	193	0.05	88 (45.60)	103 (56.37)	2 (1.04)	0 (0)	116.19	0.31
JAN (Sectors 1-8)	*91.85*	*997*	*0.08*	*413 (41.42)*	*527 (52.86)*	*55 (5.52)*	*2 (0.20)*	*407.13*	*0.76*
9	155.32	93	0.0025	0 (0)	19 (20.43)	55 (59.14)	19 (20.43)	8,744.50	0.27
10	5.32	1	0.0018	0 (0)	0 (0)	0 (0)	1 (100)	19,571.39	0.44
11	13.79	23	0.0136	0 (0)	8 (34.78)	15 (65.22)	0 (0)	2,079.28	0.35
12	34.80	0	0	0 (0)	0 (0)	0 (0)	0 (0)	0	0
13	87.65	6	0.004	0 (0)	1 (16.67)	3 (50.00)	2 (33.33)	10,263.87	0.05
14	8.84	0	0	0 (0)	0 (0)	0 (0)	0 (0)	0	0
JF (Sectors 9-14)	*305.72*	*123*	*0.002*	*0 (0)*	*28 (22.77)*	*73 (59.34)*	*22 (17.89)*	*7,660.25*	*0.20*
JAN + JF (Sectors 1-14)	*397.57*	*1,120*	*0.017*	*413 (36.88)*	*555 (49.56)*	*128 (11.42)*	*24 (2.14)*	*3,585.67*	*0.30*

The seismic phenomenon of the 13th February triggered additional thousands of landslides in the country's central sector (Fig. 5.8).

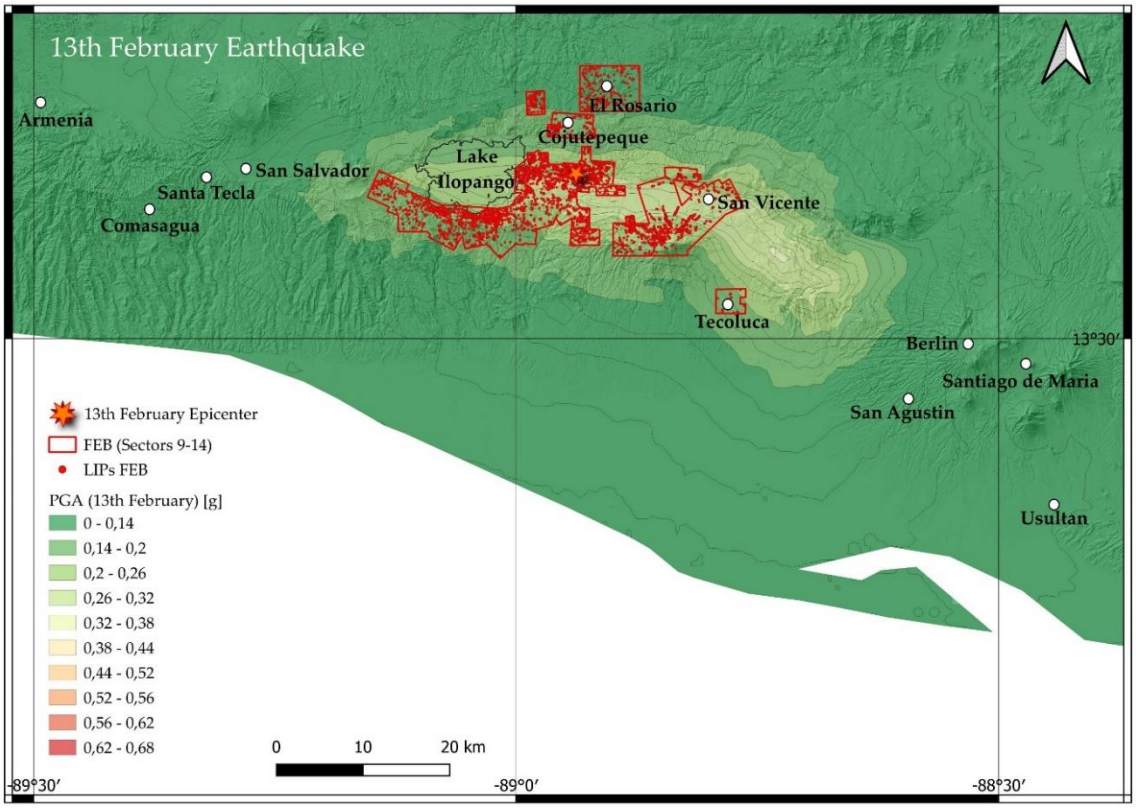

Figure 5.8 - PGA values and LIPs related to the seismic event trigger of M 6.6 of 13th February 2001 in the FEB study areas.

Aerial photos were taken a few days after the event in areas different from those of the previous month, relating to the areas that suffered the most significant damage, corresponding to sectors with high PGA values (9 to 14). The possible landslides related to these areas that were also present in the inventory of JF should have been removed, except for those landslides that have been reactivated. The comparison with Figure 5.6 showed that all landslides related to the January event were reactivated (Fig. 5.9) with enlarging and widening phenomena (Tab. 2.1); therefore, no gravitational phenomenon mapped in February was removed.

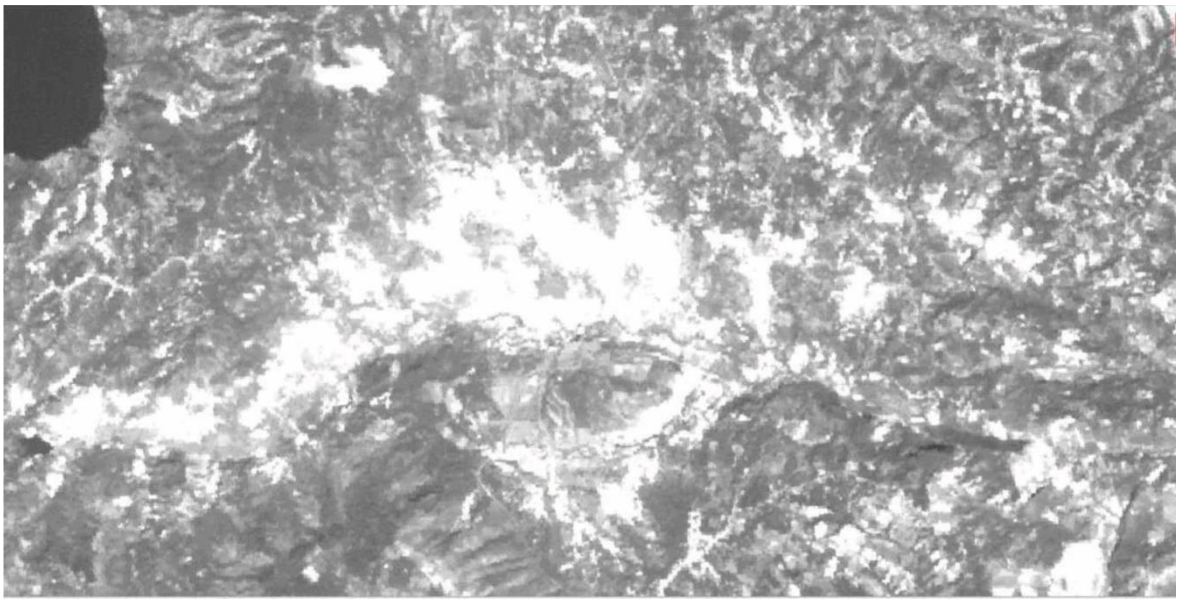

Figure 5.9 – Union of the aerial photos of February in a sector corresponding to that controlled in Figure 5.6, related to the phenomena that occurred following the 13th January event.

The resulting landslides were particularly considerable in areas characterized by thick deposits of rhyolitic tephras slightly consolidated belonging to the Tierra Blanca Formation following eruptions from the Ilopango Caldera. As a result, in the FEB inventory, the mapped LIPs were 5,371, placed in 5,344 pixels. The percentage of positive cells compared to the study area, characterized by 5,835,420 cells, equals 0.092%. The extent of the landslide cells is 123,488 pixels, 2.12% of the study area. This seismic event triggered similar landslides to the previous month, but their distribution is different. In fact, the landslides belonging to the FEB inventory are more significant and, even covering a lower spatial range, have a higher density than those of the JAN inventory (Tab. 5.7).

Table 5.7 - Amounts and characteristics of the gravitational phenomena of landslides belonging to sectors 9 to 14 related to the February earthquake (LIP = Landslide Identification Point, LAND = landslide).

Sector	Area ($km^{2)}$	N° LIPs	% LIPs	N° LANDs areas < 100 m^2 ; (%)	N° LANDs areas 100-1,000 m^2 ; (%)	N° LANDs areas 1,000-1,0000 m^2 ; (%)	N° LANDs areas > 10,000 m^2 ; (%)	LANDs areas average m^2	% LANDs
9	155.32	3650	0.10	427 (11.70)	2,145 (58.77)	955 (26.16)	123 (3.37)	1,694.63	2.47
10	5.32	186	0.33	32 (17.20)	119 (63.98)	34 (18.28)	1 (0.54)	789.50	4.68
11	13.79	279	0.16	91 (32.62)	151 (54.12)	37 (13.26)	0 (0)	554.75	1.58
12	34.80	209	0.06	6 (2.87)	144 (68.90)	57 (27.27)	2 (0.96)	1,093.83	1.16
13	87.65	1029	0.07	172 (16.72)	563 (54.71)	267 (25.95)	27 (2.62)	1,500.60	1.56
14	8.84	18	0.02	8 (44.44)	10 (55.56)	0 (0)	0 (0)	126.75	0.08
FEB (Tot 9-14)	*305.72*	*5,371*	*0.092*	*736 (13.70)*	*3,132 (58.31)*	*1,350 (25.13)*	*153 (2.85)*	*1,538.26*	*2.12*

The reasons are the magnitude value, the epicentral distance and the hypocentral depth. Indeed, all offshore areas with a high Magnitude value and focal depths greater than 30 km have strong seismic shocks enough to trigger landslides that extend over larger areas compared to shallow earthquakes (Keefer, 1984). This situation can also be seen in the January 2001 earthquake, characterized by relatively deep genesis, where MMI (Modified Mercalli Intensity) and PGA decreased their values from the hypocentre to a greater distance compared to the February 2001 earthquake, wherein these values declined rapidly. In addition, the slow decay of PGA values with the epicentral distance in seismic sources belonging to the deep and offshore genesis leads to an origin of gravitational phenomena in larger areas, unlike earthquakes belonging to the most superficial genesis, in which landslides are densely concentrated around the hypocenter. That is also evidenced by the number of gravitational phenomena between the two earthquakes and the distance at which the aerial photos were taken. The equivalent number of positive cells to the number of gravitational phenomena of landslides belonging to the January inventory shows that the spatial density of phenomena is lower than that of landslides referred to the February inventory, where several positive cells contain more than one LIP.

The areas affected by earthquakes, and then the areas where the landslides were mapped, are shown in Fig. 5.10 using graphs constructed by Keefer (1984) and Martino et al. (2014).

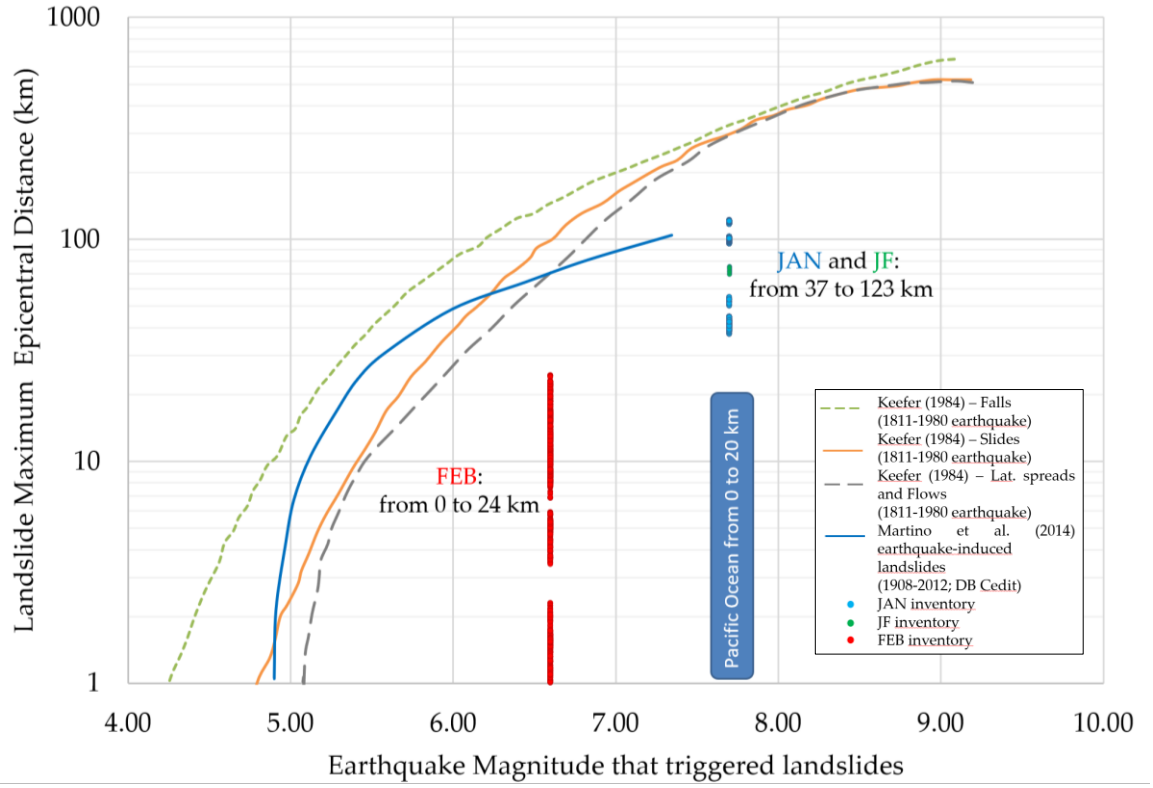

Figure 5.10 - The curves produced by Keefer (1984) and Martino et al. (2014) show the relationship between the maximum distance for the manifestation of gravitational phenomena and the Magnitude. The gravitational phenomena related to the seismic phenomena of January (JAN, JF) and February (FEB) have been placed.

The graph shows that the landslides belonging to the inventories related to JAN and JF are between 37 and 123 km away from the epicenter.

Since the seismically-induced landslides belonging to the January event were generated by an earthquake of M 7.7, they appear to be beyond the Martino's et al. (2014) curve, who have not studied earthquake-induced landslides > M 7.3 as it was the maximum Magnitude recorded in Italy. Regarding Keefer's curve, the January landslides are reliable with the data obtained from his work and appear to be under the "slide" and "flow" curves. The landslides induced by the M 6.6 earthquake in February 2001 can be compared with both Keefer's and Martino's curves and include values below both curves.

The lack of additional aerial photos at greater distances than those available makes more difficult to understand at what maximum distance the landslides were triggered; however, the results obtained show consistency with all the curves. In fact, these results do not mean that gravitational phenomena related to the January event did not occur before or after these values. In fact, the data are located only in the investigated areas, having a gap of information in the fields before and after such values. There is, however, the presence of the Pacific Ocean in the first 20 km away from the epicenter and the presence of slopes with low or null slopes up to 33 km away. As for the inventory FEB, there are phenomena from the epicenter up to 24 km, a distance beyond which there is no information about any landslides. There is to report of the presence of a sharp decline of gravitational phenomena in sector 14, corresponding to the area of Tecoluca, placed between 20 and 24 km, where the gravitational phenomena mapped are only eighteen, showing that the distribution of landslides related to the event is at the end phase. This sector, together with sector 12, corresponding to the area of Tecoluca, are those with a lower number of gravitational phenomena than their total area. These sectors confirm the relationship between the relatively high values of PGA and the number of landslides.

Further confirmation of the importance of PGA and the epicentral and hypocentral distances in the distribution and number of landslides can be seen in the case of the 1,986 intra-crustal earthquake event, which caused more than 1,500 casualties and 100,000 homeless due to different locations where the earthquakes occurred. In fact, the epicenter of 1986 occurred near the Salvadoran capital, dissimilar to 2001, which occurred in an uninhabited area between Lake Ilopango and Jiboa River (Fig. 5.11).

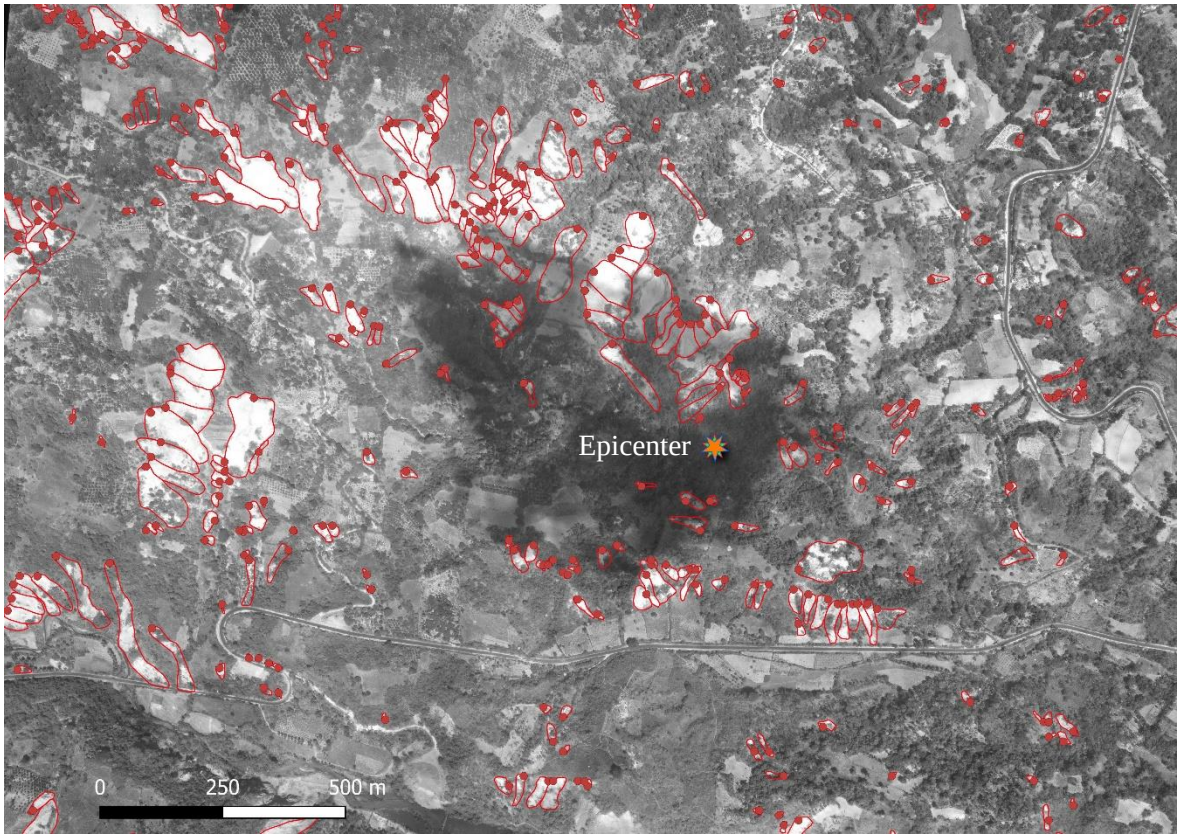

Figure 5.11 - An example of an aerial photo related to gravitational phenomena triggered by the earthquake of February 2001. An area around the 6.6 M epicenter is shown, where there are the manually mapped polygons of landslides and their relative LIPs, located in the crown of the landslides.

As mentioned, events of this type with low hypocentral depth decrease their PGA and MMI values very quickly away from the hypocenter. As a result, the February 2001 earthquake did not affect the capital, the locality with the highest population density.

Along the Jiboa River, which flows from the eastern shore of Lake Ilopango to the Ocean to the south, there have been hundreds of rotational slides and debris flows, mainly of Tierra Blanca (GEO4) (Baum et al., 2001), which created a natural dam along the watercourse. Indeed, a landslide of 12 million cubic meters blocked about 700 m of the course with debris, forming a 60 m deep lake about 2 km long. A spillway 20 m deep and 100 m long was constructed to control the lake's size and depth and decrease its maximum volume, reducing the possible catastrophic failure of the unstable landslide dam. To date, despite the inconsistent nature of the material of which the material is composed, the

landslide dam is stable. However, it is not excluded that spillway erosion may occur in years when rainfall can be higher than the average (Jibson; 2004).

5.3.2. The Ida/96E 2009 inventory

The SV inventory, elaborated by Mercurio et al. (2021), is characterized by the LIPs that have been mapped in an area of 287 km^2 along the slopes of the San Vicente Volcano area following the combined event of Hurricane Ida and the low-pressure system 96E of 7th and 8th November 2009 (Chapter 4). This intense event of rainfall-induction triggered 5,609 gravitational phenomena following 350 mm in 24 h in an area of about 400 km^2 located between Ilopango Lake and San Vicente Volcano. Following this event, numerous and extensive debris flows have caused fatalities and massive damage, with an estimated economic loss of approximately a quarter of a billion dollars (Avila, 2009a). The FSE inventory (Fig. 5.12) is generated as a result of the intersection of the areas of study from rainfall-induction (SV) and earthquake-induction (JAN+FEB).

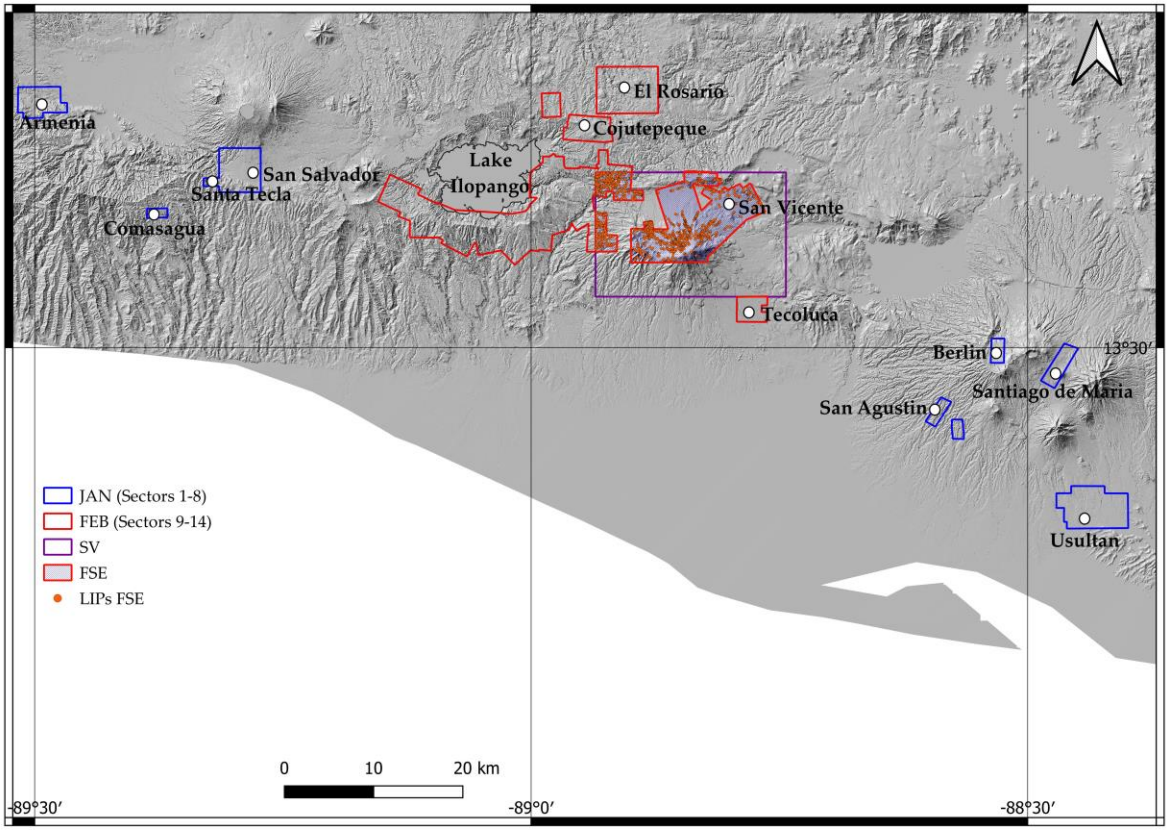

Figure 5.12 - LIPs related to the seismic event trigger M 6.6 of 13th February 2001 in the intersection between FEB and SV study areas (FSE).

The obtained result is an area of 107 km^2 that includes the entirety of sector 13 and the 12.5% of sector 9, both within the FEB study areas. It consists of 1,587 LIPs.

5.3.3. Calibration and validation of the MARS predictive models

Inventories and variables used on M1, M2, M3 and M4 models are shown in Fig.5.13a. The predictive skill of the models measured on the validation samples of the datasets JAN, FEB, JF and FSE are revealed by the boxplots of Fig. 5.13b. These reflect for each model and dataset the variability and skewness of the ten AUC values calculated by applying the calibration and validation strategy described in section 2.6. The skewness display, for each group of ten AUCs, their first quartile (Q1), median and third quartile (Q3), the minimum and maximum values within 1.5 times the interquartile range (IQR) above Q3 and below Q1 and eventually outliers outside 1.5 of IQR. Moreover, Table 5.8 shows the average and standard deviation values of the AUC groups.

(a)

Inventory for Calibration	Model M1	M2	M3	M4
SV (rainfall-induction)	X			
JAN, JF, FEB (earthquake-induction)		X	X	X

Variables

PSV	X	X		X
Static Predictors			X	X
PGA, DIST		X	X	X

Area/Inventory for Validation

JAN, JF, FEB, FSE (earthquake-induction)	X	X	X	X

(b)

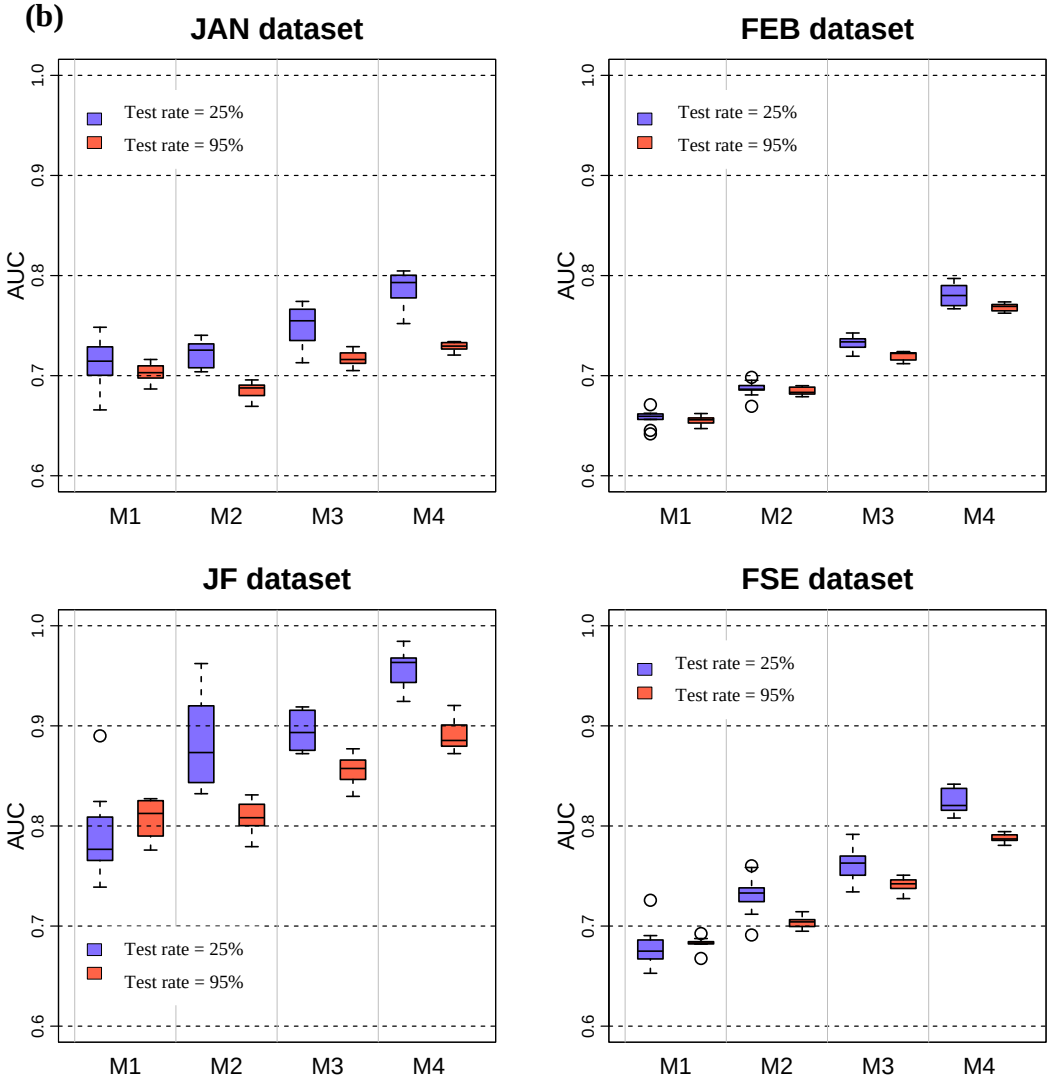

Figure 5.13 – **(a)** Inventories for calibrations, variables and inventories for validations used in M1, M2, M3, M4 models. **(b)** The Predictive skill of the M1, M2, M3 and M4 models, measured on the validation samples of the datasets JAN, FEB, JF and FSE for both scenarios (Scenario 1: test rate 25%; Scenario 2: test rate: 95%).

Table 5.8 - Average and standard deviation values of the AUC for all four models used in both scenarios (Scenario 1: test rate 25%; Scenario 2: test rate: 95%).

Scenario 1	**AUC_JAN_ mean**	AUC_JAN_ sd	**AUC_FEB_ mean**	AUC_FEB_ sd	**AUC_JF_ mean**	AUC_JF_ sd	**AUC_FSE_ mean**	AUC_FSE_ sd
M1_25	0.711	0.027	0.658	0.008	0.789	0.043	0.679	0.020
M2_25	0.723	0.013	0.687	0.008	0.880	0.042	0.731	0.020
M3_25	0.749	0.020	0.732	0.007	0.895	0.019	0.763	0.017
M4_25	0.787	0.017	0.780	0.010	0.958	0.020	0.825	0.012
Scenario 2	**AUC JAN mean**	AUC JAN sd	**AUC FEB mean**	AUC FEB sd	**AUC_JF mean**	AUC JF sd	**AUC_FSE_ mean**	AUC FSE sd
M1_95	0.703	0.009	0.655	0.004	0.808	0.019	0.683	0.006
M2_95	0.685	0.008	0.684	0.004	0.809	0.015	0.704	0.006
M3_95	0.717	0.007	0.720	0.005	0.855	0.015	0.742	0.007
M4_95	0.729	0.004	0.768	0.004	0.889	0.015	0.788	0.004

5.4. Discussion and Conclusions

In this work, four different models were produced (M1 to M4), generated with the calibration of rainfall-induction inventories related to the Ida/96E event of November 2009 (M1) and earthquake-induction inventories related to earthquakes of January and February 2001 (M2-M3-M4). Two different calibration-validation strategies were used, corresponding to two different scenarios. Scenario 1 requires 3/4 of the landslides to be used for calibration of the different inventories used in the models and the remaining 1/4 for validation on earthquake-inducted landslides. This scenario is used most for producing susceptibility models from landslides (e.g., Clerici et al., 2006; Van Den Eeckhaut et al., 2012; Costanzo et al., 2014; Martinello et al., 2020; Mercurio et al., 2021). Scenario 2 includes the calibration of only 5% of the gravitational phenomena (rainfall- or earthquake-induced landslides inventories, depending on the model), using the remaining 95% of LIPs referred to earthquake-induction phenomena for the validation. The models differ according to the independent variables used to assess their effectiveness. The following steps for each model can be drawn based on the analysis employed in this experiment.

First, the M1 models were generated using nine predictive variables elaborated by a 10-m cell DEM, rasterization of a country geological map and of the NDVI values, all referred to as the SV area, for a total of eleven variables. The results obtained through the

MARS analysis have allowed generating of a forecast map of the areas where it is most likely that rainfall-induction gravitational phenomena in the SV (PSV) area are triggered. Through the static predictive variables defined throughout the country, the model has been used as an independent variable and has been validated with the remaining 25% / 95% of LIPs related to the earthquake-induced phenomena. The resulting AUC values ranging from 0.66 for the model applied to FEB (therefore not yet acceptable, as the value is < 0.7) up to the more than acceptable values, referred to area JF, of 0.78.

Subsequently, earthquake-induction inventories were used for the remaining models, using 75% / 5% of the LIPs. The M2 model used PSV as an independent variable along with PGA and DIST seismic parameters. Following validation of the remaining earthquake-induction LIPs, there is a slight increase in average AUC values ranging from 0.69 for FEB to 0.88 for JF.

M3 models include the eleven and the two dynamic predictors, without including the presence of variables related to the Ida/96E event of 2009. The obtained earthquake-induced susceptibility model presents mean AUC values ranging from 0.73 (acceptable) for FEB to 0.90 (outstanding) for JF, showing the excellent predictive ability of earthquake-induction phenomena.

The M4 model was built using all the independent variables available. The result is a further improvement of the earthquake-induced landslide susceptibility model with mean AUC values ranging from 0.78 (almost-excellent) for FEB to 0.96 (outstanding) for JF.

The excellent results obtained by the M4 model permit saying that if all the selected independent variables are used, then both those related to the rainfall-induction (PSV) and the earthquake-induction (static and dynamic predictive variables), excellent prediction results can be obtained in areas where future earthquake-induction phenomena can occur. In fact, it is noted that the earthquake-induction landslide susceptibility model created with only earthquake-induction variables has excellent predictive capabilities. However, if the characteristics related to rainfall-induction susceptibility maps are added, the model

improves its performance, testified by the value of AUC obtained after validation on all four datasets available.

AUC values in the second scenario never vary more than 0.069 compared to the first one, with an average difference equal to 0.026, thus showing exceptional predictive performance. In addition, Scenario 2 models have much lower standard deviation values than the first scenario, showing excellent model stability.

This situation often happens immediately after a seismic or rainfall trigger, where only the main gravitative phenomena are initially mapped. It has also manifested in these two seismic phenomena, in which the inventories that until now were available are insufficient since they contain even less than 1/5 of the landslides mapped in this work. The reason was that the gravitational phenomena were mapped quickly to produce rapid reports for civil protection authorities and were not subsequently integrated with the remaining landslides. The excellent results obtained following this test suggest that, if only some of the landslides triggered by an earthquake are known, it is possible to use the approach proposed in this study to identify those sites where the other landslides are more likely to have occurred following a seismic phenomenon. Indeed, all the classic predictors used in this analysis would remain the same, excluding NDVI values, which can be obtained quickly from NASA's MODIS (Moderate Resolution Imaging Spectroradiometer) website. The additional independent variables to be generated are those related to the dynamic parameters obtained following an earthquake. In fact, it will be required to produce only the rasters linked to PGA and epicentral distances, readily available online immediately after an earthquake from the USGS website. Indeed, PGA maps can be obtained by rasterizing the shapefile via the USGS shakemap website, while epicentral distances can be generated thanks to the knowledge of the epicenter coordinates, creating a map linked to the distances from the point.

Partial mapping is never ideal in producing landslide susceptibility maps; however, the results obtained in the second scenario allow us to propose that a rapid generation of an earthquake-landslide susceptibility map induced immediately after a seismic event is possible.

These outputs obtained can be helpful both for the most affected areas of future gravitational phenomena following earthquakes with triggers comparable to those of January and February, and for the planning of post-aid events, in the situation in which a small number of LIPs are produced with ten ready-made variables and three variables that can be generated quickly after the event (NDVI of the month and PGA and epicentral distances of the seismic event).

The historical investigation of the seismic phenomena that occurred in the last century has shown a high number of earthquakes that testify to the continuous activity of the subduction of the Cocos Plate beneath the Caribbean Plate, capable of generating severe offshore earthquakes and resulting intraplate phenomena in a relatively short time. This condition must reflect that the whole country must be prepared for both types of scenarios, as, despite their differences in density and spatial distribution of landslides, they are capable of causing destruction and fatalities.

6. Prediction of the spatial distribution of landslides generated from earthquake by using an approach which combines a rainfall-induced inventory and static with seismic parameters

Chapter constructed from: Prediction of spatial distribution of landslides generated from rainfalls and earthquakes by using an approach which combines static with seismic para-meters: a test in El Salvador –Mercurio, C., Martinello, C., Azzara, G., Argueta Platero, A. A., Manno, G., Cappadonia, C., Conoscenti, C., and Rotigliano, E. (presented at EGU General Assembly 2022; https://doi.org/10.5194/egusphere-egu22-6449, 2022b)

6.1. Introduction

The main aim of this Chapter is to evaluate the ability of rainfall-induced landslide susceptibility models to predict the geographical distribution of the coseismic slope failures that occurred on 13th February 2001 seismic event. The experiment was performed in a sector of El Salvador where landslides occurred both as a result of the seismic phenomena of February 2001 and extreme rainfall phenomena related to the Ida/96E event of November 2009.

6.2. Material and methods

6.2.1. Study area

This work is concerned with predicting the position of the areas most susceptible to the manifestation of coseismic landslides by using characteristics related to both the phenomena of rain- and earthquake-induction through a rainfall-induced gravitational phenomena inventory as calibration input. In order to evaluate the predictive capabilities of the landslide susceptibility model using information related to both types of triggers, the test must be applied in an area that has been affected by the manifestation of both triggers. El Salvador, affected by both types, is an excellent test for this purpose.

As for the seismic trigger, the inventories JAN and FEB were selected, using their intersection with the other trigger event.

As the event related to the landslides triggered following extreme rainfall events, an area of study related to the Ida/96E event located around the Ilopango Caldera was used for the aim. This sector was chosen because it was located at the intersection of FEB study areas (together with the SVstudy area of Chapter 5.2.2, which has not been selected for this test); no inventory at our disposal intersects the areas of JAN (sectors 1-8, Chapter 5.2.1). This inventory comes from an article about a case study of the creation of rainfall-induced susceptibility models using different and heterogeneous inventories, named "*Investigating Limits in Exploiting Assembled Landslide Inventories for Calibrating Regional Susceptibility Models: A Test in Volcanic Areas of El Salvador*" made by Martinello, Mercurio, Cappadonia, Hernández Martínez, Reyes Martínez, Rivera Ayala, Conoscenti, Rotigliano, and published in the MDPI's Journal Applied Sciences in June 2022.

As a result, the corresponding intersection zone corresponds to the southern and southern-eastern sectors of the Ilopango Caldera, with an extension equal to 33,87 km^2 (Fig. 6.1).

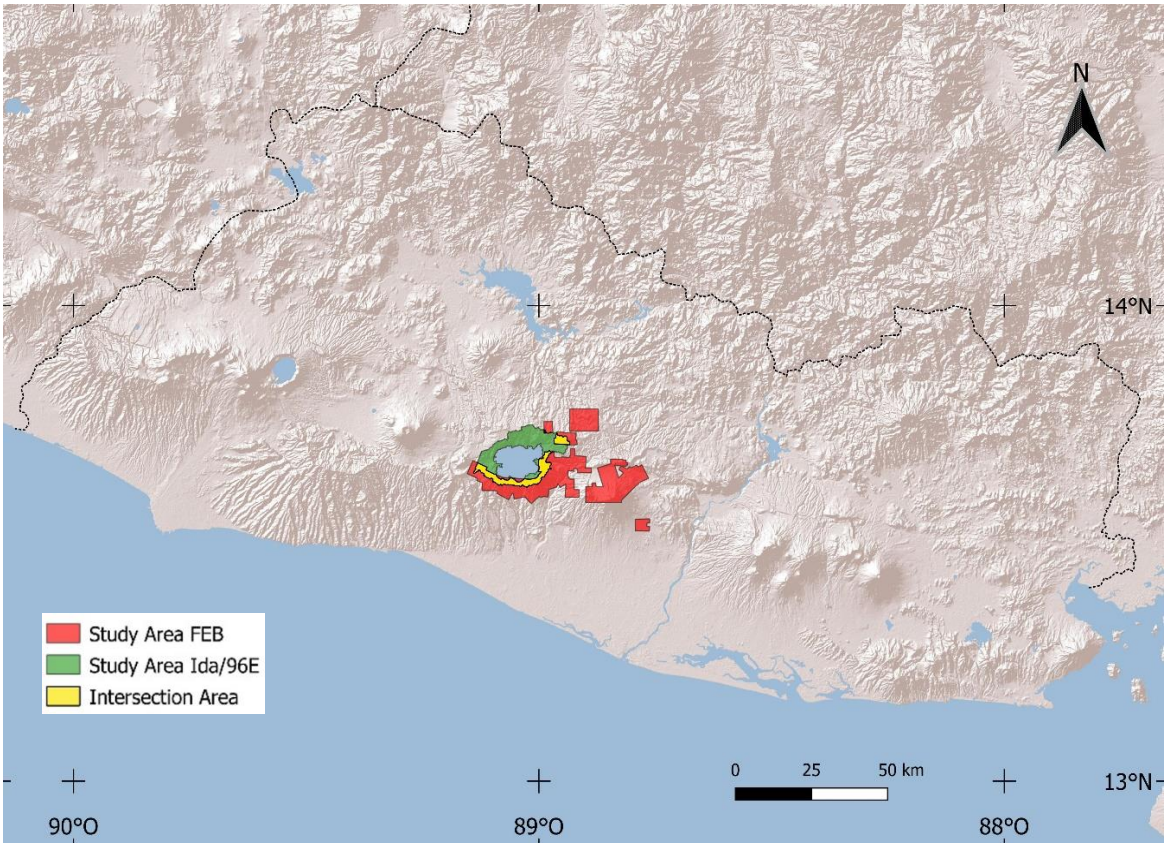

Figure 6.1 – Study area of this work (yellow polygons). That is located at the intersection of the FEB (red polygons) and the 2009 Ida/96E study areas (green polygon).

The area of Ilopango has been subject to the effect of the earthquake of 13 February 2001, as shown in Chapter 5.2.1, where it is possible to consider that the Peak Ground Accelerations related to the event of February are higher than those of January, resulting in a significantly greater number of damages than those manifested the month before. The number of triggered gravitational phenomena also confirms this data. In fact, in January, in the JF sector (landslides occurred in January related to the February aerial photo sectors, obtained following mapping of satellite images by the SPOT-4 satellite), the landslides are 997 against the 5,631 related to the FEB inventory (Tab. 5.6 and 5.7).

The earthquake of 13th February 2001 occurred during the dry season (from November to April). The analysis of the rain gauges clearly shows no abnormal rain events in the months before the earthquake (Fig. 6.2).

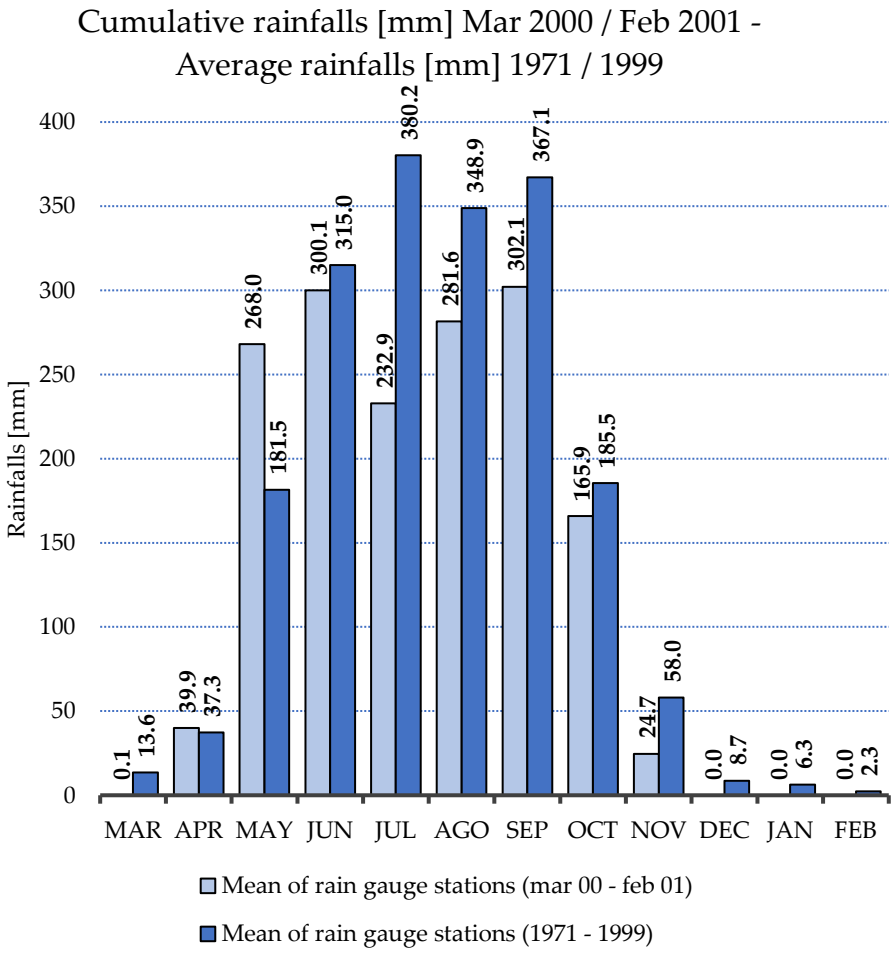

Figure 6.2 – Graph of the cumulative rains of the 12 months preceding the seismic event of February 2001 compared to the average rainfall, in the same area, in the interval 1971-1999.

The rainfall was lower than the average monthly rainfall of the period analyzed between 1971 and 1999, showing that the content of the water has not been decisive in the genesis of gravitational phenomena. In fact, the gauge stations of Ilopango Airport and Cuscatlan bridge, the closest to the study area, show that November 2000 was the last month that had rains (average of 24.7 mm), since December, January and February were completely dry. That means that there has been no physical-chemical degradation of the inconsistent volcanic outcrops, which, in the event of rain, would have led to a further decrease in cohesion, causing a more significant number and/or extent of gravitational phenomena following an earthquake. Through the analysis of the monthly averages, it is also possible to find out that, in the months of November, the average of monthly rains is equal to 58 mm, so the combined Ida/96E event of November 2009 caused about six times more rains than the November averages.

The area affected by the landslide has a high susceptibility and hazard and, in most areas, a null risk dictated by the absence of the exposed value (Chapter 2.4). However, as shown in Chapter 5.2.2, along the Jiboa River, which flows from the eastern shore of Lake Ilopango to the Ocean to the south, there have been hundreds of rotational slides and debris flows, mainly of Tierra Blanca, which generated a natural dam along the watercourse, which could have resulted in catastrophic consequences due to the potential failure of the unstable landslide dam. In addition, landslides are a significant cause of disruption to rescue lines in mountainous areas (Bird & Bommer, 2004), restricting, in this way, access to affected areas, causing delays in search and lack of rapid rescue (Nowicki et al., 2018). These factors lead to high rates of the exposed value, increasing the risk of landslides and leading to the need for risk mitigation.

6.2.2. Mapping strategy

As seen in Chapter 2.6, producing a landslide inventory is one of the foremost essential steps for generating a valuable landslide susceptibility map. The preparation of any

susceptibility map requires at least the availability or recognition of a landslide inventory which has to be related to a specific trigger (both seismic or extreme rainfall events).

The landslides selected for the analysis of landslide susceptibility related to this work are obtained in an area of intersection between the areas where gravitational phenomena related to the earthquake of February 2001 and the Ida/96E event of November 2009 occurred.

The dataset belonging to the seismic trigger of February 2001 was obtained following mapping from aerial photos obtained a few days after the earthquake by CNR and carried out in the most affected areas, corresponding to the higher PGA and MMI values obtained due to the seismic event (Chapter 5.1.2). The whole inventory (FEB), distributed over an area of about 305 km^2, consists of both 5,371 manually mapped landslide polygons and Landslide Identification Points (LIPs) located at the highest point of gravitational phenomena.

As the event related to the landslides triggered following the event Ida/96E, an inventory related to the area of the Ilopango Caldera was obtained from an inventory from Martinello et al. (2022). This inventory contains 43,867 LIPs in an area of about 367 km^2. These LIPs inventories were mapped through Google Earth orthophotos, in the first time window available, after the November 2009 trigger event. In fact, since vegetation in tropical zones is recovering rapidly, gravitational phenomena must be mapped shortly after the triggering event (Mercurio et al., 2021).

As for the 2001 seismic inventory, apart from the LIPs, landslide polygons were also available; however, these were not employed since the inventories of the 2009 rain event presented exclusively LIPs. This choice was made to have the same type of identification of the trigger in order to carry out better analysis and comparison between the outputs produced.

All inventories used for this work contain their respective LIPs in the crown of the landslides. In fact, even though there is no agreement on the best location of a point permitting to identify of the conditions which triggered a specific slope failure, several recent studies have successfully adopted LIPs on the top of the phenomena to identify pre-failure

conditions (Rotigliano et al., 2011; Lombardo et al., 2014; Cama et al., 2015; Rotigliano et al., 2018, 2019).

This study analyses the landslide susceptibility relative to the intersection between the FEB area of the seismic event of February 2001 and those related to the heavy rainfall of November 2009. The final result is an intersection area of 33.87 km^2 in which there are 1,612 LIPs related to the earthquake of 2001 (Fig. 6.3 and 6.5) and 9,176 LIPs related to the extreme rainfall event of 2009 (Fig. 6.4 and 6.5).

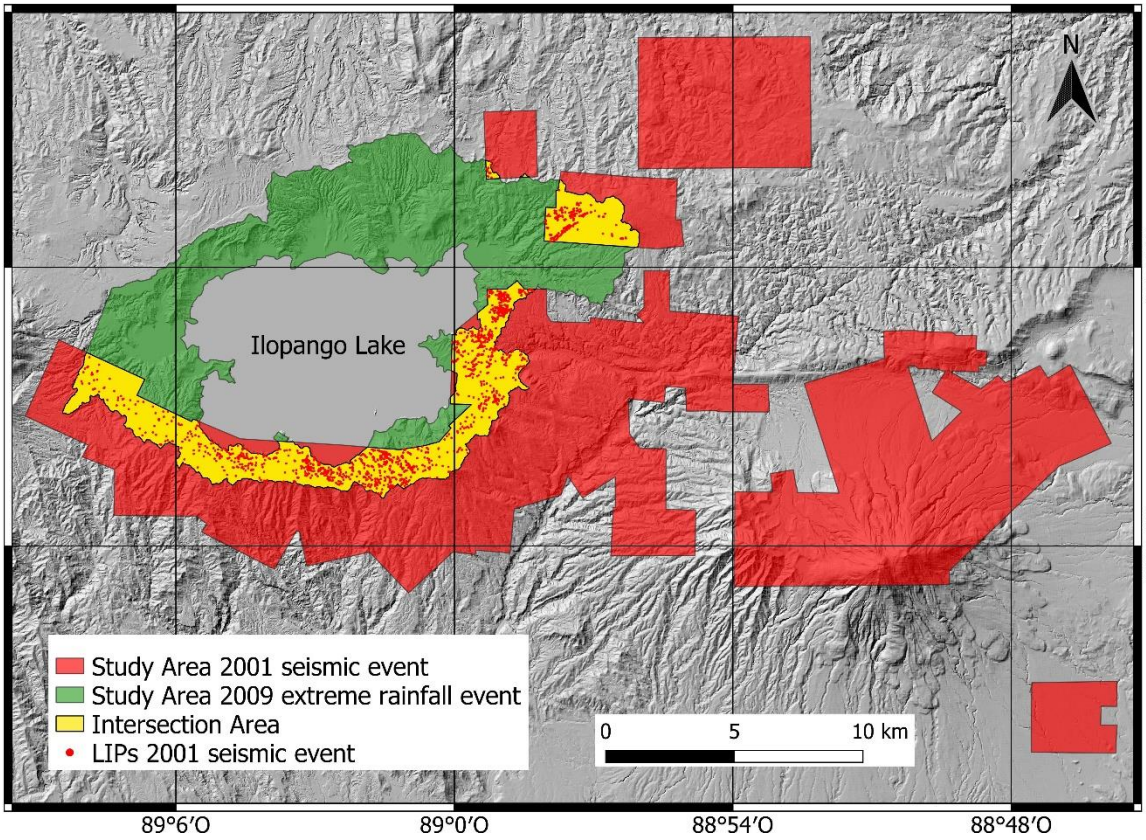

Figure 6.3 – Study area (yellow polygons) with the 1,612 LIPs related to the earthquake event of 13th February 2001.

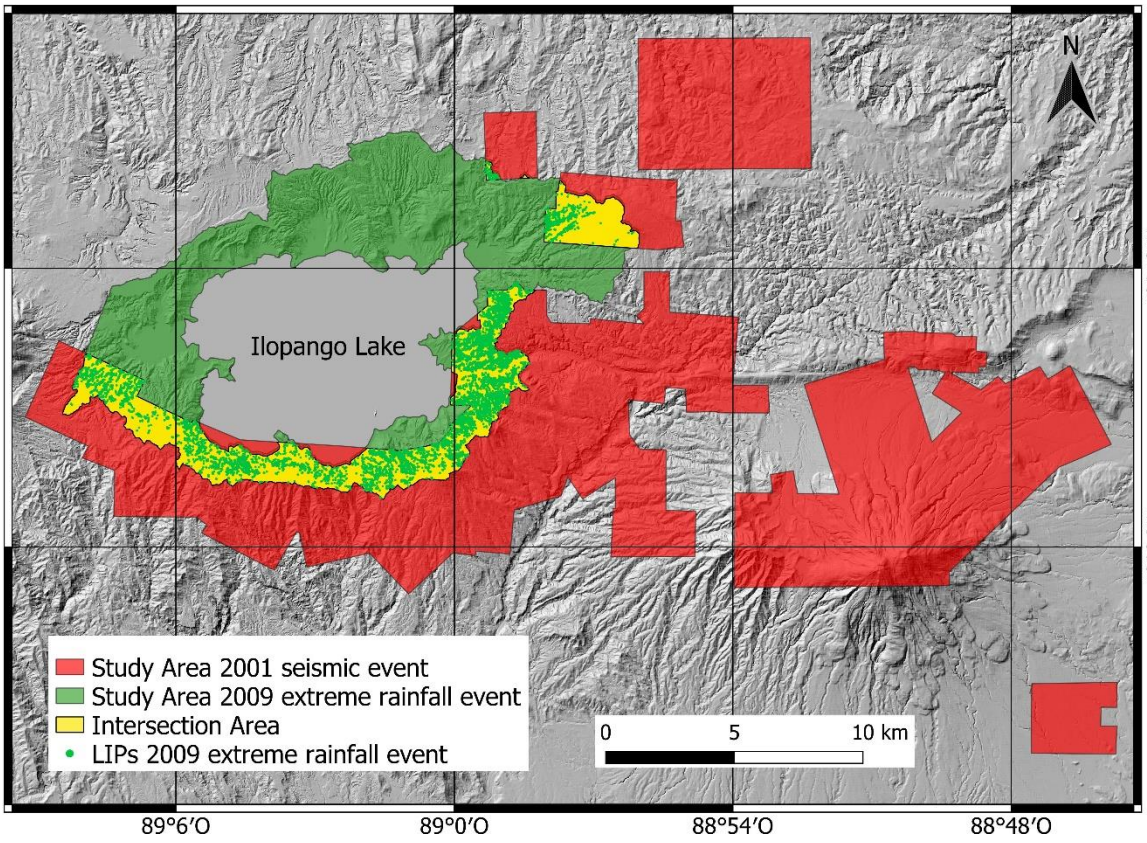

Figure 6.4 – Study area (yellow polygons) with the 9,176 LIPs related to Ida/96E event of November 2009.

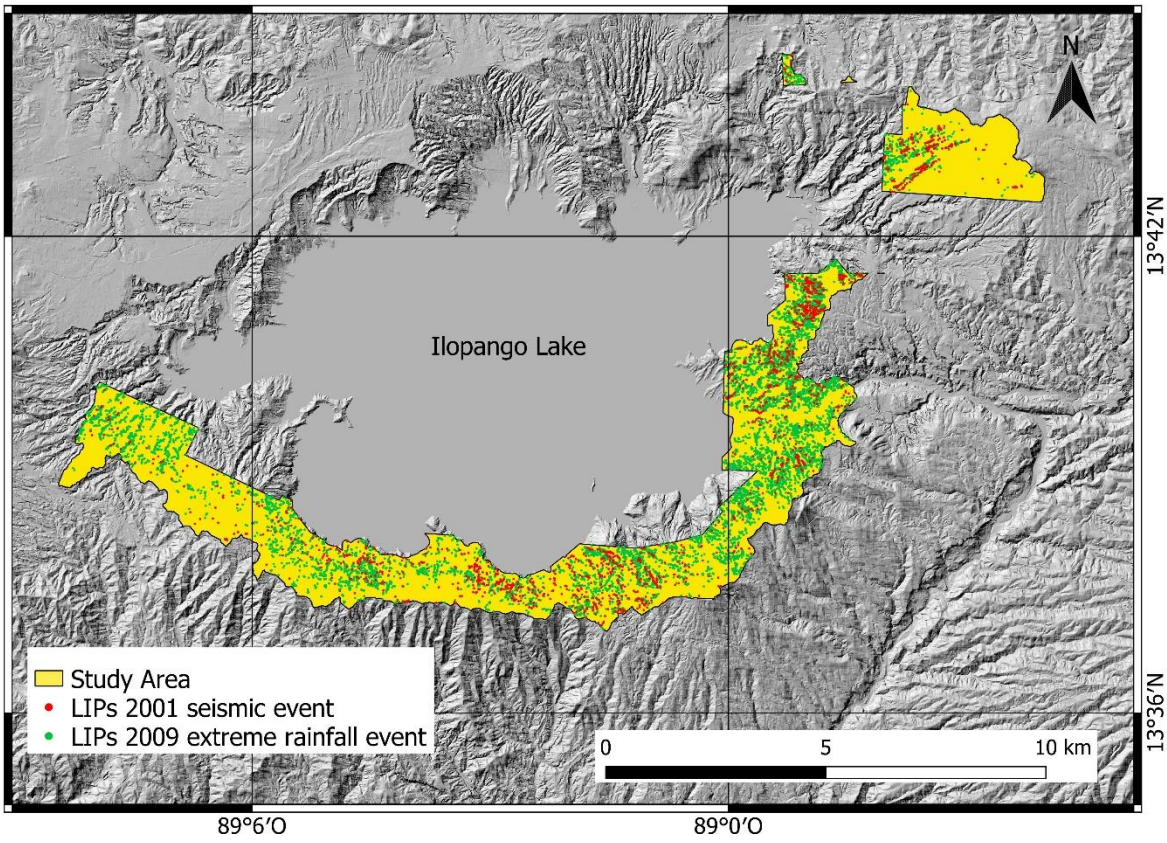

Figure 6.5 – Study area with the LIPs related to both seismic and extreme rainfall events.

6.2.3. Dependent and independent variables

In landslide susceptibility analysis made with stochastic approaches, it would be possible to assign a predictive character to gravitational phenomena through the regression functions that connect the past and present landslide conditions (dependent variable) to a series of predictors or instability factors (independent variables).

As for the binary dependent variable, as for the studies shown in Chapters 4 and 5, which involve the presence or not of the LIP within the selected mapping unit, a binary value has been assigned to each cell (0 = negative, absence; 1 = positive, presence).

As for the independent variables, ten predictive factors, that are supposed to behave as predisposing factors to both earthquake- and rainfall-induction trigger phenomena activations have been selected: *ASP* (aspect), *ELE* (elevation), *GEO* (lithology), *LCL* (landform classification), *PLC* (plan curvature), *PRC* (profile curvature), *SLO* (slope), *SPI* (stream positioning index), *TWI* (topographic wetness index) and *USE* (land use). These variables derive from the 10-m DEM through the application of tools belonging to QGIS and SAGA GIS software, except for GEO and USE, which, respectively, derived from the rasterization of a lithologic map, modified from an original geological map of the country made by Weber et al. (1975) and composed by seven classes (Table 4.1) and the rasterization from a CORINE Land Cover remote survey carried out in 2002 and composed by eleven classes (Table 4.2). All variables are continuous except for USE, LCL and GEO, which are categorical variables. The following variables were selected since they were considered predisposing factors for both the gravitational phenomena that occurred after the earthquake of February 2001 and following the low-pressure system event Ida/96E of November 2009.

Subsequently, two additional continuous variables relating exclusively to the earthquake of February 2001 were prepared. Among the potential variables that are thought to have been decisive in the occurrence of the phenomenon, the observed PGA values (*PGA*) and distances from the earthquake's epicenter (*DIST*) were chosen. PGA values in each 10 m-cell DEM were generated thanks to the rasterization of the shapefile that was made available by the USGS ShakeMap (Worden et al., 2020). That is a product of the USGS

seismic hazard prevention program, in conjunction with regional seismic systems (Wald et al., 2005). ShakeMaps provide near-real-time maps of ground movement and earthquake intensity after significant seismic phenomena. These maps are made available, easily accessible and free of charge by the official website of the USGS and can be used by governments, civil protection authorities and any other public and private figure for scientific and future planning purposes concerning what happened in the past earthquakes. The epicentral distances variable was obtained by developing a raster containing the distance values (in meters) from the epicenter coordinates obtained from the USGS ShakeMap website.

6.2.4. Modelling technique

The probability of landslide occurrence at each 10 m grid cell within the study area was calculated using the Multivariate Adaptive Regression Splines statistical modelling technique (MARS; Friedman 1991) by using the R software with the *earth* package (Milborrow; 2020).

Two different models of prediction of gravitational phenomena triggered by seismic events are carried out; one through the use of ten static variables, the other through the use of the same ten variables and the two seismic parameters. The final result is that each 10x10m-cell will contain the continuous or categorical value of each of the ten/twelve rasters used as an independent variable. Then, each of the predictive variables was analyzed to see if they had any correlations between two or more of them. In order to avoid collinearity problems, the Variance Inflation Index (VIF) has to be < 10 (Heckmann et al., 2014; Jebur et al., 2014; Bui et al., 2015; Conoscenti et al., 2016), excluding any variables with higher values.

Both models were validated by splitting 100 random samples of event and non-event 10- m pixels into training and test subsets.

The predictive skill of the models was evaluated by preparing, for each of the 100 models' run, a ROC curve and by calculating the AUC curve. In order to evaluate the

model’s performance by also using cut-off dependent metrics, an optimal cut-off value for the 100 ROC curves was calculated by using Youden's index (*J*) (Youden, 1950; Cama et al., 2017; Rotigliano et al., 2019; Conoscenti et al., 2020), which is the threshold that optimizes the sum between the sensitivity and the specificity.

6.2.5. Calibration and validation strategy

In order to assess the predictive capabilities of a model and hence its performance, calibration and validation are required. There are different types of calibration and validation; for example, these can be done with the same inventory, using a certain percentage selected for calibration and then the remaining percentage for validation. In this case, the model's final result may be affected by the size of the calibration and validation dataset (Brenning, 2005; Vorpahl et al., 2012; Vargas-Cuervo et al., 2019). However, calibration may also be performed with the entirety of a specific inventory that may be used to validate another entire different one. In the latter case, the validations can be either spatial, then carried out in another area (belonging to the same trigger event) with comparable geo-environmental characteristics or temporal if the validation is carried out in the same calibration area following a different trigger. The present work deals with verifying a forecast map of phenomena following a rainfall event to predict the areas where it is most likely that there will manifest earthquake-induction landslides in the future. As a matter of fact, a calibration of precipitation-induction phenomena and a chrono-validation of earthquake-induction phenomena in the same areas is carried out.

Differences in temporal validations between models trained under normal or extreme event triggered landslide scenarios have been examined in other articles (Rotigliano et al., 2019); however, a case where a rainfall-induction inventory could foresee areas where earthquake-induction landslides may occur has not yet been presented.

6.3. Results

6.3.1. Calibration and validation of the MARS predictive models

The main aim of this study was to evaluate the ability of rainfall-induced landslides susceptibility models to predict the geographical distribution of the coseismic slope failures that occurred in February 2001, using a backward chrono-validation.

The intersection between the areas where both events occurred, in which landslide inventories are kept for each trigger, have been divided into 403,058 10-m grid cells, corresponding to the pixels of the employed DEM. This dataset includes 8,816 positive cells (pixels that contain at least one LIP) and 394,242 negative cells (pixels not intersecting any LIP), 2.19% and 97.81% compared to the study area, respectively. In order to investigate the task of the research, the following susceptibility models were prepared and validated (Tab. 6.1).

Table 6.1 – Inventories and independent variables used for the two models.

Model	**Inventory for Calibration**	**Predictive variables**	**Inventory for Validation**
IDA2009rain	2009 Ida/96E LIPs	10 Static variables	2001 earthquake LIPs
IDA2009rain_pga_dist		10 Static + 2 Dynamic variables (PGA, DIST)	

For both models (*IDA2009rain* and *IDA2009rain_pga_dist*), the presences/absences in each 10-m cell of all the 9,176 LIPs referring to the rainfall-induction event of November 2009 were used for the calibration, while the dataset referred to the 1,612 LIPs has been used entirely and exclusively for the validation. Both models were validated by splitting 100 random samples of event and non-event 10- m pixels into training and test subsets.

The *IDA2009_rain* model was tested to recognize the earthquake-induced landslides, according to a time/trigger partition scheme, by using the ten static predictive variables. The resulting AUC mean value is 0.7, showing an acceptable performance of earthquake-

induction landslide prediction (Fig. 6.6). In addition, the standard deviation for the obtained AUC values is calculated to assess the stability of the model.

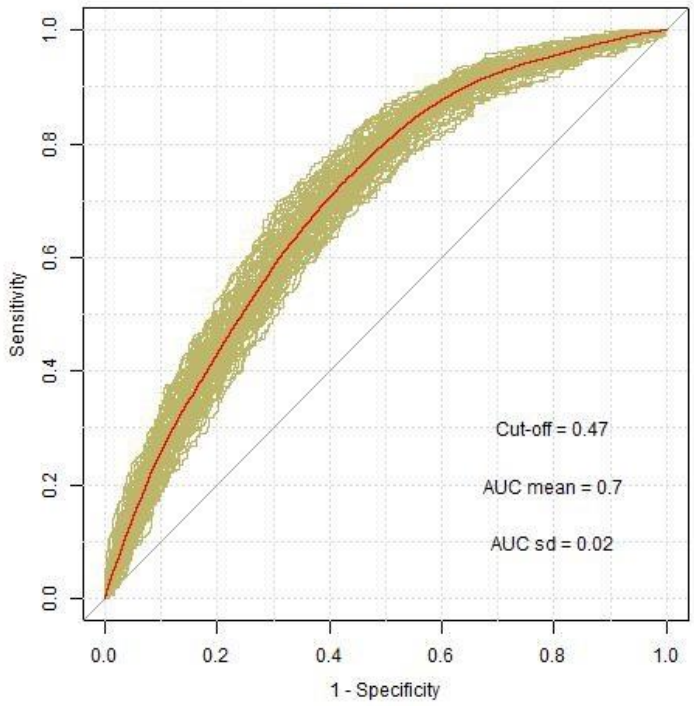

Figure 6.6 – ROC curves processed for the model *IDA2009rain* using the MARS method in the study area.

The average ROC curve was employed to calculate Youden's index *J*, which is equal to 0.47 and represents the optimal cut-off value, allowing to maximise of the sum of sensitivity and specificity. This value was employed to calculate an average confusion matrix (Tab. 6.2). The values below *J* value are predicted as negative (absence of landslide), in contrast, those above are predicted as positive (presence of landslide), thus making the susceptibility map output from landslide with binarized values. By comparing the validation dataset with the binarized map, it is possible to evaluate the model's performance with a confusion matrix by calculating the amount of true positive (TP), true negative (TN), false positive (FP) and false negatives (FN).

Table 6.2 – AUC values (mean and standard deviation), confusion matrix and sensitivity and specificity obtained following the application of the Ida2009rain model.

Model	AUC mean	AUC sd	TP	TN	FP	FN	Sensitivity	Specificity
Ida2009rain	0.7	0.02	1,203	231,341	164,349	387	0.76	0.58

Subsequently, an *IDA2009rain_pga_dist* model was obtained by combining the 2009 inventory with the ten static predictive variables and the observed PGA and epicentral distances (DIST), both related to the 13th February 2001 event, to observe a better or worse forecast of earthquake-induction phenomena following the addition of seismic parameters to the base model. An improvement in the model's predictive performance is obtained, demonstrated by the AUC mean value of 0.75, showing that the addition of seismic parameters to a model trained by rainfall events-induction leads to an improvement in the predictive performance of landslides induced by seismic phenomena (Fig. 6.7).

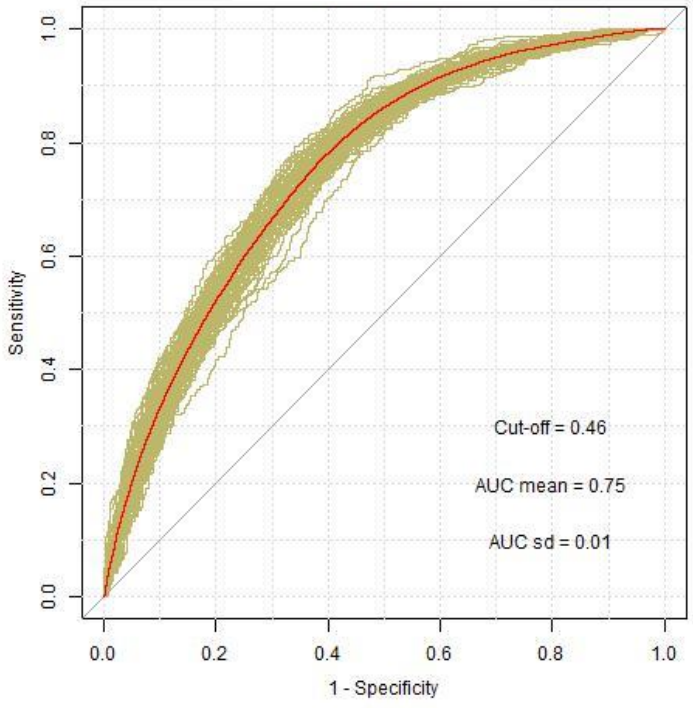

Figure 6.7 – ROC curves processed for the model *IDA2009rain_pga_dist* using the MARS method in the study area.

Also for this model, the average ROC curve was employed to calculate Youden's index *J*, which is equal to 0.47. This value was employed to calculate an average confusion matrix (Tab. 6.3).

Table 6.2 – AUC values (mean and standard deviation), confusion matrix and sensitivity and specificity obtained following the application of the Ida2009rain model.

Model	AUC mean	AUC sd	TP	TN	FP	FN	Sensitivity	Specificity
Ida2009rain_pga_dist	0.75	0.01	1,241	252,287	143,403	349	0.78	0.64

6.4. Discussion and Conclusions

In this chapter, the predictive capacity of seismic-induction landslides has been evaluated using a landslide susceptibility model (*IDA2009rain*) based on a rainfall-induction inventory and ten static predictive variables, by adopting the MARS technique. Subsequently, any improvement/worsening of predictive capabilities through the susceptibility model was evaluated *IDA2009rain_pga_dist*. The difference between the two models is in the total of independent variables used, corresponding to ten static variables, described in Cap. 6.2.3, and the same ten variables with the addition of two dynamic variables, corresponding to the values of PGA and DIST, both referred to the event of 13th February 2001. An improvement in the predictive performance of the second model compared to the first is obtained, from a value of 0.7 to 0.75.

The improvement of the AUC value of the second model is confirmed by the increase of the values of Sensitivity and Specificity, which, in turn, depend on the values of TP, TN, FP, and FN. In fact, the increase in TP and the decrease in FN leads to an increase in Sensitivity (defined as TP/(TP+FN)), while the increase in TN values and the decrease in FN FP values leads to an increase in Sensitivity (defined as TN/(TN+FP)). The increase of TP and TN and the decrease of the values of FP and FN is an essential point in the characteristics of a model, since it decreases the error. As seen in Chapter 2.5, FP represents

a "type 1 error", in which one predicts how a pixel falls when it does not manifest. It is a less serious error than the FN, a "type 2 error" in which a pixel is predicted as negative while a landslide has occurred.

In addition to the performance improvement of the second model compared to the first, there is also a decrease in the standard deviation value, testifying to better model stability.

The return times of extreme rain phenomena are shorter than those of earthquakes. That is evidenced by the extreme rainfall events and the number of earthquakes in the country in the last century. As a result, earthquake-induction landslide inventories and associated susceptibility maps are more complex to obtain than those acquired due to rainfall-induction phenomena. The results from this research suggest the possibility of coupling the susceptibility scores obtained from static modelling to the expected mechanical shaking for the earthquake-induced susceptibility assessment. Indeed, the approach proposed in the study, which to be valid had to be tested in an area where both types of triggers occurred, shows that a model calibrated on extreme rainfall events, recurring in the country due to its geographical position in a tropical sector, can acceptably predict the areas where gravitational phenomena of seismic origin may occur. The addition of typically seismic parameters, used as additional predictive variables, also increases the performance of the earthquake-induction landslide prediction model. These results allow proposing to use this methodology where inventories and susceptibility maps related to gravitational phenomena originating from seismic triggers are missing to provide valid outputs to civil protection authorities.

7. Conclusions

Since the high vulnerability of the territory of El Salvador, the high landslide hazard, occurring as a result of extreme rain and earthquake phenomena and the high rate of exposed values involved, the risk associated to gravitational phenomena is very high. In fact, El Salvador is affected both by extreme rain events due to its geographical position in a tropical setting and also by intense earthquakes that occur due to the complex geodynamic context characterized by the presence of more tectonic plates and the lithology of the outcropping volcanic rocks (pseudo-inconsistent and inconsistent). The presence of the main population centres around the active volcanoes, generated due to the geodynamic context, makes the country at high risk due to the proximity to the areas most susceptible to landslides (mainly debris flow/avalanches, falls in debris and rocks and slides). Since the associated high risk, it is essential to carry out an analysis of the areas that may be most susceptible to the manifestation of gravitational phenomena, in order to know the areas to be evacuated, in which to carry out landslide mitigation work and those in which to send aid first following such phenomena.

The case studies that have been analyzed have been that of extreme rainfall generated by the combination of hurricane Ida and the low-pressure 96E event, which occurred in November 2009 (Chapters 3.1 and 4) and the two seismic phenomena that occurred in the first two months of 2001, with a magnitude of 7.7 and 6.6 (Chapter 3.2, 5 and 6). Both types of phenomena have caused numerous victims. A study of these phenomena and a generation of maps of susceptibility serves to limit, as much as possible, the damage caused by future phenomena and to provide output to civil protection agencies. Numerous studies have shown the effectiveness of stochastic methods (statistical, indirect and objective) for producing susceptibility maps from landslides. The method used in this work was the MARS technique (Multivariate Analysis Regression Splines), which demonstrated its effectiveness for the objective in numerous works.

In Chapter 4, a study was carried out to produce a susceptibility map from a rainfall-induced landslides in an area that has been particularly affected by gravitational phenomena

(especially debris flow). This corresponds to an area of 287 km^2, where San Vicente, Guadalupe, Tepetitan and Verapaz towns are located. 5,609 Landslide Identification Points (LIPs) were used as inventory, using 75% of calibration phenomena that were validated with the remaining 25% in order to evaluate the predictive capabilities of the statistical model used. The models were validated by splitting 100 random samples of event and non-event 10 m pixels into training and test subsets. The average model has provided excellent predictive performances, testified by the AUC value of 0.80. In addition, it shows a high stability of the model, demonstrated by the standard deviation value of 0.01.

When using Youden's index as a probability threshold to discriminate between pixels predicted as positives and negatives, MARS exhibits an almost-excellent (Hosmer and Lemeshow, 2000) ability to identify the True Positives (TP), testified by the value of Sensitivity (True Positive Rate, refers to the probability of a positive test, conditioned on truly being positive) equal to 0.79. However, as already happened in further works carried out in volcanic areas of El Salvador, MARS exhibits a moderate ability to identify True Negative (TN), testified by the value of Specificity to 0.66. The final result made it possible to produce a rainfall susceptibility map with high predictive capabilities, transmitted and received by MARN (Ministerio de Medio Ambiente y Recursos Naturales), which now uses it as the official map for the metropolitan areas of Guadalupe, Tepetitan and Verapaz.

Chapter 5 aimed to create earthquake-induced landslide susceptibility maps related to two seismic phenomena that occurred in the first two months of 2001 (M 7.7, offshore at a depth of 60 km and 6.6, onshore at a depth of 10 km respectively), have caused thousands of gravitational phenomena (mainly debris flow and avalanches, slides and rock and debris falls). Both 2001 earthquakes triggered similar landslides, but their distribution varied because of different earthquake source parameters due to the magnitude value, the epicentral distance and the hypocentral depth (Keefer, 1984; Martino et al., 2014). In fact, events with deeper hypocenters can trigger landslides at a greater distance than events with lower hypocentral depths, although the latter can generate more high-density phenomena (Keefer,

1984). The objective was to predict the areas most affected by seismic-induction phenomena using two different scenarios: the first one in which a calibration with 3/4 of the landslides is carried out with which the objective is to predict the remaining 1/4 and a second scenario in which only 5% is known, therefore a minimal amount of gravitational phenomena, in order to predict the remaining 95%. That condition often occurs after earthquakes, in which only significant events are mapped to produce rapid reports for environmental management authorities. Four different landslide susceptibility models have been created, using both the rainfall-induction inventory generated in San Vicente in 2009 (M1) and the earthquake-induction inventories related to the events of 2001 (M2, M3, M4). All models used have been validated with the remaining percentage of earthquake-induction landslides. The predictive variables used in each model were different, intending to see the predictive capabilities after adding or removing sets of predictive variables. The best predictive performance model (M4) achieved acceptable to outstanding predictions of earthquake-induction landslides (depending on the dataset used) using landslides susceptibility map from rainfall-induction landslides, Static Predictors and PGA and Epicentral Distances. In fact, it is demonstrated that using only earthquake-induced landslides to predict earthquake-induction scenarios is partial. Indeed, if characteristics from the rainfall-induction analysis are added, the earthquake-induced susceptibility model improves its performance. The scenario in which only a tiny amount of gravitational phenomena are foreseen has also shown an excellent predictive ability of gravitational phenomena. The excellent results obtained following this test suggest that, if only some of the landslides triggered by an earthquake are known, it is possible to use the approach proposed in this study to identify those sites where the other landslides are more likely to have occurred following a seismic phenomenon. In this way, it would be enough to generate only the rasters of NDVI, PGA and Epicentral Distances, easily available and generated online. Partial mapping is never ideal for producing landslide susceptibility maps; however, the results obtained in the second scenario suggest that it is possible to quickly generate an earthquake-induced susceptibility map immediately after a seismic event.

Since the tropical geographical context in which El Salvador is located, the extreme rainfall phenomena exhibit relatively shorter return times than earthquakes. That means that earthquake-induction inventories and their related earthquake-induced landslide susceptibility maps are more difficult to obtain than those related to rainfall-induction landslides. Therefore, if it would be possible to figure out how to generate earthquake-induced susceptibility models using rainfall-induced inventories, which are relatively easier to find, it might be possible to generate more earthquake-induced susceptibility maps. To carry out this test and assess its validity, it is necessary to study an area affected by both types of triggers. For this reason, in Chapter 6, the aim was to create an earthquake-induced landslide susceptibility map from an inventory of rainfall-induction landslides, carrying out the analysis in a sector of the country affected by both types of triggers, corresponding to the south and south-eastern sector of the Ilopango Caldera. In fact, this sector of the country was hit by both the earthquake of February 2001 and the event Ida/96E of 2009. Using the inventory of earthquake-induced landslides of 2001 and an inventory derived from the article from Martinello et al. (2022), it was possible to carry out the analysis through two models. For both models, the presences/absences in each 10-m cell of all the 9,176 LIPs referring to the rainfall-induction event of November 2009 were used for the calibration, while the dataset referred to the 1,612 LIPs has been used entirely and exclusively for the validation.

These models differ according to the variables used. The first model (*Ida2009rain*) has ten common predictive variables for both rainfall and earthquake induction, while the second model (*Ida2009rain_pga_dist*) uses the same variables as the previous model with the addition of two dynamic variables (Peak Ground Accelerations and Epicentral Distances), relating exclusively to the earthquake-induction trigger.

The *Ida2009rain* model achieved an average AUC value of 0.70, testifying to the model's acceptable (Hosmer and Lemeshow, 2000) predictive capability. However, in the *Ida2009rain_pga_dist* model, obtained with the addition of the two dynamic variables to those used in the previous model, an improvement in predictive performance is obtained,

evidenced by the AUC value of 0.75. In addition to the value of AUC, there is an improvement also in the sensitivity and specificity values, testifying to an upgrade in the predictive ability of True Positives and Negatives. AUC values are lower than the excellent and outstanding values obtained in Chapter 5. That is because an earthquake-induced landslide susceptibility map is generated from a rainfall-induced landslide inventory, not from earthquake-induced landslides. However, the results are more than acceptable (Hosmer and Lemeshow, 2000). Since it is possible to generate earthquake-induction susceptibility maps by combining rainfall-induction landslide inventories with seismic parameters, it would be possible to produce earthquake-induction landslide susceptibility maps everywhere, even when seismic-induction inventories are missing.

Table 7.1 shows the results obtained for the applications made in Chapters 4, 5 and 6.

Table 7.1 – Inventories, variables and results obtained for each of the seven models used in this thesis.

Chapter	Inventory for Calibration	Variables	Inventory for Validation	Results
4	Rainfall-induced landslides (75%)	10 predictive variables	Rainfall-induced landslides (25%)	Excellent prediction of **rainfall-induced landslides** using MARS
5	Rainfall-induced landslides (Scenario 1: 75%; Scenario 2: 5%);	*Model 1*: Probability of occurrences of rainfall-induced lanslides by using 11 predictive variables (PSV)	Earthquake-induced landslides (Scenario 1: 25%; Scenario 2: 95%)	Acceptable to Outstanding predictions of **earthquake-induced landslides** using landslides susceptibility map from rainfalls-induction landslides, Static Predictors and PGA and Epicentral Distances. The use of only earthquake-induced landslides to predict earthquake-induction scenarios is partial. Indeed, if we add information from the rainfall-induction analysis the earthquake-induced susceptibility model improves its performance. Scenario 2 models (95% validation) also performed very well.
	Earthquake-induced landslides (Scenario 1: 75%; Scenario 2: 5%);	*Model 2*: PSV; 2 Dynamic predictors (PGA, Epicentral distances)		
	Earthquake-induced landslides (Scenario 1: 75%; Scenario 2: 5%);	*Model 3*: 11 Static predictors; 2 Dynamic predictors (PGA, Epicentral distances)		
	Earthquake-induced landslides (Scenario 1: 75%; Scenario 2: 5%);	*Model 4:* PSV; 11 Static predictors; 2 Dynamic predictors (PGA, Epicentral distances)		
6	Rainfall-induced landslides (100%);	*Ida2009rain:* 10 Static predictors	Earthquake-induced landslides (100%)	Improving performances predicting **earthquake-induced landslides** when PGA and Epicentral Distances are added to the rainfall-induced landslides susceptibility model. Since it is possible to generate earthquake-induction susceptibility maps by combining rainfall-induction landslide inventories with seismic parameters, it would be possible to produce earthquake-induction landslide susceptibility maps even where seismic-induction inventories are missing
		Ida2009rain_pga_dist: 10 Static predictors; 2 Dynamic predictors (PGA, Epicentral distances)		

References

Carrara, Agnesi, Macaluso, Monteleone, Pipitone. **1986**. “Slope Movements Induced by the Southern Italy Earthquake of November 1980.” IAEG 2: 237–50.

Agnesi, Carrara, Macaluso, Monteleone, Pipitone, M. Sorriso-Valvo. **1982**. “Preliminary Observations of Slope Instability Phenomena Induced by the Earthquake of November 1980 on the Upper Valley of Sele River” Geologia Applicata e Idrogeologia 17 (1): 79–93.

Agnesi, Carrara, Macaluso, Monteleone, Pipitone, Sorrivo-Valvo. **1983**. “Elementi Tipologici e Morfologici Dei Fenomeni Di Instabilityà Dei Versanti Indotti Dal Sisma Del 1980 (Alta Valle Del Sele).” Geologia Applicata e Idrogeologia XVIII (I): 309–41.

Agnesi, Camarda, Conoscenti, Di Maggio, Diliberto, Madonia, Rotigliano. **2005**. “A Multidisciplinary Approach to the Evaluation of the Mechanism That Triggered the Cerda Landslide (Sicily, Italy).” Geomorphology 1–2 (65): 101–16. https://doi.org/10.1016/J.GEOMORPH.2004.08.003.

Allison. **1999**. “Logistic Regression Using the SAS System: Theory and Application, SAS Institute Inc., Cary, NC.” 1999. http://www.sciepub.com/reference/248083.

Avelar, Netto, Lacerda, Becker, Mendonça. **2013**. “Mechanisms of the Recent Catastrophic Landslides in the Mountainous Range of Rio de Janeiro, Brazil.” In Landslide Science and Practice: Global Environmental Change. https://doi.org/10.1007/978-3-642-31337-0-34.

Avila, Cangialosi. **2009a**. “Tropical Cyclone Report.”

Avila. **2009b**. “Síntesis de Los Informes de Evaluación Técnica de Las Lluvias Del 7 y 8 de Noviembre 2009 En El Salvador: Análisis Del Impacto Físico Natural y Vulnerabilidad Socio Ambiental”.

Bent, Evans. **2004**. “The MW 7.6 El Salvador Earthquake of 13 January 2001 and Implications for Seismic Hazard in El Salvador.” Special Paper of the Geological Society of America 375: 397–404. https://doi.org/10.1130/0-8137-2375-2.397.

Bird, Bommer. **2004**. “Earthquake losses due to ground failure”, Eng. Geol., 75, 147–179.

Bommer, Benito, Ciudad-Real, Lemoine, López-Menjívar, Madariaga, Mankelow. **2002**. “The El Salvador Earthquakes of January and February 2001: Context, Characteristics and Implications for Seismic Risk.” Soil Dynamics and Earthquake Engineering. https://doi.org/10.1016/S0267-7261(02)00024-6.

Brabb. **1984**. “Innovative Approaches for Landslide Hazard Evaluation”. IV International Symposium on Landslides, Toronto, 307-323. - References - Scientific Research Publishing.” n.d. Accessed November 16, 2020.

Brenning. **2005**. Spatial prediction models for landslide hazards: review, comparison and evaluation. Nat. Hazards Earth Syst. Sci. 5, 853–862. http://dx.doi.org/10.5194/ nhess-5-853-2005.

Bui, Tuan, Klempe, Pradhan, Revhaug. **2015**. Spatial prediction models for shallow landslide hazards: a comparative assessment of the efficacy of support vector machines, artificial neural networks, kernel logistic regression, and logistic model tree. Landslides http://dx.doi.org/10.1007/s10346-015-0557-6.

Cama, Lombardo, Conoscenti, Agnesi, Rotigliano. **2015**. “Predicting Storm-Triggered Debris Flow Events: Application to the 2009 Ionian Peloritan Disaster (Sicily, Italy).” Natural Hazards and Earth System Sciences 15 (8): 1785–1806. https://doi.org/10.5194/nhess-15-1785-2015.

Cama, Conoscenti, Lombardo, Rotigliano. **2016**. “Exploring Relationships between Grid Cell Size and Accuracy for Debris-Flow Susceptibility Models: A Test in the Giampilieri Catchment (Sicily, Italy).” Environmental Earth Sciences 75 (3): 1–21. https://doi.org/10.1007/s12665-015-5047-6.

Cama, Lombardo, Conoscenti, Rotigliano. **2017**. “Improving Transferability Strategies for Debris Flow Susceptibility AssessmentApplication to the Saponara and Itala Catchments (Messina, Italy).” Geomorphology 288 (July): 52–65. https://doi.org/10.1016/j.geomorph.2017.03.025.

Carrara, Cardinali, Guzzetti, Reichenbach. **1995**. “Gis Technology in Mapping Landslide Hazard.” In , 135–75. Springer, Dordrecht. https://doi.org/10.1007/978-94-015-8404-3_8.

Carrara, Crosta, Frattini. **2008**. “Comparing Models of Debris-Flow Susceptibility in the Alpine Environment.” Geomorphology. https://doi.org/10.1016/j.geomorph.2006.10.033.

Castillo, Sotela, Roman. **2011**. “Efectividad De La Metodología Mora-Vahrson Modificada En El Caso De Los Deslizamientos Provocados Por El Terremoto De Cinchona, Costa Rica.” Revista Geográfica de América Central 2(47):141–62. https://www.revistas.una.ac.cr/index.php/geografica/article/view/3970.

Chen, **2006**. “Controlling Factors of Hazardous Debris Flow in Taiwan.” Quaternary International 147 (1): 3–15. https://doi.org/10.1016/J.QUAINT.2005.09.002.

Chung, Fabbri. **2003**. “Validation of Spatial Prediction Models for Landslide Hazard Mapping.” Natural Hazards. Vol. 30.

Chung, Fabbri. **2008**. “Predicting Landslides for Risk Analysis - Spatial Models Tested by a Cross-Validation Technique.” Geomorphology 94 (3–4): 438–52. https://doi.org/10.1016/j.geomorph.2006.12.036.

Clerici, Perego, Tellini, Vescovi. **2006**. “A GIS-Based Automated Procedure for Landslide Susceptibility Mapping by the Conditional Analysis Method: The Baganza Valley Case Study (Italian Northern Apennines).” Environmental Geology 50 (7): 941–61. https://doi.org/10.1007/s00254-006-0264-7.

Conoscenti, Di Maggio, Rotigliano. **2008**. “GIS Analysis to Assess Landslide Susceptibility in a Fluvial Basin of NW Sicily (Italy).” Geomorphology. https://doi.org/10.1016/j.geomorph.2006.10.039.

Conoscenti, Angileri, Cappadonia, Rotigliano, Agnesi, Märker. **2014**. “Gully Erosion Susceptibility Assessment by Means of GIS-Based Logistic Regression: A Case of Sicily (Italy).” Geomorphology 204 (January): 399–411. https://doi.org/10.1016/j.geomorph.2013.08.021.

Conoscenti, Ciaccio, Caraballo-Arias, Gómez-Gutiérrez, Rotigliano, Agnesi. **2015**. “Assessment of Susceptibility to Earth-Flow Landslide Using Logistic Regression and Multivariate Adaptive Regression Splines: A Case of the Belice River Basin (Western Sicily, Italy).” Geomorphology 242 (August): 49–64. https://doi.org/10.1016/j.geomorph.2014.09.020.

Conoscenti, Rotigliano, Cama, Caraballo-Arias, Lombardo, Agnesi. **2016**. “Exploring the Effect of Absence Selection on Landslide Susceptibility Models: A Case Study in Sicily, Italy.” Geomorphology 261 (May): 222–35. https://doi.org/10.1016/j.geomorph.2016.03.006.

Conoscenti, Agnesi, Cama, Caraballo-Arias, Rotigliano. **2018**. “Assessment of Gully Erosion Susceptibility Using Multivariate Adaptive Regression Splines and Accounting for Terrain Connectivity.” Land Degradation and Development 29 (3): 724–36. https://doi.org/10.1002/ldr.2772.

Conoscenti, Rotigliano. **2020**. “Predicting Gully Occurrence at Watershed Scale: Comparing Topographic Indices and Multivariate Statistical Models.” Geomorphology 359 (June). https://doi.org/10.1016/j.geomorph.2020.107123.

Conrad, Bechtel, Bock, Dietrich, Fischer, Gerlitz, Wehberg, Wichmann, Böhner. **2015**. “System for Automated Geoscientific Analyses (SAGA) v. 2.1.4.” Geoscientific Model Development 8 (7): 1991–2007. https://doi.org/10.5194/gmd-8-1991-2015.

Costanzo, Rotigliano, Irigaray, Jiménez-Perálvarez, Chacón. **2012**. “Factors Selection in Landslide Susceptibility Modelling on Large Scale Following the Gis Matrix Method: Application to the River Beiro Basin (Spain).” Natural Hazards and Earth System Sciences 12 (2): 327–40. https://doi.org/10.5194/nhess-12-327-2012.

Costanzo, Chacón, Conoscenti, Irigaray, Rotigliano. **2014**. “Forward Logistic Regression for Earth-Flow Landslide Susceptibility Assessment in the Platani River Basin (Southern Sicily, Italy).” Landslides 11 (4): 639–53. https://doi.org/10.1007/s10346-013-0415-3.

Crone, Baum, Lidke, Sather, Bradley, Tarr. **2001**. “Landslides Induced by Hurricane Mitch in El Salvador -- an Inventory and Descriptions of Selected Features.” Open File Report 01-444.

Cruden, Varnes. **1996**. Landslide Types and Processes. In Turner, A.K. and Shuster, R.L., Eds., Landslides Investigation and Mitigation, Transportation Research Board, Special Report No. 247, 36-75. - References - Scientific Research Publishing.” n.d. Accessed November 16, 2020. https://www.scirp.org/(S(czeh2tfqyw2orz553k1w0r45))/reference/ReferencesPapers.aspx?ReferenceID=1855371.

Desio. **1973**. Geologia Applicata all’Ingegneria, Hoepli Editore, Milano;

Dewey, Suárez. **1991**. “Seismotectonics of Middle America.” Neotectonics of North America, April, 309–21. https://doi.org/10.1130/DNAG-CSMS-NEO.309.

Earle. **2015**. Physical Geology

EPOCH. **1993**. The temporal occurrence and forecasting of landslides in the European community (Ed: Flageollet, J. C.). Contract No. 90 0025, 3 Volumes.

Evans, Bent. **2004**. “The Las Colinas Landslide, Santa Tecla: A Highly Destructive Flowslide Triggered by the January 13, 2001, El Salvador Earthquake.” Special Paper of the Geological Society of America 375: 25–37. https://doi.org/10.1130/0-8137-2375-2.25.

Frattini, Crosta, Carrara. **2010**. “Techniques for Evaluating the Performance of Landslide Susceptibility Models.” Engineering Geology 111 (1–4): 62–72. https://doi.org/10.1016/J.ENGGEO.2009.12.004.

Friedman. **1991**. “Multivariate Adaptive Regression Splines.” The Annals of Statistics 19 (1): 1–67. https://doi.org/10.1214/aos/1176347963.

Galli, Ardizzone, Cardinali, Guzzetti, Reichenbach. **2008**. “Comparing Landslide Inventory Maps.” Geomorphology 94 (3–4): 268–89. https://doi.org/10.1016/J.GEOMORPH.2006.09.023.

García-Rodríguez, Malpica, Benito, Díaz. **2008**. “Susceptibility Assessment of Earthquake-Triggered Landslides in El Salvador Using Logistic Regression.” Geomorphology 95 (3–4): 172–91. https://doi.org/10.1016/j.geomorph.2007.06.001.

García-Rodríguez, Malpica. **2010**. “Assessment of Earthquake-Triggered Landslide Susceptibility in El Salvador Based on an Artificial Neural Network Model.” Natural Hazards and Earth System Science 10 (6): 1307–15. https://doi.org/10.5194/nhess-10-1307-2010.

Garosi, Sheklabadi, Pourghasemi, Besalatpour, Conoscenti, Van Oost. **2018**. “Comparison of Differences in Resolution and Sources of Controlling Factors for Gully Erosion Susceptibility Mapping.” Geoderma 330 (November): 65–78. https://doi.org/10.1016/j.geoderma.2018.05.027.

Gutiérrez, Schnabel, Lavado-Contador. **2009**. “Using and Comparing Two Nonparametric Methods (CART and MARS) to Model the Potential Distribution of Gullies.” Ecological Modelling 220 (24): 3630–37. https://doi.org/10.1016/j.ecolmodel.2009.06.020.

Gutiérrez, Conoscenti, Angileri, Rotigliano, Schnabel. **2015**. “Using Topographical Attributes to Evaluate Gully Erosion Proneness (Susceptibility) in Two Mediterranean Basins: Advantages and Limitations.” Natural Hazards 79 (1): 291–314. https://doi.org/10.1007/s11069-015-1703-0.

Guzzetti, Carrara, Cardinali, Reichenbach. **1999**. “Landslide Hazard Evaluation: A Review of Current Techniques and Their Application in a Multi-Scale Study, Central Italy.” In Geomorphology, 31:181–216. Elsevier. https://doi.org/10.1016/S0169-555X(99)00078-1.

Guzzetti, Reichenbach, Cardinali, Galli, and Ardizzone. **2005**. “Probabilistic Landslide Hazard Assessment at the Basin Scale.” Geomorphology 72 (1–4): 272–99. https://doi.org/10.1016/j.geomorph.2005.06.002.

Guzzetti, Reichenbach, Ardizzone, Cardinali, Galli. **2006**. “Estimating the Quality of Landslide Susceptibility Models.” Geomorphology 81 (1–2): 166–84. https://doi.org/10.1016/j.geomorph.2006.04.007.

Hair, Black, Babin, Anderson. **2010**. “Multivariate Data Analysis: A Global Perspective: Pearson Education International.” In New Jersey.

Hansen.**1984**. Landslide Hazard Analysis. In: Brunsden, D. & Prior, D.B. (Eds.), Slope Instability, John Wiley and Sons, New York, Pp. 523-602.” n.d. Accessed October 1, 2022. http://www.sciepub.com/reference/209033.

Hayashi, Self. **1992**. “A Comparison of Pyroclastic Flow and Debris Avalanche Mobility.” Journal of Geophysical Research: Solid Earth 97 (B6): 9063–71. https://doi.org/10.1029/92JB00173.

Heckmann, Gegg, Gegg, Becht. **2014**. “Sample Size Matters: Investigating the Effect of Sample Size on a Logistic Regression Susceptibility Model for Debris Flows.” Natural Hazards and Earth System Sciences 14 (2): 259–78. https://doi.org/10.5194/nhess-14-259-2014.

Hosmer, Lemeshow. **2000**. Applied Logistic Regression. Applied Logistic Regression. Hoboken, NJ, USA: John Wiley & Sons, Inc. https://doi.org/10.1002/0471722146.

Hungr, Leroueil, Picarelli. **2014**. "The Varnes Classification of Landslide Types, an Update." Landslides. https://doi.org/10.1007/s10346-013-0436-y.

Hutchinson. **1988**. General Report: Morphological and geotechnical parameters of landslides in relation to geology and hydrogeology. Proceedings, Fifth International Symposium on Landslides (Ed: Bonnard, C.), 1, 3-35

Major, Schilling, Pullinger, Escobar, Howell. **2001**. "USGS Open-File Report 01-367: Volcano-Hazard Zonation for San Vicente Volcano, El Salvador." 2001. https://pubs.usgs.gov/of/2001/0367/.

Javidan, Kavian, Pourghasemi, Conoscenti, Jafarian, Rodrigo-Comino. **2021**. "Evaluation of Multi-Hazard Map Produced Using MaxEnt Machine Learning Technique." Scientific Reports 2021 11:1 11 (1): 1–20. https://doi.org/10.1038/s41598-021-85862-7.

Jebur, Pradhan, Tehrany. **2014**. Optimization of landslide conditioning factors using very high-resolution airborne laser scanning (LiDAR) data at catchment scale. Re- mote Sens. Environ. 152, 150–165. http://dx.doi.org/10.1016/j.rse.2014.05.013.

Jibson, Crone, Harp, Baum, Major, Pullinger, Escobar, Martínez, Smith. **2004**. "Landslides Triggered by the 13 January and 13 February 2001 Earthquakes in El Salvador." Special Paper of the Geological Society of America. https://doi.org/10.1130/0-8137-2375-2.69.

Keefer. **1984**. "Landslides Caused by Earthquakes." Geological Society of America Bulletin 95 (4): 406–21.

Keith. **2014**. Multiple Regression and Beyond. Multiple Regression and Beyond. https://doi.org/10.4324/9781315749099.

Kopačková, Šebesta. **2007**. "An Approach for GIS-Based Statistical Landslide Susceptibility Zonation: With a Case Study in the Northern Part of El Salvador." Remote Sensing for Environmental Monitoring, GIS Applications, and Geology VII 6749 (October): 67492R. https://doi.org/10.1117/12.737835.

Larsen. **2006**. "Geomorphic Effects of Large Debris Flows and Flash Floods, Northern Venezuela, 1999." Zeitschrift Fur Geomorphologie, Supplementband.

Larsen. **2008**. "Rainfall-Triggered Landslides, Anthropogenic Hazards, and Mitigation Strategies." Advances in Geosciences. https://doi.org/10.5194/adgeo-14-147-2008.

Legros. **2002**. "The Mobility of Long-Runout Landslides." Engineering Geology 63 (3–4): 301–31. https://doi.org/10.1016/S0013-7952(01)00090-4.

Lombardo, Cama, Maerker, Rotigliano. **2014**. "A Test of Transferability for Landslides Susceptibility Models under Extreme Climatic Events: Application to the Messina 2009 Disaster." Natural Hazards 74 (3): 1951–89. https://doi.org/10.1007/s11069-014-1285-2.

Lomnitz, Rodriguez. **2001**. "El Salvador 2001: Earthquake Disaster and Disaster Preparedness in a Tropical Volcanic Environment." Seismological Research Letters 72 (3): 346–51. https://doi.org/10.1785/GSSRL.72.3.346.

Major, Schilling, Pullinger, Escobar. **2004**. "Debris-Flow Hazards at San Salvador, San Vicente, and San Miguel Volcanoes, El Salvador." Special Paper of the Geological Society of America 375: 89–108. https://doi.org/10.1130/0-8137-2375-2.89.

Martinello, Cappadonia, Conoscenti, Agnesi, Rotigliano. **2020**. "Optimal Slope Units Partitioning in Landslide Susceptibility Mapping." Journal of Maps. https://doi.org/10.1080/17445647.2020.1805807.

Martinello, Mercurio, Cappadonia, Hernández-Martínez, Reyes-Martínez, Rivera-Ayala, Conoscenti, Rotigliano. **2022**. "Investigating Limits in Exploiting Assembled Landslide Inventories for Calibrating Regional Susceptibility Models: A Test in Volcanic Areas of El Salvador." Applied Sciences (Switzerland) 12 (12). https://doi.org/10.3390/APP12126151.

Martino, Prestininzi, Romeo. **2014**. "Earthquake-Induced Ground Failures in Italy from a Reviewed Database." Natural Hazards and Earth System Sciences 14 (4): 799–814. https://doi.org/10.5194/NHESS-14-799-2014.

Méndez Alfaro. **2022**. "Modelación de flujos de escombros en el flanco norte del volcán de San Vicente usando modelos numéricos". Bachelor tesis, Universidad de El Salvador. El Salvador, Central America.

Mercurio, Martinello, Rotigliano, Argueta-Platero, Reyes-Martínez, Rivera-Ayala, Conoscenti. **2021**. "Mapping Susceptibility to Debris Flows Triggered by Tropical Storms: A Case Study of the San Vicente Volcano Area (El Salvador, CA)." https://doi.org/10.3390/earth2010005.

Mercurio, Martinello, Argueta-Platero, Azzara, Rotigliano, Conoscenti. **2022a**. "Predicting earthquake-induced landslides by using a stochastic modelling approach which combines preparatory and triggering factors: a case study of the coseismic landslides occurred on January and February 2001 in El Salvador" – presented at 10th IAG International Conference on Geomorphology (ICG) https://doi.org/10.5194/icg2022-543.

Mercurio, Martinello, Azzara, Argueta Platero, Manno, Cappadonia, Conoscenti, Rotigliano. **2022b**. "Prediction of spatial distribution of landslides generated from rainfalls and earthquakes by using an approach which combines static with seismic para-meters: a test in El Salvador" – presented at EGU General Assembly 2022; https://doi.org/10.5194/egusphere-egu22-6449.

Milborrow. **2020**. "Notes on the Earth Package."

Mora, Vahrson. **1994**. Macrozonation Methodology for Landslide Hazard Determination. Bulletin of Association of Engineering Geologists, 31, 49-58

Naimi, **2015**. "Uncertainty Analysis for Species Distribution Models | R Software Package. https://www.researchgate.net/publication/303174794_Usdm_Uncertainty_analysis_for_species_distribution_models.

Nowicki, Hamburger, Allstadt, Wald, Robeson, Tanyas, Hearne, Thompson. **2018**. A global empirical model for near-real-time assessment of seismically induced landslides. Journal of Geophysical Research: Earth Surface, 123, 1835–1859. https://doi.org/10.1029/2017JF004494.

Ohlmacher. **2007**. "Plan Curvature and Landslide Probability in Regions Dominated by Earth Flows and Earth Slides." Engineering Geology 91 (2–4): 117–34. https://doi.org/10.1016/j.enggeo.2007.01.005.

Quesada, Feoli-Boraschi. **2018**. "Comparación de La Metodología Mora-Vahrson y El Método Morfométrico Para Determinar Áreas Susceptibles a Deslizamientos En La Microcuenca Del Río Macho, Costa Rica." Revista Geográfica de América Central 2 (61): 17–45. https://doi.org/10.15359/RGAC.61-2.1.

Quesada, Campos-Durán. **2022**. "Natural Disaster Risk Inequalities in Central America." Papers in Applied Geography. https://doi.org/10.1080/23754931.2022.2081814.

Reichenbach, Rossi, Malamud, Mihir, Guzzetti. **2018**. "A Review of Statistically-Based Landslide Susceptibility Models." Earth-Science Reviews. Elsevier B.V. https://doi.org/10.1016/j.earscirev.2018.03.001.

Rolo, Bommer, Houghton, Vallance, Berdousis, Mavrommati, Murphy. **2004**. "Geologic and Engineering Characterization of Tierra Blanca Pyroclastic Ash Deposits." Special Paper of the Geological Society of America 375: 55–67. https://doi.org/10.1130/0-8137-2375-2.55.

Rotigliano, Agnesi, Cappadonia, Conoscenti, Agnesi, Cappadonia, and Conoscenti. **2011**. "The Role of the Diagnostic Areas in the Assessment of Landslide Susceptibility Models: A Test in the Sicilian Chain." Springer 58: 981–99. https://doi.org/10.1007/s11069-010-9708-1.

Rotigliano, Cappadonia, Conoscenti, Costanzo, and Agnesi. **2012**. "Slope Units-Based Flow Susceptibility Model: Using Validation Tests to Select Controlling Factors." Natural Hazards 61 (1): 143–53. https://doi.org/10.1007/s11069-011-9846-0.

Rotigliano, Martinello, Agnesi, Conoscenti. **2018.** "Evaluation of Debris Flow Susceptibility in El Salvador (CA): A Comparison between Multivariate Adaptive Regression Splines (MARS) and Binary Logistic Regression (BLR)." Hungarian Geographical Bulletin 67 (4): 361–73. https://doi.org/10.15201/hungeobull.67.4.5.

Rotigliano, Martinello, Hernandéz, Agnesi, and Conoscenti. **2019**. "Predicting the Landslides Triggered by the 2009 96E/Ida Tropical Storms in the Ilopango Caldera Area (El Salvador, CA): Optimizing MARS-Based Model Building and Validation Strategies." Environmental Earth Sciences 78 (6). https://doi.org/10.1007/s12665-019-8214-3.

Shao, Xu. **2022**. "Earthquake-Induced Landslides Susceptibility Assessment: A Review of the State-of-the-Art." Natural Hazards Research, March. https://doi.org/10.1016/J.NHRES.2022.03.002.

Steger, Brenning, Bell, Glade. **2016**. "The Propagation of Inventory-Based Positional Errors into Statistical Landslide Susceptibility Models." Natural Hazards and Earth System Sciences 16 (12): 2729–45. https://doi.org/10.5194/NHESS-16-2729-2016.

Steger, Brenning, Bell, Glade. **2017**. "The Influence of Systematically Incomplete Shallow Landslide Inventories on Statistical Susceptibility Models and Suggestions for Improvements." Landslides 14 (5): 1767–81. https://doi.org/10.1007/S10346-017-0820-0.

USAID. **2005**. USAID Responds to Flooding in Central America and Mexico. https://web.archive.org/web/20111031003901/http:/usaid.gov/locations/latin_america_caribbean/ca_flooding/

USGS. **1977.** "Landslides", Earthquake Information Bulletin.

USGS. **2005**. "Landslides Induced by Hurricane Mitch in El Salvador— An Inventory and Descriptions of Selected Features" - Crone, Baum, Lidke, Sather, Bradley, Tarr

Van Den Eeckhaut, Reichenbach, Guzzetti, Rossi, Poesen. **2009**. "Combined Landslide Inventory and Susceptibility Assessment Based on Different Mapping Units: An Example from the Flemish Ardennes, Belgium." Natural Hazards and Earth System Science. https://doi.org/10.5194/nhess-9-507-2009.

Van Den Eeckhaut, Hervás, Jaedicke, Malet, Montanarella, Nadim. **2012**. "Statistical Modelling of Europe-Wide Landslide Susceptibility Using Limited Landslide Inventory Data." Landslides 9 (3): 357–69. https://doi.org/10.1007/S10346-011-0299-Z/TABLES/5.

Vargas-Cuervo, Rotigliano, Conoscenti. **2019**. "Prediction of Debris-Avalanches and -Flows Triggered by a Tropical Storm by Using a Stochastic Approach: An Application to the Events Occurred in Mocoa (Colombia) on 1 April 2017." Geomorphology 339 (August): 31–43. https://doi.org/10.1016/j.geomorph.2019.04.023.

Varnes. **1978**. Slope Movement Types and Processes. In: Schuster, R.L. and Krizek, R.J., Eds., Landslides, Analysis and Control, Transportation Research Board, Special Report No. 176, National Academy of Sciences, 11-33.

Varnes & IAG. **1984**. "Commission on Landslides" - Landslide Hazard Zonation - a review of principles and practice. UNESCO Paris. 63pp

Verstappen. **1983**. "Geomorphology of the Agri Valley, Southern Italy." ITC Journal.

Vorpahl, Elsenbeer, Märker, Schröder. **2012**. How can statistical models help to determine driving factors of landslides? Ecol. Model. 239, 27–39. http://dx.doi.org/ 10.1016/j.ecolmodel.2011.12.007.

Wald. **2005**. ShakeMap® Manual - Technical Manual, Users Guide, And Software Guide

Weber, Wiesemann, Lorenz, Schmidt-Thome. **1975**. "Mapa Geológico de La República de El Salvador/América Central = Geologische Karte Der Republik El Salvador/Mittelamerika." Accessed November 16, 2020. https://nla.gov.au/nla.obj-726140200/view.

White. **1993**. Bulletin of the Seismological, and undefined 1993. "Destructive Upper-Crustal Earthquakes of Central America since 1900." Pubs.Geoscienceworld.Org 83 (4): 1115–42. https://pubs.geoscienceworld.org/ssa/bssa/article-abstract/83/4/1115/119725.

Worden. **2020**. ShakeMap v4 Documentation.

Youden. **1950**. "Index for Rating Diagnostic Tests." Cancer 3 (1): 32–35. https://doi.org/10.1002/1097-0142(1950)3:1<32::AID-CNCR2820030106>3.0.CO;2-3.